Photometry and Transit-Timing Analysis for Eleven Transiting Exoplanets

by

Katherine Rebecca de Kleer

Submitted to the Department of Physics
in partial fulfillment of the requirements for the degree of

Bachelor of Science

at the

MASSACHUSETTS INSTITUTE OF TECHNOLOGY

June 2009

Author .....
Department of Physics
May 8, 2009

Certified by .....
Joshua N. Winn
Assistant Professor
Thesis Supervisor

Accepted by .....
David E. Pritchard
Chairman, Department Committee on Undergraduate Theses

Photometry and Transit-Timing Analysis for Eleven Transiting Exoplanets

by

Katherine Rebecca de Kleer

Submitted to the Department of Physics
on May 8, 2009, in partial fulfillment of the
requirements for the degree of
Bachelor of Science

Abstract

This thesis presents time-series photometry of transits of 11 different extrasolar planets. Observations were conducted with the Fred L. Whipple Observatory 1.2m telescope and the Wise Observatory 1m telescope, in standard optical bandpasses. The number of transits observed for each planet ranges between one and 20 transits, and differential aperture photometry is performed for each transit observation. For the system TrES-2, this thesis examines 14 different different transit observations. Because of this large quantity of data, the parameters R_p/R_*, b, a/R_*, and i are also fitted for with precision using the Markov Chain Monte Carlo technique, and the resultant parameter values are presented. Transit-timing analysis is performed on all systems: CoRoT-2, GJ436, HAT-P-1, HD17156, HD189733, TrES-1, TrES-2, WASP-2, WASP-3, XO-1, XO-2, and XO-3. Transit timing is important both for constraining the orbital period and to search for variations in the transit-to-transit interval that could indicate the presence of an unseen companion planet. The transit center times for nearly all observations are found, and the planetary periods for all systems are calculated. In many cases these periods are determined with much greater precision than previously known. It is found that systems XO-2 and HAT-P-1 are consistent with a constant period, but our data are not conclusive with regards to the other systems.

Thesis Supervisor: Joshua N. Winn
Title: Assistant Professor

Acknowledgments

I would first like to thank Joshua Winn for advising this thesis and for all of his assistance, encouragement, and patience. I am also grateful to Anjali Tripathi, Joshua Carter and Saul Rappaport for their assistance along the way. I am thankful to Gilbert Esquerdo for teaching me how to use the observing facilities at the Fred Lawrence Whipple Observatory, and to Tsevi Mazeh for sharing his data. Finally, I would like to acknowledge Krishna Rajagopal for inspiring and motivating me on this thesis and in physics research in general.

Contents

List of Figures

List of Tables

Chapter 1

Introduction

1.1 Transiting Exoplanets and the Transit-Timing Variation Method

With the numerous discoveries of planets around other stars over the past two decades, the study of these 'exoplanets' has become one of the largest and most-followed new fields in astrophysics. The main goals of these observations are to determine as accurately as possible the orbital parameters of the planet-star system as well as the individual masses and radii of the star and orbiting planet. With these values in hand, more informed theories of planet formation and structure can be developed. Many techniques have been employed for observing and determining the orbital parameters of exoplanetary systems, but one of the most productive of these has been photometric transit observations.

Transit observations are unique because they give a direct measurement of the planetary radius ratio R_p/R_*, the scaled semi-major axis a/R_*, and the orbital inclination i. Knowledge of the inclination i can be combined with radial velocity measurements of $M_p\sin(i)$ to get a value for the planetary mass M_p. This mass can be combined with the planetary radius to calculate the planetary density and thus give information about the composition of the planet.

In addition, transit observations could potentially yield the discovery of additional

planets in those same systems, even though they may be invisible to other observing techniques. A recently-proposed method involves obtaining precise timings of transits and studying the variations in the planetary period over time. An Earth-sized planet in orbit with a transiting planet could cause detectable variations in the period that would be observable by finding exact times of mid-transit. Through looking for these variations, the presence of a smaller planet or even a satellite of the transiting body could be inferred (Agol et al. 2005, Holman & Murray 2005).

1.2 Overview

This thesis will look at eleven systems with known transiting planets, for each of which we have between one and 20 transit observations. Data reduction and aperture photometry were done on all data sets (data listed in Table A.1), and the majority of observations were fit with a theoretical model. The final light curves with the best-fitting models are presented in Figures B-1 through B-63. Because we have an abundance of high-quality data for the system TrES-2, precise parameters for this system were calculated using the Markov chain Monte Carlo technique, and the results are tabulated in Tables 3.1 and 3.2 and compared to previously published values.

In addition, precise transit times were calculated for each transit with occasional exceptions for poor quality data (presented in Table A.4). The Markov Chain Monte Carlo technique was used to obtain accurate error bars for the transit times. From these transit times, precise periods were calculated for nine systems with our data alone. In addition, in most cases we combined our results with published transit times to determine higher-precision periods (presented in Table A.6). The transit-time residuals for these systems were calculated and are plotted in Figures B-64 through B-71. The consistency of these times with a constant orbital period is discussed.

Chapter 2

Observations and Data Reduction

2.1 Observations

The majority of data was taken on the 1.2 m (48 inch) telescope at the Fred Lawrence Whipple Observatory (FLWO) on Mt. Hopkins, Arizona. The detector KeplerCam was used, which was constructed for a photometric survey of the target field of the Kepler satellite mission. The camera is a 4096 x 4096 CCD with four amplifiers for a total field of view of 23' x 23'. After 2x2 binning, the pixel scale is 0.68"/pixel.

A small fraction of data was also taken on the 1 m (40 inch) telescope at Wise Observatory in the Negev Desert, Israel. The instrument used was a Princeton Instruments (PI) VersArray camera with a back-illuminated CCD. The detector has a 1300 x 1300 pixel array with a pixel scale of 0.58"/pixel and a field of view of 13.0' x 12.6'.

For the data taken at the FLWO, a specific observing procedure was followed on each night of observation. Each night, 20 bias images were taken at the beginning and end of the night for a total of 40 bias images. In addition, dome flats were taken for each filter used. The durations of flat exposures were chosen to achieve approximately 20,000 counts per pixel. At the FLWO, Sloan filters r, i, and z were used for observations. At Wise Observatory, a Bessel R filter was used.

The precise field of view for each target was selected to include as many comparison stars as possible of similar magnitude to the target. Once the telescope was focused

and the desired field pointing was established, the telescope was defocused if needed with a goal of 30,000 counts for the target star. The exposure times were held constant over the course of the observation, despite changing airmass or weather conditions. This was not the case for the data taken at Wise Observatory; for this data, the exposure times were changed throughout the night to maintain a constant photon count for the target star.

A number of observations produced poor light curves. The GJ436 observation on 2008-06-19, the TrES-4 observation, and the WASP-3 observation on 2008-07-14 were not used because poor weather affected the data. The GJ436 observations on 2008-03-05, 2008-03-16 and 2008-04-09 were of poor quality for unknown reason, and the 2008-04-09 observation was so poor it was not used. The GJ436 observation on 2008-05-05 experienced weather problems, but the data was still used.

All observations are tabulated in Table A.1, including important information and any notes.

2.2 Data Reduction and Aperture Photometry

The data were reduced and calibrated using IRAF procedures. Images were read into IRAF as four-segment FITS files. Using the IRAF procedure IMSTAT, each bias and flat field was examined for anomalous pixel counts. These occurred infrequently, but the frames containing such pixels were not used in the reduction. Using the procedure ZEROCOMBINE, the bias images were then calibrated for the overscan correction and trimmed, and a master bias image was created. Using the procedure FLATCOMBINE, the flat fields were also calibrated for the overscan correction and trimmed, the master bias was subtracted from them, and they were combined to produce a master flat field. Finally, the procedure CCDPROC was used on the data images to calibrate for overscan correction, trim the images, subtract the master bias image, divide by the master flat field, and merge the four FITS segments into one standard FITS file. The output of this process is a set of reduced data images in standard FITS format.

In most cases, the telescope guider functioned as expected, and the images were aligned within a few pixels. However, guiding failure occurred occasionally due to temporary cloud obstruction of the guide star, and images needed to be aligned manually. In these cases, the IRAF procedure IMALIGN was used to align the images to each other. Bright stars were identified by hand in one image, and the procedure used their relative coordinates to shift all images to match this image. Shifts were always made in integer pixel amounts to avoid pixel interpolation. Occasionally, images were misaligned by over 30 pixels and manual shifting was needed prior to running of the IMALIGN procedure.

Aperture photometry was performed on each reduced data set to obtain photon counts of the target star and numerous comparison stars in the field. Then differential photometry was carried out to correct for overall brightness trends, and the flux for the target star was normalized to its out-of-transit flux.

The aperture photometry was performed using IRAF procedures. First, comparison stars were identified by hand, and coordinates were recorded. In general, most of the stars in the field between half and twice the brightness of the target star were recorded as comparison stars; the number ranged by target based on the density of the field but was generally between six and twenty. The airmass over the course of each observation was calculated from the time and observatory location. The FWHM of the target star was calculated for each image using the IRAF procedure PSFMEASURE. Based on the average FWHM value, a range of at least nine integer pixel aperture sizes were chosen. The range always included the pixel value nearest twice the average FWHM. For each of these aperture sizes, photometry was done on the target star and each comparison star using the IRAF procedure PHOT. This procedure calculates the flux inside an aperture surrounding each star and subtracts from it an estimate for the sky background based on an annular aperture at a radius of 30 pixels from the star's center. The final result of this procedure is an array for each night of observation containing background-subtracted electron counts for each selected star per aperture size.

2.3 Differential Photometry and Light Curve Production

At this point data were exported from IRAF; all further work was done using IDL scripts. The first modification to the data was the manual identification and exclusion of unusuable data. Frequently the first few data points were excluded because their pointing or exposure time was not consistent with the rest of the data. In a few cases, the flux of all stars dipped significantly during a part of the observation; this was attributed to a passing cloud, and the data in these regions were excluded. In general, if flux of all stars dropped temporarily below 50% of the average flux near that airmass, all data from this time period were excluded. Ideally, dividing the target flux by the comparison flux should eliminate any weather-related problems. However, because passing clouds cause differential extinction and the comparison stars all have different spectra from the target star, differential photometry does not remove all atmospheric effects. Even in the comparison-divided target light curves, cloud effects are often clearly visible. Occasionally the comparison or target light curves contained a single data point deviating considerably from the rest of the data; these data points were generally excluded as well. Such data points were identified as follows. The target light curve was smoothed over 50 data points (out of approximately 300 total), and if the deviation of any single data point from the smoothed light curve was above a certain threshold, this entire data frame was excluded from analysis. For the comparison stars, if the deviation of any single data point from the mean was above a threshold value, that data point was replaced by the mean count value for the star. These threshold values were variable based on the quality of the observation, but usually were around 15% of the mean or out-of-transit flux.

After the exclusion of unusable data, the aperture size and comparison stars were chosen from those selected during reduction. The out-of-transit region of each observation was identified by eye on the target light curve, and combinations of aperture size and comparison star subset were tried until the standard deviation of the out-of-transit target flux was minimized. This process somewhat moderates the problem of

the different extinctions of differently-coloured comparison stars, since it selects for comparison stars that have spectra nearer that of the target. In general, the aperture sizes that minimized noise were 2-3 times the FWHM of the target star.

Once these values were selected, the chosen comparison stars were averaged to make a composite comparison light curve. First, each comparison star was weighted based on the standard deviation in its flux. The weighting scheme was chosen from

$$\begin{aligned} \text{weight} &\propto \frac{1}{\sigma^2} \\ \text{weight} &\propto \frac{1}{\sqrt{\sigma}} \\ \text{weight} &\propto \frac{1}{|\sigma|} \end{aligned}$$

based on which minimized the standard deviation of the out-of-transit flux of the target. In most cases, the σ^2 weighting was chosen, which is stastically optimal assuming Gaussian, uncorrelated noise. The reference light curve was then constructed from the comparison stars as the mean-normalized sum of the weighted light curves, or:

$$F_{ref} = \frac{\sum \text{weight}_i F_{comp,i}}{\sum \text{weight}_i} \tag{2.1}$$

where the comparison light curves $F_{comp,i}$ are normalized to their mean value. The target light curve was then divided by this reference flux and normalized to its mean out-of-transit flux.

The final step in the light curve production process was to look at correlations between out-of-transit flux and other variables. The variables that were examined for correlation were the x and y pixel coordinates on the chip, the ellipticity of the target star, the FWHM of the target star, time, position angle, and reference flux. In addition, the correlation between magnitude (log(flux)) and airmass z was examined. For each of these pairs of variables, a correlation coefficient was computed. A correlation was identified when the correlation coefficient was above 0.2. In these cases, possible reasons for correlation were explored, and the light curve was 'decorrelated.' This

process consists of fitting a line to the out-of-transit flux (or magnitude) vs the variable, and dividing all the data by this function. The most common correlations were between magnitude and airmass and between flux and FWHM or time. However, after decorrelating the magnitude against airmass, there were generally no significant correlations remaining. In the Wise Observatory data, where the guiding was not as successful, flux was occasionally correlated with pixel coordinate.

The final result of this procedure is a collection of normalized, low-noise light curves. Both the theoretical and the actual noise were computed for each night of observation. The theoretical noise was calculated as the quadrature sum of the median photon noise and the median scintillation noise, where each of these is calculated as follows:

$$\begin{aligned} \sigma_{photon} &= \sqrt{\frac{1}{G f_{obs} t_{exp}}} \\ \sigma_{scint} &= 0.09 D^{-0.67} z^{1.75} e^{-h/8000} (2t_{exp})^{-0.5} \\ \sigma_{theoretical} &= \sqrt{\sigma_{photon}^2 + \sigma_{scint}^2}, \end{aligned}$$

where G is the CCD gain (electrons per count), f_{obs} is the flux of the target star in counts/seconds, t_{exp} is the exposure time in seconds, D is the telescope diameter in cm, and h is the altitude of the site in m. The actual noise was calculated as the standard deviation of the out-of-transit data points. In general, the actual noise was 1.5 - 2 times higher than the theoretical noise.

Chapter 3

TrES-2: Precise Parameter Determination

3.1 Introduction: Transit Parameters

In order to understand and analyze an exoplanetary system, it is important to know quite precisely the system parameters. Though some parameters cannot be found from transit photometry alone, it is possible to measure a number of useful values. A light curve is described completely by six parameters (see figure 3-1): the transit center time T_c, the depth δ, the width T, the ingress and egress time τ, and the limb darkening coefficients u_1 and u_2. However, the parameters T, τ, and δ are not of physical significance; of more scientific interest are the radius ratio R_p/R_*, the inclination angle i, the impact parameter b, and the planet's semi-major axis a/R_*. These parameters can be obtained from the transit light curve (see Mandel & Agol 2002), but the relationship is roughly as follows. The physically significant parameters can be expressed approximately in terms of measurable parameters as

$$\begin{aligned} \frac{R_p}{R_*} &\approx \sqrt{\delta} \\ b^2 &\approx 1 - \sqrt{\delta}\frac{T}{\tau} \end{aligned}$$

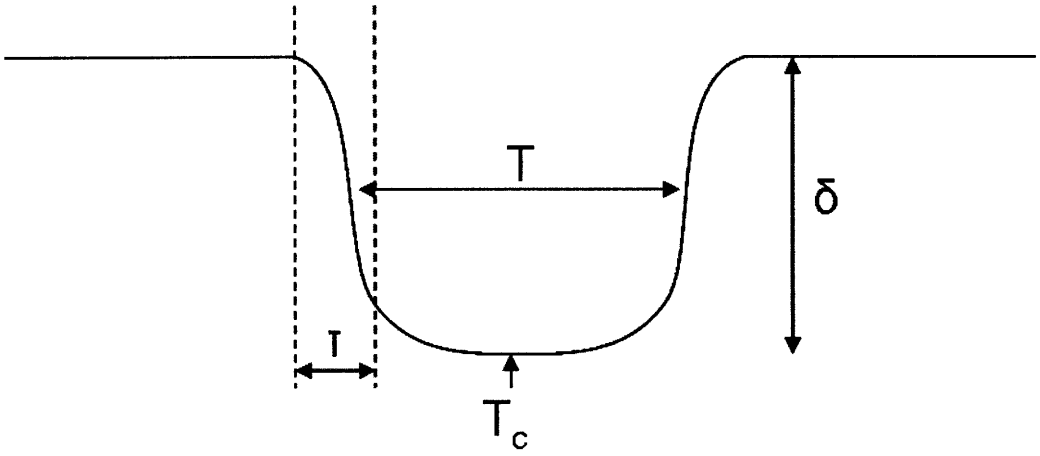

Figure 3-1: Light Curve Parameters: An illustration of the four main parameters describing a transit light curve: the transit center time T_c, the depth δ, the width T, and the ingress and egress time τ.

$$\begin{aligned} \frac{a}{R_*} &\approx \frac{\sqrt{1-b^2}P}{\pi T} \\ i &\approx \arccos\left(bR_*/a\right), \end{aligned}$$

where the inverse equations are

$$\begin{aligned} \delta &\approx \left(\frac{R_p}{R_*}\right)^2 \\ T &\approx \frac{PR_*\sqrt{1-b^2}}{a\pi} \\ \tau &\approx \frac{PR_*\sqrt{\delta}}{a\pi\sqrt{1-b^2}}, \end{aligned}$$

P is the period, and equations are given for a circular orbit.

3.2 Parameter Determination

In order to determine the most precise system parameters and assign credible error intervals, the Markov chain Monte Carlo technique was used.

To maximize precision, model-fitting was done for composite instead of individual light curves. Because limb darkening effects vary across the spectrum, it was necessary

to fit the light curves for each filter separately to find the limb darkening coefficients u_1 and u_2. Within each filter, composite light curves were produced by first determining the best-fitting value for T_c for each light curve, then combining the light curves together by aligning their transit-center points. The light curves that were used in the final fitting were generally binned to a time sampling of one data point per 45-60 seconds, since the fitting process was relatively time-intensive.

For the TrES-2 system there were 15 nights of observation (see Table A.1): six in the z-band taken at the FLWO, six in the i-band taken at the FLWO, and seven in the R-band taken at Wise Observatory. Of these seven, one was of very poor quality and was discarded. In many cases, the flux of the star was affected by the changing airmass z over the course of the observation. Since this effect is not symmetric about the center of the transit, this would lead to a skewed calculated T_c. Thus when the best-fitting T_c value was being fit for, a flux-airmass relation was fit for simultaneously. It was assumed that the un-obstructed magnitude of the central star would vary linearly with the airmass. Thus the flux-airmass relation looks like

$$f = f_0 e^{-kz} \tag{3.1}$$

where f is the observed flux, f_0 is the unobstructed flux, and k is a coefficient describing the relationship between airmass and flux. Thus the fitting involved using the IDL function AMOEBA to find the values of (T_c,f_0,k) that minimized

$$\chi^2 = \sum \left(\frac{f_i - f_{i,calc}}{\sigma_f} \right)^2, \tag{3.2}$$

where f_i is an elements from the array of observed fluxes, $f_{i,calc}$ is an element from the array of theoretical fluxes calculated from the current values of the parameters using the code from Mandel and Agol (2002), and σ_{f_i} is the error on each data point. For the individual light curves, σ_f for each data point was given the value of the standard deviation of the out-of-transit data. For the binned light curves, σ_f was

assigned to each data point as

$$\sigma_f = \frac{1}{n}\sqrt{\sum \sigma_{f,i}^2} \tag{3.3}$$

where n is the number of data points averaged to produce a given binned point, and the $\sigma_{f,i}$ are the errors on all these points. As is generally the case throughout this thesis, this procedure assumes the errors to be Gaussian and uncorrelated.

With known transit center times, it was possible to combine the light curves from different nights to create the composite light curves for each filter, which are shown in Figures B-72,B-75,and B-78.

For each of the composite light curves, fitting was done for the six parameters (T_c, R_p/R_*, T, b, i, u_1, u_2). However, some of these variables are correlated to each other, so for the purposes of fitting this set of variables was converted to the less-correlated set (T_c, R_p/R_*, T, b, $u_{\rm sum}$, $u_{\rm diff}$), where

$$\begin{aligned} u_{\rm sum} &= u_1 + u_2 \\ u_{\rm diff} &= u_1 - u_2. \end{aligned}$$

Both $u_{\rm sum}$ and $u_{\rm diff}$ were very poorly constrained. Thus only $u_{\rm sum}$ was actually fit for, while $u_{\rm diff}$ was fixed at the tabulated value (given in Table A.3).

The MCMC program ran as follows (see Winn et al. 2007, Tegmark et al. 2004, Holman et al. 2006, Ford 2005). For each step, the initial χ^2 was calculated exactly as in Equation 3.2. A parameter was then chosen at random from the set of five above. This parameter was varied by an amount chosen from a Gaussian distribution centered at the current parameter value with a width set at the beginning to be approximately the expected error. The new χ^2 value was then calculated and compared to the previous value. If the parameter variation decreased the value of χ^2, the new parameter value was kept. If it increased the value of χ^2, the new value was kept with probability

$$\text{prob} = e^{-\frac{\chi_i^2 - \chi_{i-1}^2}{2}} \tag{3.4}$$

where χ_i^2 is the current χ^2 value and χ_{i-1}^2 is the value before the variation. Thus if χ^2 increased significantly due to the variation, it is improbable that the new value is be kept, but if the increase is slight, there is a reasonable probability for this. If the new value is not kept, the parameter is returned to its value at the start of the step.

The distribution of values each parameter took over the run was treated as the probability distribution for that parameter. The distributions for the parameters (u_1, u_2, a/R_* and i) were derived from their values over the course of the simulation as calculated from the the parameters (R_p/R_*, T, b, $u_{\rm sum}$, $u_{\rm diff}$) used in the fitting. The median and 68.3% confidence limits were then read directly from the distribution. This approach was used and implemented based on its description by Tegmark et al. (2004).

All of the system parameters converged well and were calculated to good precision. However, the limb darkening coefficients were very poorly constrained. They were included in the fitting in order to accurately find the uncertainty in the system parameters. The limb darkening coefficients are covariant with the system parameters, and error in these coefficients thus causes corresponding error in the other parameters.

While the above parameters were derived from the light curves alone, it is possible to calculate additional parameters given external knowledge of the stellar mass M_*. Using the value given by Torres et al. 2008 (listed in Table 3.2, the stellar radius, planetary radius, semi-major axis, and stellar mean density were calculated for TrES-2. The stellar radius was calculated from Kepler's Third Law

$$\left(\frac{P}{2\pi}\right)^2 = \left(\frac{a}{R_*}\right)^3 \frac{R_*^3}{G(M_* + M_p)}, \tag{3.5}$$

where G is the universal gravitational constant and M_p is assumed to be negligible and is thus neglected. The values for the planetary radius, semi-major axis, and stellar mean density follow immediately from the stellar radius and mass when combined with the known transit parameters R_p/R_* and a/R_*.

Table 3.1: TrES-2 Fitted Parameters

filter	R_p/R_*	b	a/R_*	i(deg)	(u_1,u_2)	Source
z	0.1260 ± 0.0018	0.858 ± 0.017	7.45 ± 0.17	83.41 ± 0.27	(0.23,0.36) ± 0.10	(1)
R	0.1264 ± 0.0028	0.856 ± 0.017	7.93 ± 0.25	83.81 ± 0.32	(0.27,0.30) ± 0.09	(1)
i	0.1237 ± 0.0017	0.846 ± 0.014	7.74 ± 0.16	83.73 ± 0.22	(0.26,0.34) ± 0.09	(1)
	0.1253 ± 0.0010	0.858 ± 0.017	7.62 ± 0.11	83.57 ± 0.14		(2)

Source (1) is this thesis and (2) is Torres et al. 2008.

The errors on these values were established by creating artificial probability distributions for P, M_*, and a/R_* assuming Gaussian distributions and combining these distributions to find resultant probability distributions for the stellar and planetary radii, the semi-major axis, and the stellar mean density.

3.3 Discussion

The resultant parameter values are tabulated in Table 3.1. The distributions for the relevant parameters are shown in Figures B-74, B-77, and B-80, and the resultant probability distributions are plotted in Figures B-73, B-76, and B-79.

Since each filter was treated separately, we obtained three values for each parameter. The radius ratio was found to be 0.1260 ± 0.0018, 0.1264 ± 0.0028, and 0.1237 ± 0.0017 for the z-band, R-band, and i-band fits respectively. These are consistent (within 1σ) with the published value of 0.1253 ± 0.0010 (Torres et al. 2008). The impact parameter was found to be 0.858 ± 0.017, 0.856 ± 0.017, and 0.846 ± 0.014, again consistent (within 1σ) with the published value of 0.8540 ± 0.0062. The scaled semi-major axis was found to be 7.45 ± 0.17, 7.93 ± 0.25, and 7.74 ± 0.16. All three values fall within 1.2σ of the published value of 7.62 ± 0.11 (Torres et al. 2008). The inclination angle was found to be 83.41^o ± 0.27^o, 83.81^o ± 0.32^o, and 83.73^o ± 0.22^o, where all these values and the above are again reported for the z-band, R-band, and i-band respectively. These values for the inclination angle are consistent (within 1σ) with the published value of 83.57^o ± 0.14^o (Torres et al. 2008). Thus all of our parameter values are consistent with previously published values. The errors in our values are larger than the errors in the published parameters despite our larger num-

ber of data sets (we had six observation nights each in the z-band and R-band, while Holman et al. (2007) and Torres et al. (2008) had only three). This is most likely due to the fact that we were fitting for these parameters as well as the limb darkening coefficients, while Torres et al. (2008) fit only for the system parameters and fixed the limb darkening coefficients at the tabulated values. It was found that fitting for these coefficients simultaneously greatly increased the uncertainty in the system parameters because the coefficients were poorly constrained by the data. However, due to the covariance between the system parameters and limb darkening coefficients, we believe that these higher error bars more accurately represent the true uncertainty.

Assuming a value for M_* of 0.983 ± 0.063 (Torres et al. 2008), the stellar radius, planetary radius, semi-major axis, and stellar mean density were calculated. We found a stellar radius of 1.027 ± 0.031 solar radii, a planetary radius of 1.258 ± 0.043 Jupiter radii, a semi-major axis of 0.03556 ± 0.00073 AU, and a stellar mean density of 1.282 ± 0.087 g cm^{-3}. These values are tabulated in Table 3.2 along with those obtained by Torres et al. (2008). The two sets of parameter values are consistent and of similar precision. Thus we see no need to modify the interpretation of TrES-2 as a gas giant planet, slightly larger than predicted by planetary models.

Table 3.2: TrES-2 System Parameters

Parameter	This Thesis	Torres et al. 2008
P	2.4706130 ± 0.0000007	2.47063
R_p/R_*	0.1260 ± 0.0018	0.1253 ± 0.0010
b	0.858 ± 0.017	0.8540 ± 0.0062
a/R_*	7.45 ± 0.17	7.62 ± 0.11
i(deg)	83.41 ± 0.27	83.57 ± 0.14
$M_*(M_\odot)$		0.983 ± 0.06
$R_*(R_\odot)$	1.027 ± 0.031	1.003 ± 0.033
$R_p(R_{Jup})$	1.258 ± 0.043	1.224 ± 0.041
$M_p(M_{Jup})$		1.200 ± 0.053
$\log(g_p)$(cgs)		3.298 ± 0.016
$\log(g_*)$(cgs)	4.408 ± 0.022	4.427 ± 0.021
a (AU)	0.03556 ± 0.00073	0.03558 ± 0.00077
ρ_p (g cm^{-3})		0.813 ± 0.096
ρ_* (g cm^{-3})	1.282 ± 0.087	1.372 ± 0.061

Values given for parameters derived from transit light curves alone are all presented from the z-band data, since there were the highest number of good light curves in this band.

Chapter 4

Transit Timing

4.1 Introduction to the Transit Timing Method

The transit timing method is a technique that uses known transiting extrasolar planets to attempt to detect unobserved companion planets. Though it has not yet been used to make a successful detection, it has been proposed and discussed in Holman & Murray (2005), Agol et al. (2005), Simon (2007) and others, and used to place constraints on potential companion planets in various systems (Steffen et al. 2008, Hrudkova et al. 2008).

The method utilizes the fact that an unseen companion planet would gravitationally influence the transiting planet, causing the transit-to-transit interval to be non-uniform. While a single planet around a star would have a constant or nearly-constant period, a planet with a companion could have period variations on the order of minutes (Holman & Murray 2005). In this section, we perform a transit timing analysis on eleven systems with known transiting planets. We determine the transit center time of each observation, and look for evidence of deviations from a constant period.

4.2 Finding Transit Center Times

In order to look for transit timing variations in each of the systems, the exact transit times with error bars needed to be found for each night of observation. For each light curve, the best-fitting parameters were found. These parameters were then fixed, and the transit times and errors were found using the Markov Chain Monte Carlo (MCMC) technique.

First, the tabulated values of the limb-darkening coefficients u_1 and u_2 were taken from Claret et al. (2000) based on various stellar parameters (see Table A.3) and held constant at these values throughout the fitting. This was done because there was generally too much noise in an individual light curve to meaningfully constrain these coefficients. However, the use of potentially incorrect limb darkening coefficients should not affect the final transit time since they affect the model light curve in a way that is a symmetric about the center point.

For each light curve, the values for T_c, R_p/R_*, b and i were found by minimizing χ^2 using the IDL function AMOEBA, though T_c was later determine more precisely, as explained below. To avoid varying highly correlated variables simultaneously, the transit width T (see Section 3.1) was used instead of i during the minimization and converted back afterwards. For observations of partial transits, these parameters were initiated at the best-fitting values for the full transits of the same system and were not permitted to deviate far from these values. The minimization function took in the parameter values, calculated a theoretical light curve f_{th} using the equations and code from Mandel & Agol (2002), and calculated χ^2 as follows:

$$\chi^2 = \sum \left(\frac{f - f_{th}}{\sigma_f} \right)^2, \tag{4.1}$$

where f is the observed flux and σ_f is the error on each flux point, which is fixed across each observation at the standard deviation of the out-of-transit flux.

Once the optimal system parameters (R_p/R_*, b, i) were found, they were fixed at these best-fitting values while the transit center time was varied. For each observation, we used a 50,000-step MCMC, varying the values for T_c as well as the airmass

coefficients k, and f_0 (see Equation 3.1 for exact definition of these). Though this step number is relatively small, it was found that these three parameters converged almost immediately, and the final values and error bars did not change between a 10,000-step chain and a 50,000-step chain. The choice of k and f_0 as additional variables to vary was made because they do not affect the light curve in a symmetric way. While the transit center time is not correlated with variables that affect the light curve in a symmetric way, it should be correlated with all variables that have asymmetric effects. Thus variations in R_p/R_*, b or i should not affect the final value for T_c, but variations in k or f_0 would. This is also the reason that the system parameters were optimized for each light curve individually, rather than found more accurately using composite light curves, as was done for TrES-2 (Chapter 3). The slight inaccuracies in these system parameters should have no effect on the calculated transit center time.

4.3 Fitting for Periods and Searching for Variations

Once all the transit center times were known precisely, an arbitrary 'zero epoch' transit was chosen, and the epoch number of each other transit was easily found from known estimates for the planet's period (epoch numbers of each observation are tabulated in Table A.4). A linear fit was then done to the transit center times versus their epoch number, to get a precise period. This fit was then subtracted from the data to obtain the timing residuals and thus determine whether any timing anomalies were present. A value of χ^2 was determined for each fit, where

$$\chi^2 = \sum \left(\frac{T_c(calc) - T_c(pre)}{\sigma_{Tc}} \right)^2. \tag{4.2}$$

$T_c(pre)$ is the predicted transit time based on the linear fit, and σ_{Tc} is the error on the calculated transit center time. This value helps assess how well the data fit a linear model, and thus how consistent the data are with a constant orbital period.

4.4 Discussion & Future Work

Transit center times for all systems are tabulated in Table A.4. Ephemerides were produced for all systems for which we had two or more observations, and these are tabulated in Table A.6.

The cited error bars for transit center times are the errors directly from the probability distributions given by the Markov chains. However, we believe that these errors are generally under-estimated, as is discussed at the end of this section. In order to obtain the most precise estimates for the period, only light curves with relatively low and uncorrelated noise were used in fitting for the period (see Table A.4 for which observations were used). After these were fit, the error bars on all transit times were scaled up by the square root of χ^2 per degree of freedom, so that the calculated period would fit the 'good' data points with a χ^2 per degree of freedom of one. The actual calculated ephemerides and errors are based on only these low-noise observations and are based on the scaled-up error bars. In most cases, our data were combined with published transit center times to produce more precise ephemerides as well. The ephemerides based on our data alone, and those based on our data combined with published times, are tabulated in Table A.6. The results stated here are based only on our own data.

For GJ436, 12 observations were used to fit for the planetary period. The ephemeris was found to be $HJD_0 = 2454510.80069 \pm 0.00015$ and $P = 2.643896 \pm 0.000004$. This is consistent with the published period of 2.64386 ± 0.00003 (Shporer et al. 2009). The fit with original error bars gave a χ^2 value (see Equation 4.2) of 54, which is high considering that only 12 observations were used. The uncertainties used in the ephemeris fitting were scaled up to give a χ^2 value of 10. With this rescaling of uncertainties, the data is generally consistent with a constant period.

For HAT-P-1, four observations were used. The ephemeris was found to be $HJD_0 = 2454390.73871 \pm 0.00016$ and $P = 4.4653094 \pm 0.0000037$, consistent with the published period of 4.46543 ± 0.00014 (Winn et al. 2007). In this case the χ^2 value based on the original error bars was 2.2, which shows that our data is completely

consistent with a constant period.

The fitting for TrES-1 was done using only two observations. The calculated ephemeris is $HJD_0 = 2454204.91020 \pm 0.00037$ and $P = 3.0300823 \pm 0.0000037$. This period is about 3σ off from the published value of 3.0300737 ± 0.0000013 (Winn et al. 2007b).

Ten observations were used for the TrES-2 fit. The calculated ephemeris is $HJD_0 = 2454313.402728 \pm 0.00024$ and $P = 2.470613 \pm 0.0000022$. The published value of $P = 2.470621 \pm 0.000017$ (Holman et al. 2007) is consistent with this period. The χ^2 value for this system was again quite high, with a value of 76 prior to the rescaling of error bars.

Only two observations were used for the WASP-2 fit. The calculated ephemeris is $HJD_0 = 2454619.96275 \pm 0.00038$ and $P = 2.1522117 \pm 0.0000072$. This is nearly 2σ from the published period of 2.152226 ± 0.000004 (Collier Cameron et al. 2007).

For WASP-3, the period was fit for using three observations. The ephemeris was found to be $HJD_0 = 2454627.72109 \pm 0.00073$ and $P = 1.84689 \pm 0.00008$, again consistent with the published period of 1.846835 ± 0.000002 (Gibson et al. 2008). The χ^2 from the original fit was 21.

The fitting for XO-1 was done using only two transit observations. The calculated ephemeris is $HJD_0 = 2454143.94454 \pm 0.00020$ and $P = 3.9415075 \pm 0.0000023$. The published period of 3.941634 ± 0.000137 (Fernandez et al. 2009) is consistent with this.

For XO-2, three transit observations were used. The calculated ephemeris is $HJD_0 = 2454479.96429 \pm 0.00032$ and $P = 2.615843 \pm 0.000041$, which is consistent with the published period of 2.615819 ± 0.000014 (Fernandez et al. 2009). The χ^2 for from the original fit was 4.2 for three data points, so we conclude that our results are consistent with a constant period for XO-2 even without error re-scaling.

Four transit observations were used for XO-3. The ephemeris was found to be $HJD_0 = 2454449.86703 \pm 0.00041$ and $P = 3.1914418 \pm 0.000031$. This value for the period is nearly 3σ from the published value of 3.1915239 ± 0.0000068 (Winn et al. 2009). The χ^2 value for the original fit was 13.1.

When our data were combined with the published transit times, the values of χ^2 per degree of freedom were generally much close to one, indicating overall consistency with a constant period.

For nearly all of the above cases, the χ^2 value for the model fit was significantly higher than the number of degrees of freedom, and errors were scaled up correspondingly. We believe the errors produced by the Markov Chain were under-estimated in a number of ways, so it is difficult to assess the success of the model in describing the data. Our analysis did not account for correlated noise in the data, although it was clearly present in a number of cases. In particular, many light curves were not perfectly symmetric, and some deviated significantly from symmetry about the center point. In these cases, the value for T_c that minimized χ^2 may have been skewed by the asymmetries despite having converged well in the Markov Chain. The uncertainty in the transit times for partial observations (ingress or egress only) is much larger than calculated because of our two-step method of optimizing the system parameters and then fitting for the transit time. Often the best-fitting system parameters were much different for partial transits as for full transits, and fixing these parameters at slightly incorrect values could affect the transit time significantly for partial transits. However, since for a given set of parameters the transit time should converge quite well in a Markov Chain, this extra error is not represented in the calculated parameter distribution. For clean, full transits without much correlated noise, we believe that the uncertainties in the transit times are accurate. However, our stated uncertainties for light curves with asymmetries or correlated noise are likely quite under-estimated.

The next step to be taken with these results would be to work out the correct transit time uncertainties, correcting for some of the under-estimated error in poor-quality light curves. With more accurate error bars in hand, an analysis could be done on each system to determine whether the data is consistent with a constant period. If any inconsistencies are found, the potential for an unobserved companion planet could be explored, and perhaps an upper limit on the mass of such a planet could be determined.

Appendix A

Tables

Table A.1: List of Observations

Target	Date	Dur(h)	Telescope	Filter	$t_{\exp}$(s)	z	Segment	Weather
CoRoT-2	09-06-08	2.3	FLWO	i	60	1.1-1.3	ingress	clear
GJ436	05-22-07	3.6	FLWO	z	10	1.0-1.8	full	haze
GJ436	05-30-07	2.5	FLWO	z	10	1.0-1.3	full	haze
GJ436	12-14-07	2.2	FLWO	z	10	1.0-1.2	full	clear
GJ436	12-30-07	2.2	FLWO	z	10	1.2-2.2	full	clear
GJ436	01-02-08	3.4	Wise	R	15-17	1.0-1.7	full	
GJ436	01-20-08	2.7	FLWO	r	20	1.0-1.2	full	haze
GJ436	02-05-08	2.0	FLWO	r	20	1.0-1.2	full	haze
GJ436	02-13-08	2.6	FLWO	r	20	1.0-1.3	full	haze
GJ436	03-05-08	2.7	FLWO	r	20	1.0-1.5	full	clear
GJ436	03-13-08	2.7	FLWO	r	20	1.0-1.2	full	clouds
GJ436	03-16-08	3.5	Wise	R	10-30	1.0-1.8	full	
GJ436	03-21-08	1.6	FLWO	r	20	1.0	full	clear
GJ436	03-24-08	2.6	Wise	R	9-18	1.0-1.4	full	
GJ436	03-29-08	2.9	FLWO	r	20	1.0-1.1	full	clear
GJ436	04-01-08	3.0	Wise	R	20-28	1.0-1.1	full	
GJ436	04-06-08	1.9	Wise	r	20	1.0-1.2	full	clear

Target	Date	Dur(h)	Telescope	Filter	t_{exp}(s)	z	Segment	Weather
GJ436	05-05-08	2.5	FLWO	r	20	1.0-1.3	full	clouds
GJ436	05-13-08	2.4	FLWO	r	20	1.0-1.1	full	clear
GJ436	06-19-08	2.0	FLWO	r	15	1.2-1.8	full	clouds
HAT-P-1	09-18-06	5.2	FLWO	z	15	1.1-1.3	full	
HAT-P-1	10-07-07	5.0	FLWO	z	15	1.1-1.7	full	
HAT-P-1	10-16-07	5.5	FLWO	z	15	1.1-1.5	full	haze
HAT-P-1	10-25-07	4.3	FLWO	z	15	1.1	full	
HAT-P-1	12-31-07	2.6	FLWO	z	15	1.1-1.7	ingress	
TrES-1	04-13-07	4.6	FLWO	z	30	1.0-2.2	full	clouds
TrES-2	09-10-06	4.6	FLWO	z	30	1.1-1.7	full	clouds
TrES-2	09-15-06	3.1	FLWO	z	30	1.1-1.3	full	clear
TrES-2	11-01-06	3.5	FLWO	z	30	1.1-2.0	full	clouds
TrES-2	03-24-07	3.5	FLWO	z	30	1.2-2.2	full	clouds
TrES-2	05-10-07	3.6	FLWO	z	30	1.1-1.4	full	haze
TrES-2	07-26-07	4.1	Wise	R	30-55	1.1-1.7	full	
TrES-2	07-31-07	3.3	Wise	R	20-30	1.1-1.3	full	
TrES-2	10-03-07	2.6	FLWO	z	30	1.1-1.4	ingress	clouds
TrES-2	11-07-07	2.9	Wise	R	120	1.2-2.3	egress	clouds
TrES-2	05-20-08	3.7	Wise	R	50-60	1.1-1.8	full	
TrES-2	05-27-08	3.8	FLWO	i	30	1.1-1.5	full	clear
TrES-2	06-01-08	3.3	FLWO	i	30	1.1-1.8	full	clouds
TrES-2	06-26-08	4.1	Wise	R	45-55	1.1-1.2	full	
TrES-2	07-01-08	3.5	Wise	R	40-55	1.1-1.2	full	
TrES-4	06-10-08	3.3	FLWO	i	60	1.0-1.4	ingress	clear
WASP-2	06-01-08	2.4	FLWO	z	30	1.1-1.3	ingress	clouds
WASP-3	05-14-08	3.8	FLWO	i	20	1.0-1.3	full	clouds
WASP-3	06-09-08	4.4	FLWO	i	20	1.0-2.2	full	clear
WASP-3	06-20-08	5.6	FLWO	i	20	1.2-1.3	full	clear
WASP-3	07-27-08	3.3	FLWO	i	30	2.1	full	clouds

Target	Date	Dur(h)	Telescope	Filter	$t_{\rm exp}$(s)	z	Segment	Weather
XO-1	02-11-07	4.2	FLWO	z	30	1.0-2.1	full	
XO-1	06-10-08	3.2	FLWO	i	30	1.1	egress	
XO-2	12-31-07	5.1	FLWO	z	30	1.1-1.3	full	clear
XO-2	01-13-08	2.6	FLWO	z	45	1.1-1.3	ingress	clear
XO-2	02-11-08	5.0	FLWO	z	25	1.2	full	haze
XO-3	10-24-07	5.0	FLWO	z	15	1.1-1.6	full	haze
XO-3	12-14-07	5.8	FLWO	z	15	1.1-1.6	full	clear
XO-3	01-12-08	3.3	FLWO	z	10	1.1-1.3	egress	clouds
XO-3	01-15-08	6.0	FLWO	z	10	1.1-2.1	full	clouds
XO-3	01-31-08	5.2	FLWO	z	10	1.1-2.1	ingress	clouds
XO-3	02-16-08	4.7	FLWO	z	10	1.1-1.9	full	haze

[a] Dates are in PST at the start of the observation night. Dur gives the duration of the observation and z gives the airmass range over the course of this observation. The filters are Sloan r, i, and z filters and the Bessel R filter. Approximate weather is given based on sky camera feed from Mt. Hopkins, AZ where the FLWO is located.
[b] A number of observations produced poor light curves. The GJ436 observation on 2008-06-19, the TrES-4 observation, and the WASP-3 observation on 2008-07-14 were not used because poor weather affected the data. The GJ436 observations on 2008-03-05, 2008-03-16 and 2008-04-09 were of poor quality for unknown reason, but the 2008-04-09 observation was not used. The GJ436 observation on 2008-05-05 experienced poor weather problems, but the data was still used.

Table A.2: Aperture Photometry Statistics

Target	Date	FWHM (pix)	Aperture (pix)	rms_{pre}	rms_{obs}
CoRoT-2	09-06-08	2.6	7	0.00084	0.00078
GJ436	05-22-07	4.6	13	0.00092	0.0016
GJ436	05-30-07	3.7	16	0.00084	0.0017
GJ436	12-14-07	6.9	11	0.00079	0.0017
GJ436	12-30-07	4.5	17	0.0013	0.0019
GJ436	01-02-08	4.2	13	0.0009	0.0017
GJ436	01-20-08	4.1	17	0.00063	0.00093
GJ436	02-05-08	3.7	15	0.00066	0.00083
GJ436	02-13-08	5.5	18	0.00067	0.0013
GJ436	03-05-08	6.7	17	0.00073	0.0017
GJ436	03-13-08	4.0	17	0.00065	0.00094
GJ436	03-16-08	3.1	11	0.00010	0.00020
GJ436	03-21-08	3.8	15	0.00063	0.00086
GJ436	03-24-08	3.4	12	0.00010	0.00018
GJ436	03-29-08	3.8	14	0.00064	0.00089
GJ436	04-01-08	4.6	12	0.00057	0.0015
GJ436	04-06-08	4.0	16	0.00069	0.0010
GJ436	05-05-08	3.8	16	0.00066	0.0016
GJ436	05-13-08	3.5	11	0.00065	0.0013
GJ436	06-19-08	4.4	16	0.0010	0.0018
HAT-P-1	09-18-06	-	6	0.00098	0.0011
HAT-P-1	10-07-07	2.6	6	0.0011	0.0015
HAT-P-1	10-16-07	2.6	6	0.0010	0.0022
HAT-P-1	10-25-07	2.4	8	0.00099	0.0013
HAT-P-1	12-31-07	3.6	6	0.0011	0.0011
TrES-1	04-13-07	2.2	11	0.0025	0.0012
TrES-2	09-10-06	3.3	7	0.0011	0.0014

Target	Date	FWHM (pix)	Aperture (pix)	rms_{pre}	rms_{obs}
TrES-2	09-15-06	3.2	6	0.0011	0.0012
TrES-2	11-01-06	2.9	8	0.0011	0.0012
TrES-2	03-24-07	2.96	8	0.0011	0.0020
TrES-2	05-10-07	4	10	0.0011	0.0014
TrES-2	07-26-07	3.4	15	0.00062	0.0013
TrES-2	07-31-07	2.6	7	0.00086	0.0020
TrES-2	10-03-07	2.2	7	0.0012	0.0017
TrES-2	11-07-07	4.5	14	0.00044	0.00052
TrES-2	05-20-08	2.2	12	0.00067	0.0022
TrES-2	05-27-08	2.5	10	0.00085	0.0013
TrES-2	06-01-08	3	12	0.00089	0.0015
TrES-2	06-26-08	3.5	9	0.00061	0.0014
TrES-2	07-01-08	4.0	12	0.00050	0.0011
TrES-4	06-10-08	3.0	12	0.00063	0.0012
WASP-2	06-01-08	2.5	5	0.0012	0.0012
WASP-3	05-14-08	2.4	8	0.00077	0.0011
WASP-3	06-09-08	2.6	13	0.00088	0.0016
WASP-3	06-20-08	2.5	11	0.00079	0.0015
WASP-3	07-27-08	3.14	8	0.00082	0.0027
XO-1	02-11-07	3.7	8	0.0010	0.0012
XO-1	06-10-08	3.2	8	0.00074	0.0016
XO-2	12-31-07	3.5	10	0.00089	0.0012
XO-2	01-13-08	2.5	11	0.00073	0.0012
XO-2	02-11-08	2.1	10	0.00097	0.0015
XO-3	10-24-07	3.5	11	0.00098	0.0025
XO-3	12-14-07	5	20	0.00094	0.0019
XO-3	01-12-08	3.0	12	0.0012	0.0019
XO-3	01-15-08	3.2	10	0.0012	0.0020
XO-3	01-31-08	4.0	12	0.0013	0.0018

Target	Date	FWHM (pix)	Aperture (pix)	rms_{pre}	rms_{obs}
XO-3	02-16-08	3.5	16	0.0012	0.0025

[a] The FWHM given is an average full width at half maximum of the target star over the observation, and the aperture listed is the aperture used in the photometry. rms_{pre} is the calculated predicted noise from scintillation and photon noise, and rms_{obs} is the rms in the out-of-transit flux for the observation.

Table A.3: Stellar Parameters and Calculated Limb Darkening Coefficients from Claret 2000

System	$T_{\rm eff}$(K)	log(g) cm/s^2	[M/H]	$v_{\rm micro}$(km/s)	filter	u_1	u_2
CoRoT-2	5625	4.52	0.0	2	i	0.33	0.29
GJ436	3684	4.77	-0.3	2	z	0.10	0.56
					r	0.57	0.23
					R	0.33	0.41
HAT-P-1	5975	4.40	0.1	2	z	0.24	0.31
HD17156	6079	4.21	0.2	2	z	0.23	0.31
TrES-1	5250	4.55	0.0	2	z	0.29	0.30
TrES-2	5850	4.44	-0.1	2	z	0.20	0.33
					i	0.25	0.33
					R	0.31	0.34
WASP-2	5200	4.53	0.0	2	z	0.29	0.29
					i	0.38	0.27
WASP-3	6400	4.30	0.0	2	i	0.27	0.31
XO-1	5750	4.50	0.0	2	z	0.25	0.30
					i	0.32	0.29
XO-2	5340	4.47	0.4	2	z	0.28	0.30
XO-3	6429	4.24	-0.2	2	z	0.22	0.30

Table A.4: Transit Center Times

System	Date	T_c	χ^2	DOF	χ^2/DOF	Epoch	Comment
CoRoT-2	2008-06-09	2454627.96486 ± 0.00041	563	114	4.94	0	1
GJ436	2007-05-22	2454243.76666 ± 0.00026	590	537	1.10	-101	1
	2007-05-30	2454251.69968 ± 0.00031	318	365	0.87	-98	1
	2007-12-14	2454449.99197 ± 0.00028	412	340	0.74	-23	1
	2007-12-30	2454465.85403 ± 0.00026	353	315	1.12	-17	1
	2008-01-02	2454468.49922 ± 0.00035	238	250	0.95	-16	0
	2008-01-20	2454487.00572 ± 0.00021	278	287	0.97	-9	1
	2008-02-05	2454502.86872 ± 0.00018	244	218	1.12	-3	1
	2008-02-13	2454510.80073 ± 0.00026	287	281	1.02	0	1
	2008-03-05	2454531.95258 ± 0.00028	278	288	0.96	8	0
	2008-03-13	2454539.88276 ± 0.00021	434	287	1.51	11	1
	2008-03-16	2454542.53752 ± 0.00031	381	298	1.28	12	0
	2008-03-21	2454547.81534 ± 0.00018	197	170	1.16	14	1
	2008-03-24	2454550.45670 ± 0.00023	274	241	1.14	15	0
	2008-03-29	2454555.74686 ± 0.00018	288	302	0.95	17	1
	2008-04-01	2454558.29197 ± 0.00033	205	186	1.10	18	1
	2008-04-06	2454563.67888 ± 0.00021	174	206	0.85	20	1
	2008-05-05	2454592.76067 ± 0.00025	396	252	1.57	31	0
	2008-05-13	2454600.69217 ± 0.00025	261	257	1.02	34	0
HAT-P-1	2006-09-18	2453997.79151 ± 0.00022	670	665	1.01	-88	1
	2006-09-27	2454006.71766 ± 0.00031	722	655	1.10	-86	0
	2007-10-07	2454381.80845 ± 0.00029	523	606	0.91	-2	1
	2007-10-16	2454390.73863 ± 0.00031	596	632	0.94	0	1
	2007-10-25	2454399.66916 ± 0.00022	569	522	1.09	2	1
	2007-12-31	2454466.64817 ± 0.00040	507	238	1.55	17	0
HD17156	2007-12-24	2454459.70211 ± 0.00045	617	749	0.82	0	1
TrES-1	04-13-2007	2454204.91034 ± 0.00036	269	374	0.72	0	1

System	Date	T_c	χ^2	DOF	χ^2/DOF	Epoch	Comment
	05-17-2008	2454604.8811 ± 0.00032	142	128	1.11	132	1
TrES-2	09-10-2006	2453989.7526 ± 0.00024	413	400	1.03	-131	1
	09-15-2006	2453994.6938 ± 0.00023	293	265	1.10	-129	1
	11-01-2006	2454041.6360 ± 0.00024	326	300	1.09	-110	1
	03-24-2007	2454184.9299 ± 0.00027	408	270	1.51	-52	0
	05-10-2007	2454231.8714 ± 0.00024	288	291	0.99	-33	1
	07-26-2007	2454308.4604 ± 0.00025	220	188	1.17	-2	1
	07-31-2007	2454313.4032 ± 0.00027	202	223	0.91	0	1
	10-03-2007	2454377.6386 ± 0.00027	181	157	1.16	26	0
	11-07-2007	2454412.2252 ± 0.00029	180	53	3.40	40	0
	05-20-2008	2454607.4049 ± 0.00037	91	112	0.81	119	0
	05-27-2008	2454614.8170 ± 0.00024	295	310	0.95	122	1
	06-01-2008	2454619.7600 ± 0.00028	183	204	0.90	124	1
	06-26-2008	2454644.4654 ± 0.00026	156	186	0.84	134	1
	07-01-2008	2454649.4059 ± 0.00024	102	138	0.74	136	1
WASP-2	2008-06-01	2454619.96275 ± 0.00038	213	173	1.23	0	1
	2008-10-30	2454770.61757 ± 0.00033	219	115	1.91	70	1
WASP-3	2008-05-14	2454601.8649 ± 0.00029	606	403	1.50	-14	1
	2008-06-09	2454627.7198 ± 0.00034	600	469	1.28	0	1
	2008-06-20	2454638.8028 ± 0.00022	558	591	0.96	6	1
	2008-07-27	2454675.7413 ± 0.00031	132	196	0.67	26	0
XO-1	2007-02-11	2454143.94454 ± 0.00020	601	350	1.72	0	1
	2008-06-10	2454628.74996 ± 0.00020	143	263	0.55	123	1
XO-2	2007-12-31	2454466.88488 ± 0.00023	410	422	0.97	-5	1
	2008-01-13	2454479.96485 ± 0.00033	147	164	0.90	0	1
	2008-02-11	2454508.73847 ± 0.00023	558	455	1.23	11	1
XO-3	2007-10-24	2454398.80370 ± 0.00032	692	625	1.11	-16	1
	2007-12-14	2454449.86779 ± 0.00028	775	716	1.08	0	1
	2008-01-12	2454478.59831 ± 0.00041	383	493	0.78	9	0

System	Date	T_c	χ^2	DOF	χ^2/DOF	Epoch	Comment
	2008-01-15	2454481.78076 ± 0.00031	867	806	1.08	10	1
	2008-01-31	2454497.73964 ± 0.00037	729	365	2.00	15	0
	2008-02-16	2454513.69605 ± 0.00032	670	783	0.86	20	1

[a] Under comment header, (1) indicates that this observation was used in the fitting for the ephemeris, (0) indicates that it was not, usually due to obvious correlated noise.

[b] χ^2 value is calculated according to Equation 4.1, and DOF is the number of degrees of freedom, in this case approximately the number of data points.

[c] Transit time errors listed here are as given by the Markov Chain parameter distributions, without any subsequent rescaling

Table A.5: Transit Center Times from Literature

System	Source	T_c
CoRoT-2	Alonso et al. 2008	2454237.53562 ± 0.00014
	Veres et al. 2008	2454706.4041 ± 0.0030
HAT-P-1	Winn et al. 2007	2453979.92994 ± 0.00069
	Bakos et al. 2007	2453984.39700 ± 0.00900
	Winn et al. 2007	2453988.86197 ± 0.00076
	Winn et al. 2007	2453997.79200 ± 0.00054
	Winn et al. 2007	2453997.79348 ± 0.00047
	Winn et al. 2007	2454006.72326 ± 0.00059
	Winn et al. 2007	2454015.65338 ± 0.00107
	Winn et al. 2007	2454069.23795 ± 0.00290
	Johnson et al. 2008	2454363.94601 ± 0.00091
	Johnson et al. 2008	2454381.80849 ± 0.00125
HD17156	Barbieri et al., 2007	2454353.61 ± 0.02
	Narita et al. 2008	2454417.2645 ± 0.0021
TrES-1	M. Vanko et al. 2009	2454174.60958 ± 0.00150
	Charbonneau et al. 2005	2452847.4363 ± 0.0015
	Charbonneau et al. 2005	2452850.4709 ± 0.0016
	Charbonneau et al. 2005	2452856.5286 ± 0.0015
	Charbonneau et al. 2005	2452868.6503 ± 0.0022
	Charbonneau et al. 2005	2453171.6523 ± 0.0019
	Charbonneau et al. 2005	2453174.6864 ± 0.0004
	Charbonneau et al. 2005	2453183.7752 ± 0.0005
	Charbonneau et al. 2005	2453186.8061 ± 0.0003
	Charbonneau et al. 2005	2453189.8354 ± 0.0019
	Charbonneau et al. 2005	2453192.8694 ± 0.0015
	Charbonneau et al. 2005	2453247.4075 ± 0.0004
	Winn et al. 2007b	2453895.84297 ± 0.00018

System	Source	T_c
	Winn et al. 2007b	2453898.87341 ± 0.00014
	Winn et al. 2007b	2453901.90372 ± 0.00019
	Hrudkova et al. 2008	2454356.41417 ± 0.00010
	Hrudkova et al. 2008	2454359.44431 ± 0.00015
	Hrudkova et al. 2008	2454362.47424 ± 0.00020
WASP-3	Gibson et al. 2008	2454605.55956 ± 0.00035
	Gibson et al. 2008	2454714.52210 ± 0.00036
XO-1	Wilson et al. 2006	2453127.0385 ± 0.0058
	Wilson et al. 2006	2453142.7818 ± 0.0218
	Wilson et al. 2006	2453150.6855 ± 0.0106
	Wilson et al. 2006	2453154.6250 ± 0.0026
	Wilson et al. 2006	2453158.5663 ± 0.0034
	Wilson et al. 2006	2453162.5137 ± 0.0025
	Wilson et al. 2006	2453166.4505 ± 0.0025
	Wilson et al. 2006	2453170.3917 ± 0.0037
	Wilson et al. 2006	2453229.5143 ± 0.0045
	Wilson et al. 2006	2453237.4043 ± 0.0032
	Wilson et al. 2006	2453241.3410 ± 0.0067
	Holman et al. 2006	2453875.92305 ± 0.00036
	Holman et al. 2006	2453879.8640 ± 0.0011
	Holman et al. 2006	2453883.80565 ± 0.00019
	Holman et al. 2006	2453887.74679 ± 0.00016
	M. Vanko et al. 2009	2454171.53188 ± 0.00130
XO-2	Fernandez et al. 2009	2454466.88512 ± 0.00021
	Fernandez et al. 2009	2454479.96393 ± 0.00039
	Fernandez et al. 2009	2454508.73864 ± 0.00026
	Fernandez et al. 2009	2454521.81778 ± 0.00072
	Fernandez et al. 2009	2454529.66433 ± 0.00043
	Fernandez et al. 2009	2454532.27978 ± 0.00074

System	Source	T_c
XO-3	Winn et al. 2008	2454360.50866 ± 0.00173
	Winn et al. 2008	2454382.84500 ± 0.00265
	Winn et al. 2008	2454382.84523 ± 0.00112
	Winn et al. 2008	2454392.41999 ± 0.00130
	Winn et al. 2008	2454395.61179 ± 0.00167
	Winn et al. 2008	2454398.80332 ± 0.00066
	Winn et al. 2008	2454411.56904 ± 0.00161
	Winn et al. 2008	2454449.86742 ± 0.00067
	Winn et al. 2008	2454465.82610 ± 0.00038
	Winn et al. 2008	2454478.59308 ± 0.00119
	Winn et al. 2008	2454481.78455 ± 0.00070
	Winn et al. 2008	2454507.31319 ± 0.00118
	Winn et al. 2008	2454513.69768 ± 0.00090

Table A.6: Ephemerides for transiting planet systems

System	Source	HJD_0	P	χ^2	n_{obs}	χ^2/DOF
CoRoT-2	This Thesis(2)	2454627.96496 ± 0.000040	1.7429882 ± 0.0000019			
	Alonso et al., 2008	2454237.53562 ± 0.000014	1.7429964 ± 0.0000017			
GJ436	This Thesis(1)	2454510.80069 ± 0.00015	2.643896 ± 0.000004	54	12	5.4
	Shporer et al., 2009	2454235.8355 ± 0.0001	2.64386 ± 0.00003			
HAT-P-1	This Thesis(1)	2454390.73871 ± 0.00016	4.4653094 ± 0.0000037	2.2	4	1.1
	This Thesis(2)	2454390.73870 ± 0.00016	4.4653036 ± 0.0000026	20.6	14	1.7
	Winn et al., 2007	2453997.79258 ± 0.00029	4.46543 ± 0.00014			
HD17156	This Thesis(2)	2454459.70211 ± 0.00045	21.2188 ± 0.0010			
	Winn et al., 2009	2454459.69987 ± 0.00045	21.2168 ± 0.00044			
TrES-1	This Thesis(1)	2454204.91020 ± 0.00037	3.0300823 ± 0.0000037		2	
	This Thesis(2)	2454204.910619 ± 0.000058	3.0300727 ± 0.0000005	34	20	1.9
	Winn et al., 2007b	2453186.80603 ± 0.00028	3.0300737 ± 0.0000013			
TrES-2	This Thesis(1)	2454313.402728 ± 0.00024	2.470613 ± 0.0000022	76	10	9.5
	Holman et al., 2007	2453957.63479 ± 0.00038	2.470621 ± 0.000017			
WASP-2	This Thesis(1)	2454619.96275 ± 0.00038	2.1522117 ± 0.0000072		2	
	Collier Cameron et al., 2007	2453991.5146 ± 0.0044	2.152226 ± 0.000004			
WASP-3	This Thesis(1)	2454627.72109 ± 0.00073	1.84689 ± 0.00008	21	3	21
	This Thesis(2)	2454627.72137 ± 0.00027	1.8468242 ± 0.0000083	1.8	5	0.6
	Gibson et al., 2008	2454605.55915 ± 0.00023	1.846835 ± 0.000002			
XO-1	This Thesis(1)	2454143.94454 ± 0.00020	3.9415075 ± 0.0000023		2	
	This Thesis(2)	2454143.94476 ± 0.000091	3.9415047 ± 0.0000012	21.3	18	1.3
	Wilson et al., 2006	2453150.6849 ± 0.0018	3.941634 ± 0.000137			
XO-2	This Thesis(1)	2454479.96429 ± 0.00032	2.615843 ± 0.000041	4.2	3	4.2
	This Thesis(2)	2454479.96425 ± 0.00014	2.615822 ± 0.000014	7.1	9	1.0
	Fernandez et al., 2009	2454466.88514 ± 0.00019	2.615819 ± 0.000014			
XO-3	This Thesis(1)	2454449.86703 ± 0.00041	3.1914418 ± 0.000031	13.1	4	6.6
	This Thesis(2)	2454449.86782 ± 0.00020	3.191500 ± 0.000016	30.8	17	1.8
	Winn et al., 2009	2454449.86816 ± 0.00023	3.1915239 ± 0.0000068			

[a] Thesis(1) ephemeris is based on only 'good' observations (see Table A.4), with transit timing errors scaled up so that χ^2 per degree of freedom is equal to one. The χ^2 values given in this ephemeris are *prior* to this rescaling.

[b] Thesis(2) ephemeris includes data from this thesis and published transit times tabulated in Table A.5. Published values were used whenever available, except with the systems GJ436 and TrES-2, since we already had a number of good data sets

Appendix B

Figures

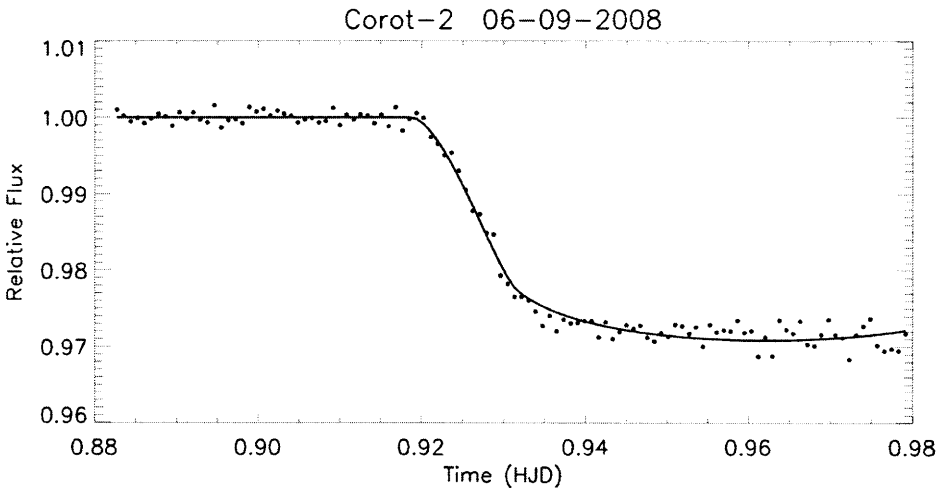

Figure B-1: CoRoT-2 observation (epoch 0) on FLWO 1.2m on 06-09-2008 with model fit. $T_c = 2454627.96486 \pm 0.00041$.

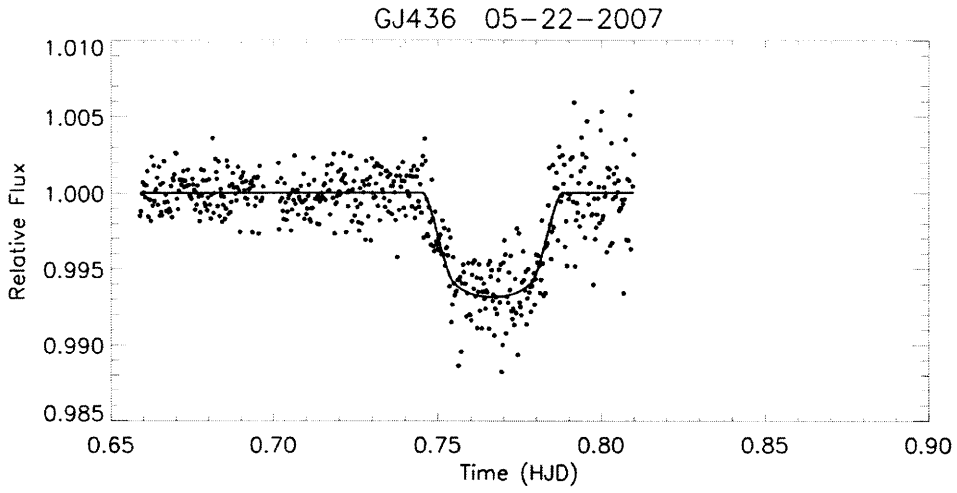

Figure B-2: GJ436 observation (epoch -101) on FLWO 1.2m on 05-22-2007 with model fit. $T_c = 2454243.76666 \pm 0.00026$.

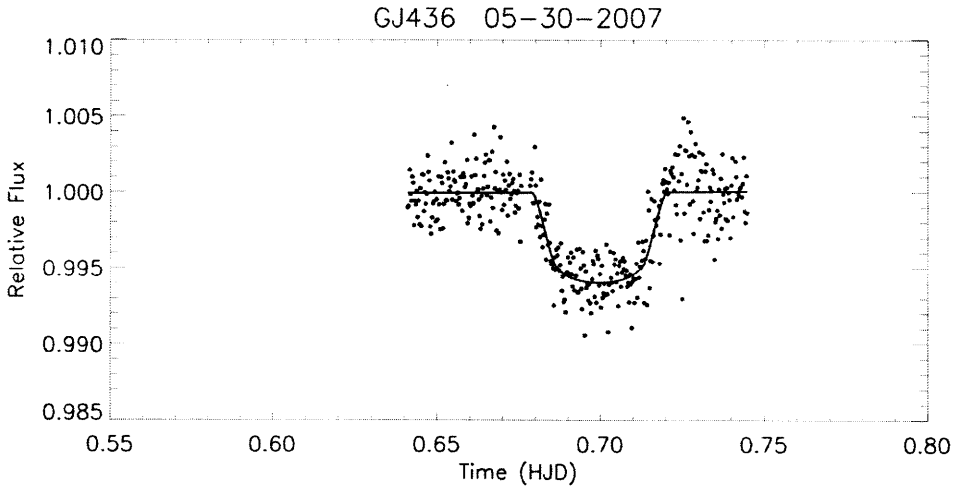

Figure B-3: GJ436 observation (epoch -98) on FLWO 1.2m on 05-30-2007 with model fit. $T_c = 2454251.69968 \pm 0.00031$.

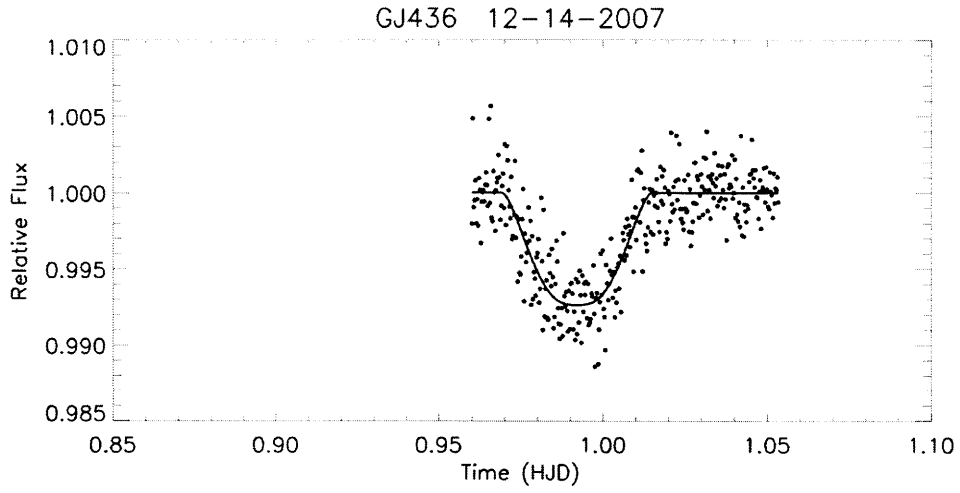

Figure B-4: GJ436 observation (epoch -23) on FLWO 1.2m on 12-14-2007 with model fit. $T_c = 2454449.99197 \pm 0.00028$.

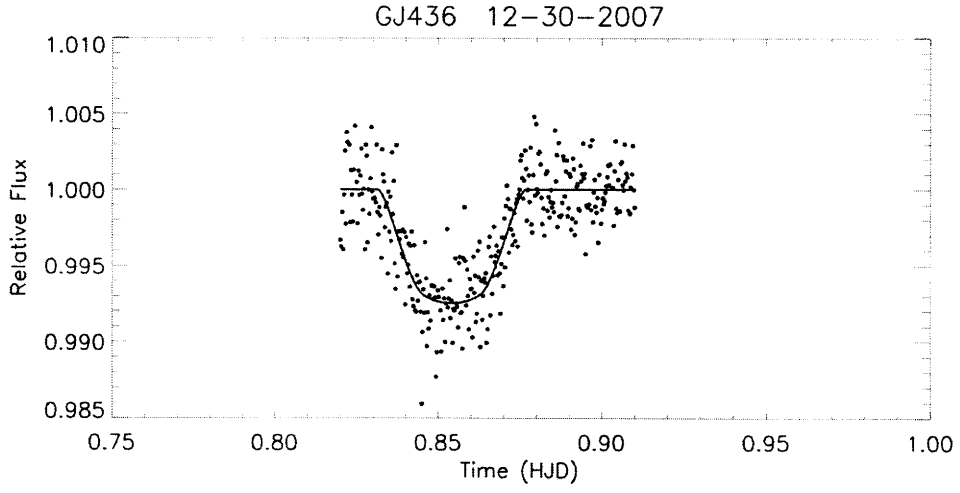

Figure B-5: GJ436 observation (epoch -17) on FLWO 1.2m on 12-30-2007 with model fit. $T_c = 2454465.85403 \pm 0.00026$.

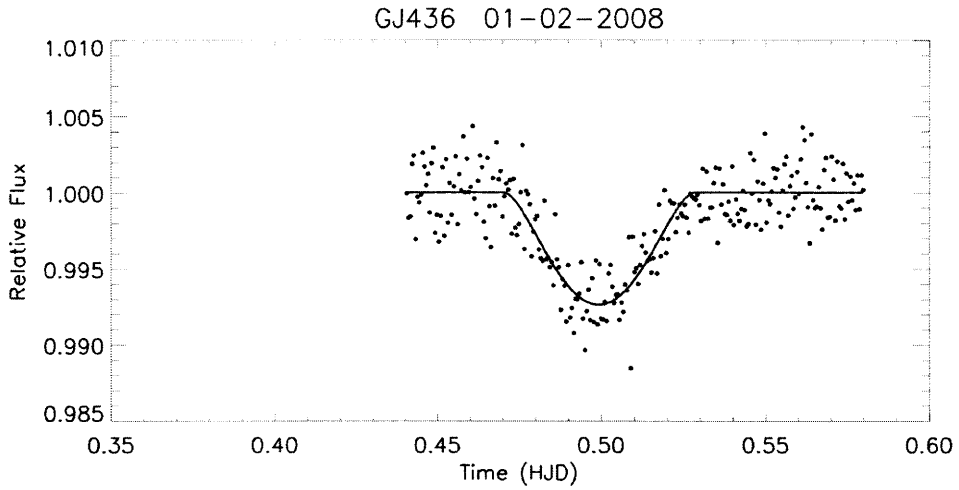

Figure B-6: GJ436 observation (epoch -16) on Wise 1m on 01-02-2008 with model fit. $T_c = 2454468.49922 \pm 0.00035$. Light curve appears to have correlated noise and was not used fitting for the ephemeris.

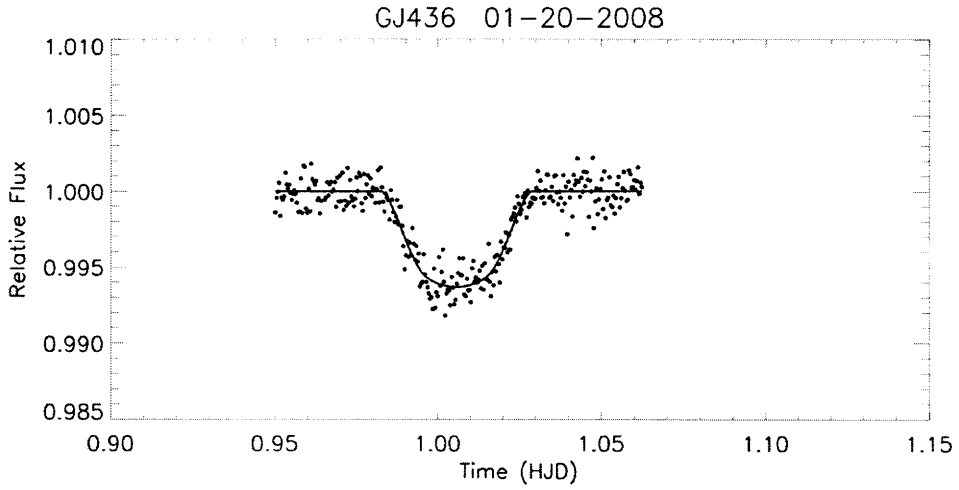

Figure B-7: GJ436 observation (epoch -9) on FLWO 1.2m on 01-20-2008 with model fit. $T_c = 2454487.00572 \pm 0.00021$.

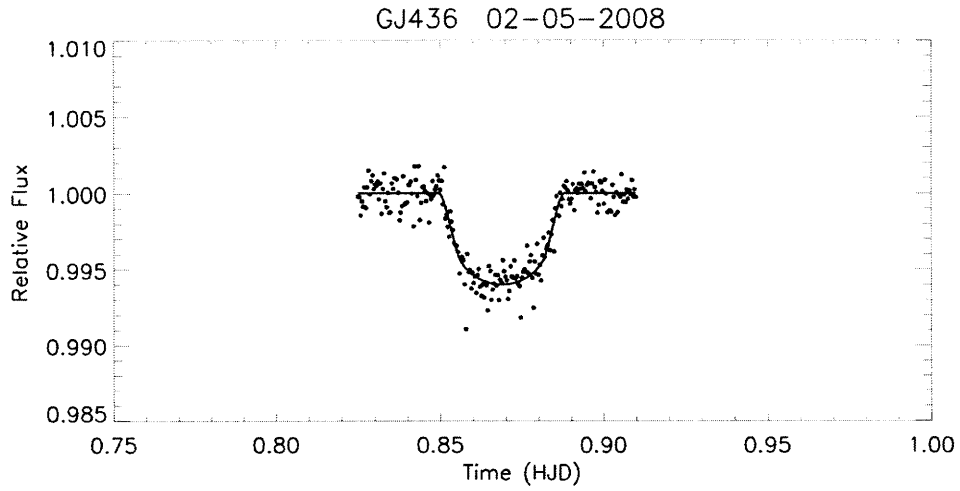

Figure B-8: GJ436 observation (epoch -3) on FLWO 1.2m on 02-05-2008 with model fit. $T_c = 2454502.86872 \pm 0.00018$.

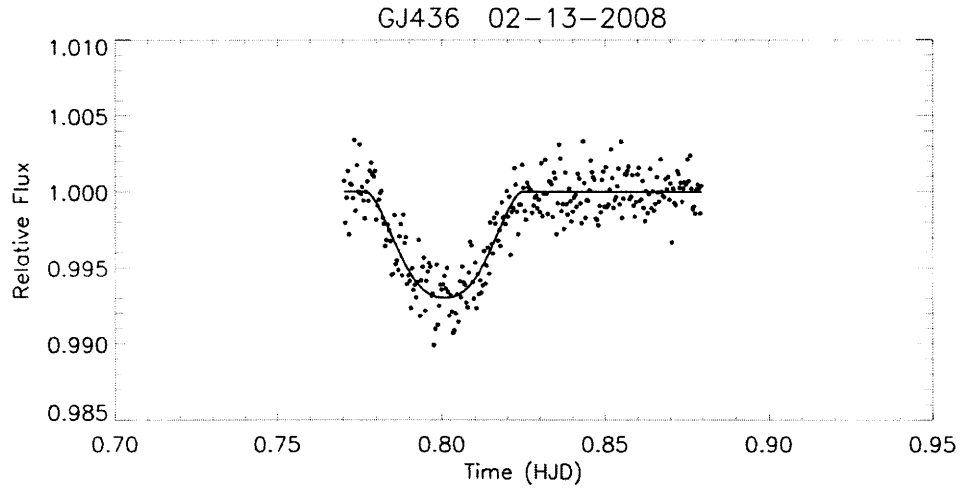

Figure B-9: GJ436 observation (epoch 0) on FLWO 1.2m on 02-13-2008 with model fit. $T_c = 2454510.80073 \pm 0.00026$.

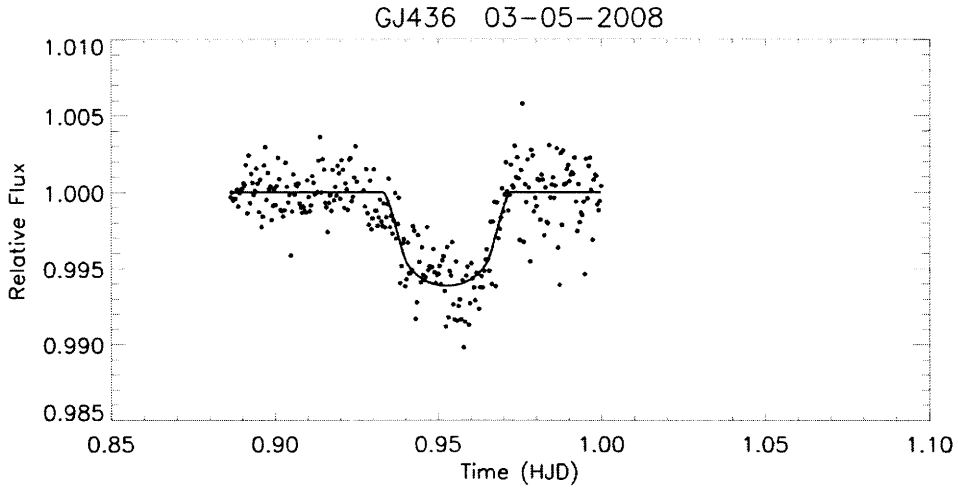

Figure B-10: GJ436 observation (epoch 8) on FLWO 1.2m on 03-05-2008 with model fit. $T_c = 2454531.95258 \pm 0.00028$. Light curve appears poor; the reason for this is unknown, but this data was not used in fitting for the ephemeris.

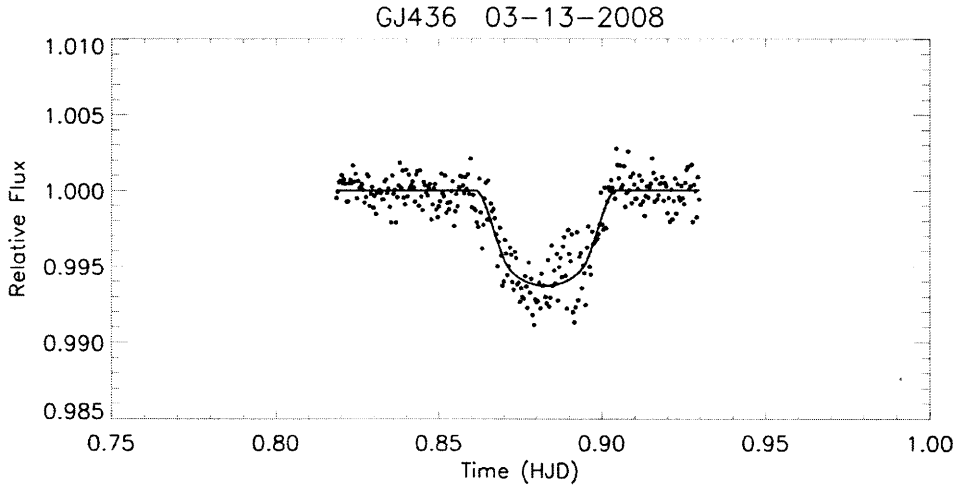

Figure B-11: GJ436 observation (epoch 11) on FLWO 1.2m on 03-13-2008 with model fit. $T_c = 2454539.88276 \pm 0.00021$.

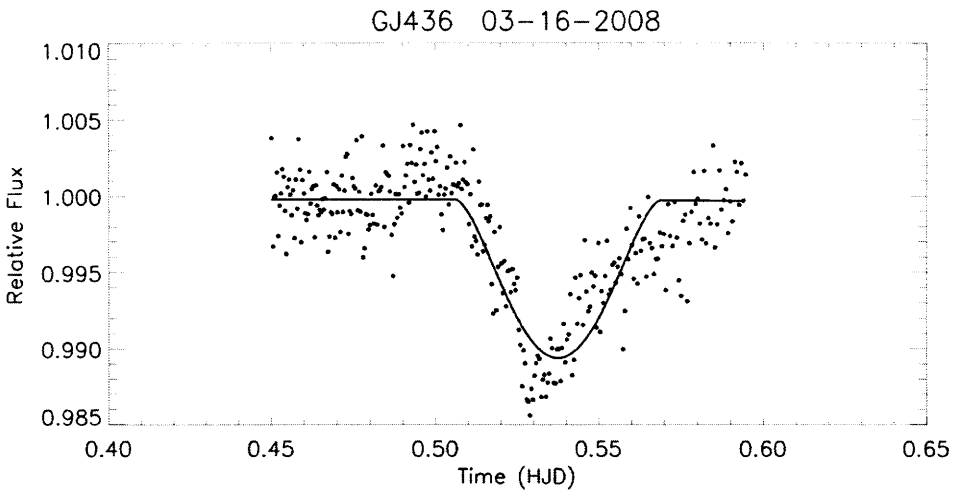

Figure B-12: GJ436 observation (epoch 12) on Wise 1m on 03-16-2008 with model fit. $T_c = 2454542.53752 \pm 0.00031$. Light curve looks very poor; the reason for this is unknown, but data was not used in fitting for the ephemeris.

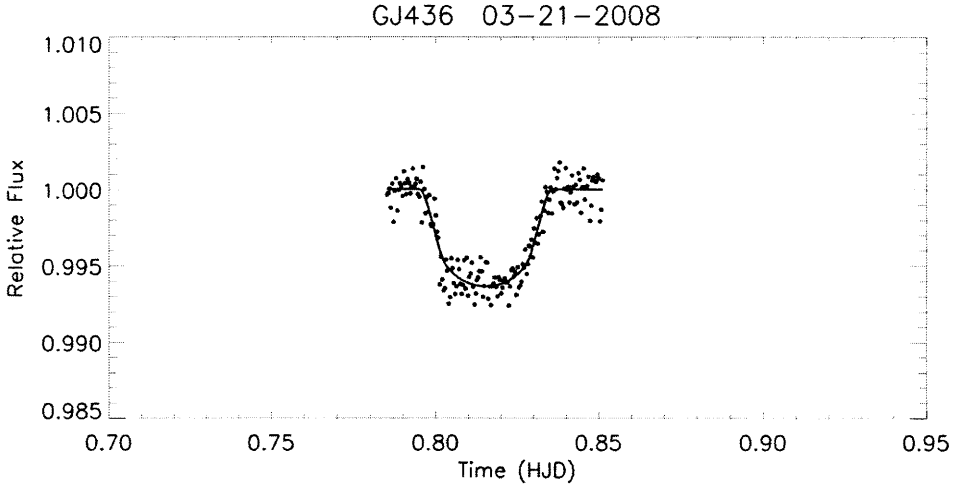

Figure B-13: GJ436 observation (epoch 14) on FLWO 1.2m on 03-21-2008 with model fit. $T_c = 2454547.81534 \pm 0.00018$.

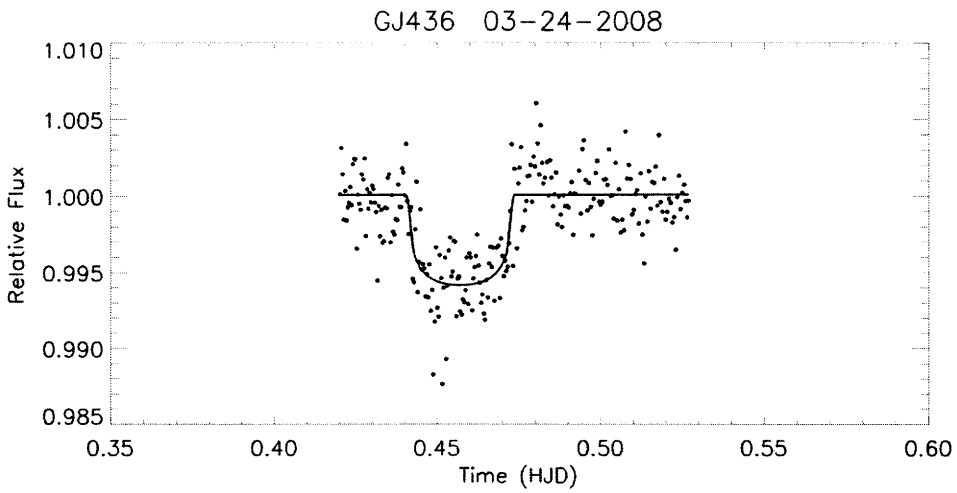

Figure B-14: GJ436 observation (epoch 15) on Wise 1m on 03-24-2008 with model fit. $T_c = 2454550.45670 \pm 0.00023$. Some correlated noise appears to be present, and the data was thus not used in fitting for the ephemeris.

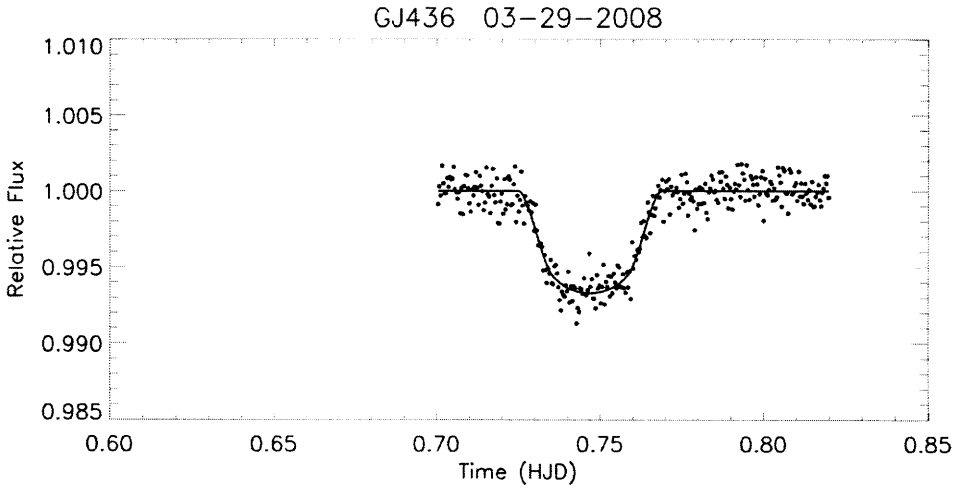

Figure B-15: GJ436 observation (epoch 17) on FLWO 1.2m on 03-29-2008 with model fit. $T_c = 2454555.74686 \pm 0.00018$.

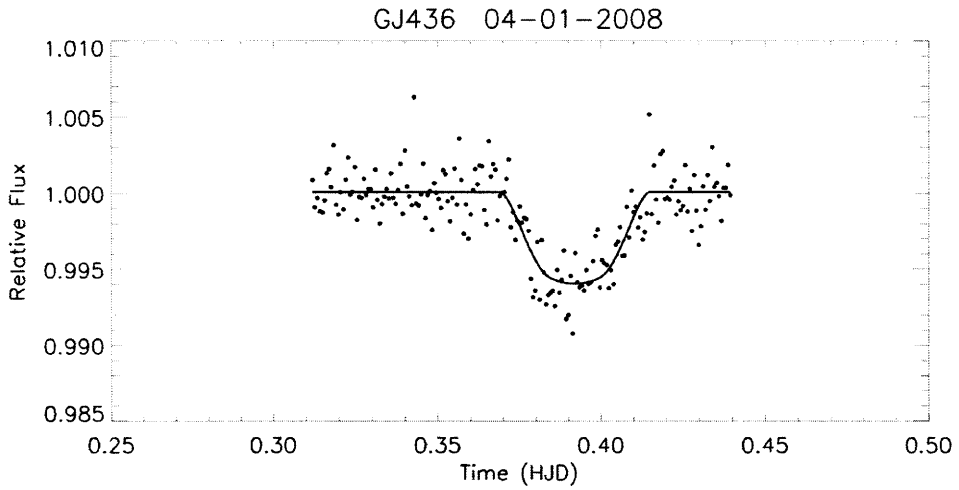

Figure B-16: GJ436 observation (epoch 18) on Wise 1m on 04-01-2008 with model fit. $T_c = 2454558.29197 \pm 0.00033$.

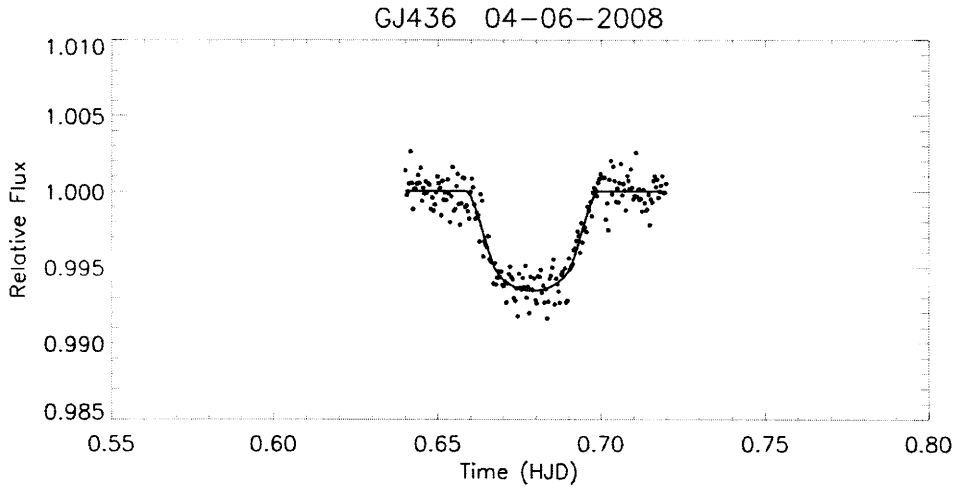

Figure B-17: GJ436 observation (epoch 20) on FLWO 1.2m on 04-06-2008 with model fit. $T_c = 2454563.67888 \pm 0.00021$.

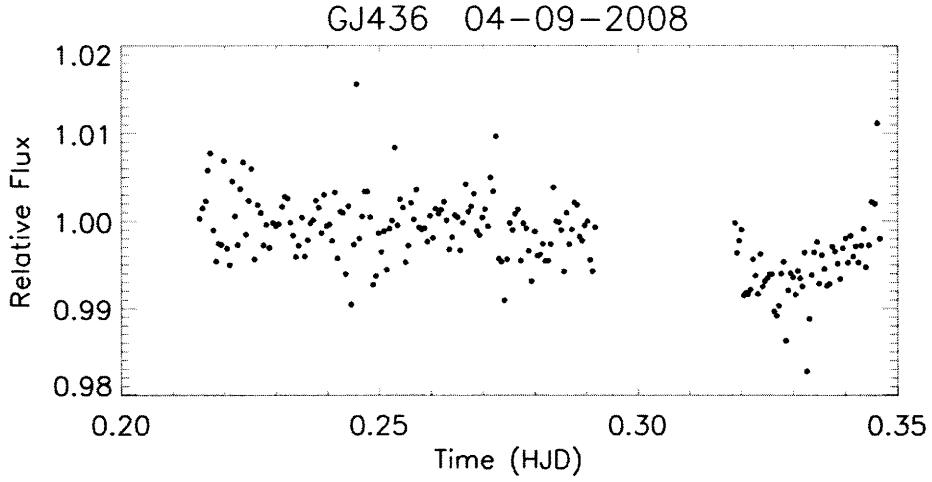

Figure B-18: GJ436 observation on FLWO 1.2m on 04-09-2008. Light curve is poor and was not fit or used for transit timing.

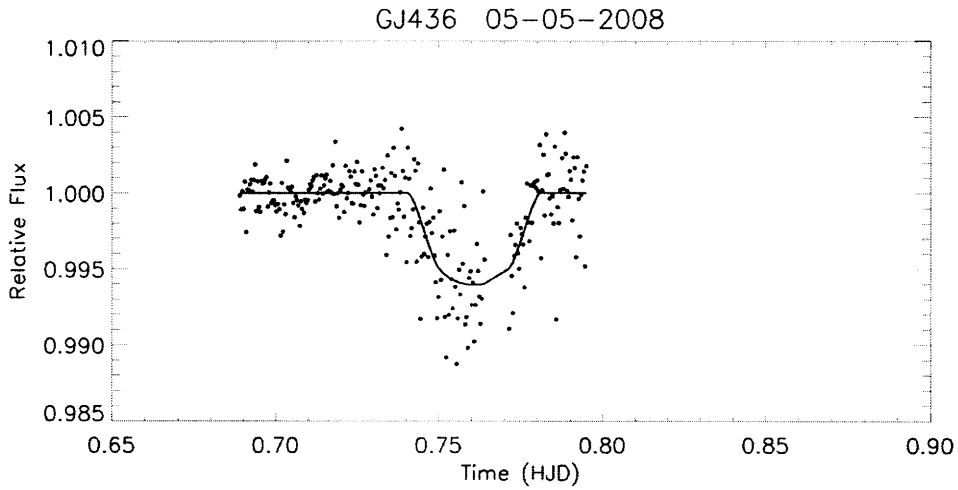

Figure B-19: GJ436 observation (epoch 31) on FLWO 1.2m on 05-05-2008 with model fit. $T_c = 2454592.76067 \pm 0.00025$. Light curve apperas very noisy, likely due to poor weather during observation. As a result, data was not used in fitting for the ephemeris.

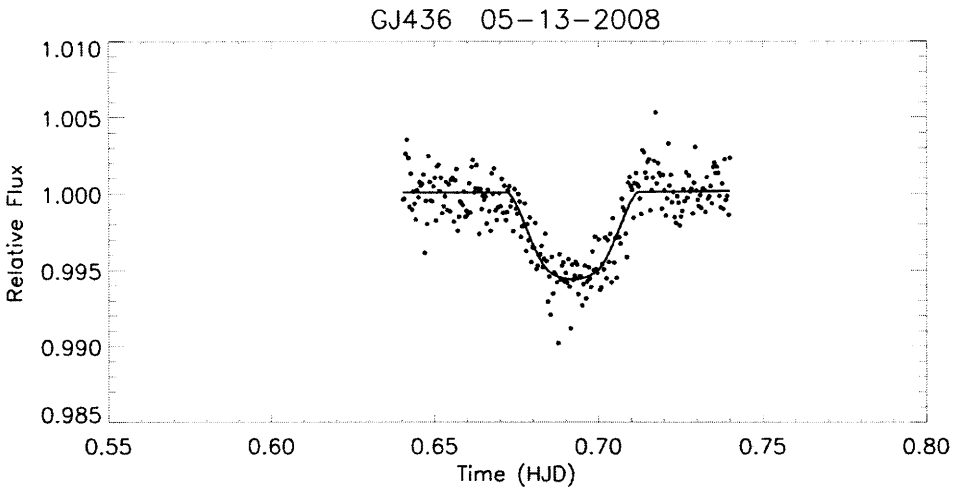

Figure B-20: GJ436 observation (epoch 34) on FLWO 1.2m on 05-13-2008 with model fit. $T_c = 454600.69217 \pm 0.00025$. Data exhibits asymmetries and was thus not used in fitting for the ephemeris.

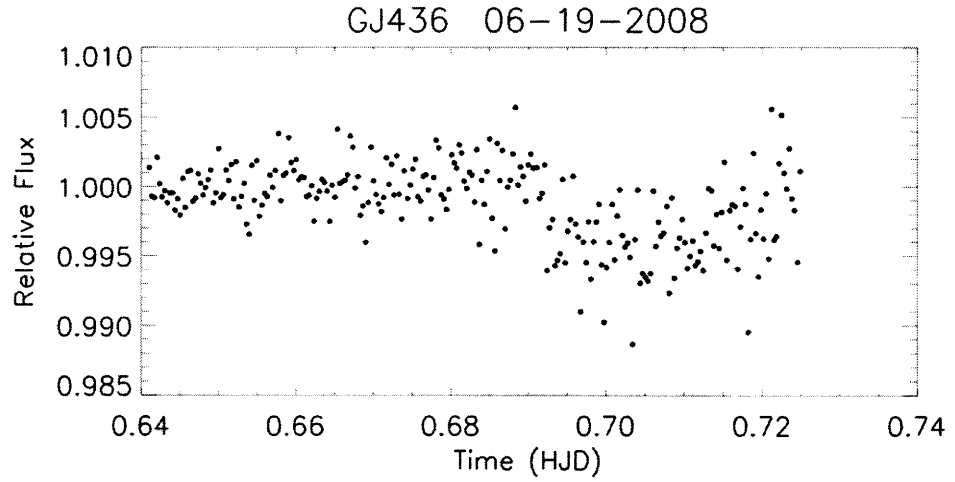

Figure B-21: GJ436 observation on FLWO 1.2m on 06-19-2008 with model fit. The weather was poor during this observation. Data is very noisy and was not fit or used for transit timing.

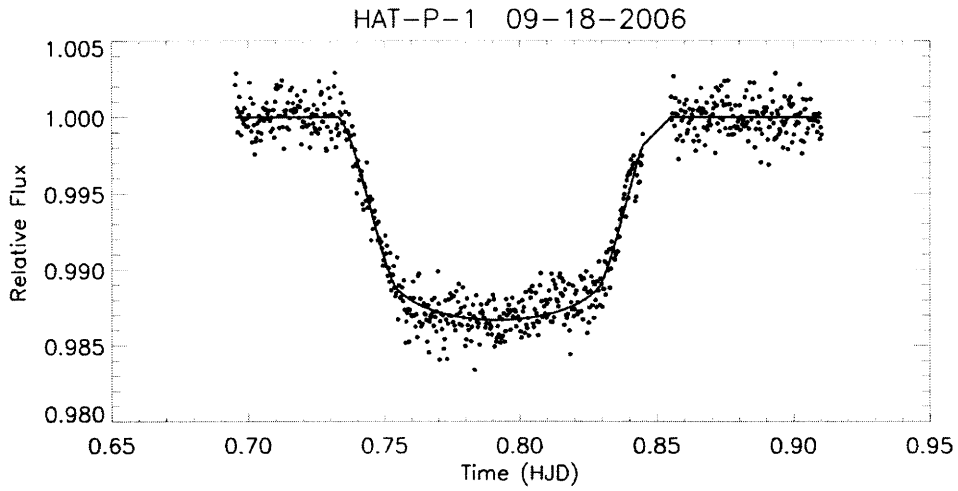

Figure B-22: HAT-P-1 observation (epoch -88) on FLWO 1.2m on 09-18-2006 with model fit. $T_c = 2453997.79151 \pm 0.00022$.

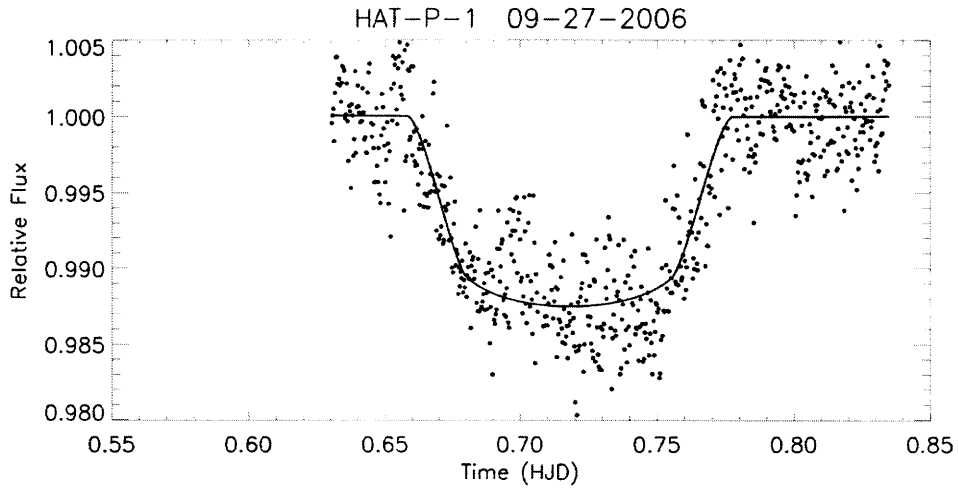

Figure B-23: HAT-P-1 observation (epoch -86) on FLWO 1.2m on 09-27-2006 with model fit. $T_c = 2454006.71766 \pm 0.00031$. Data appears to have correlated noise, and was thus not used in fitting for the ephemeris.

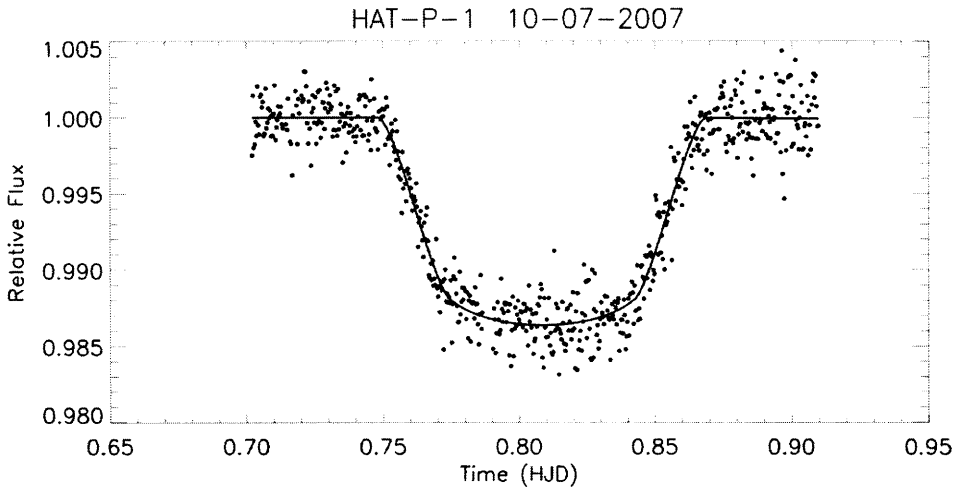

Figure B-24: HAT-P-1 observation (epoch -2) on FLWO 1.2m on 10-07-2007 with model fit. $T_c = 2454381.80845 \pm 0.00029$.

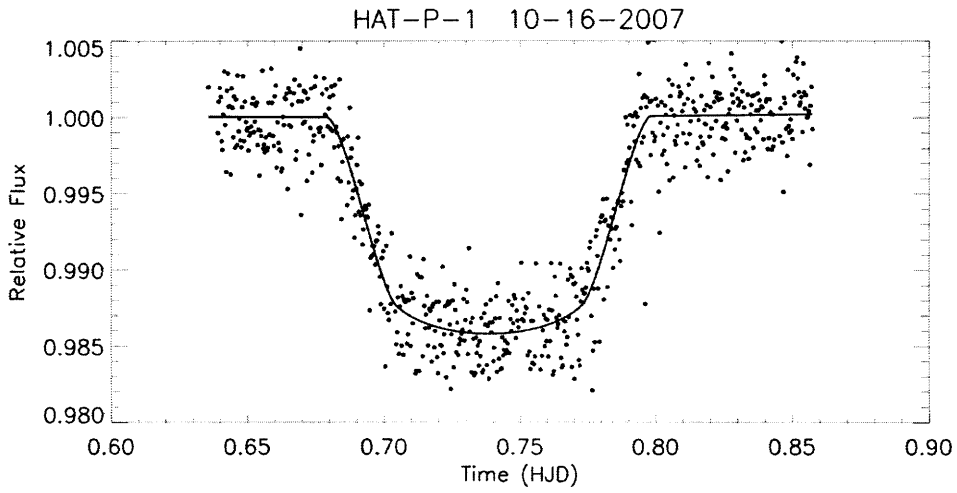

Figure B-25: HAT-P-1 observation (epoch 0) on FLWO 1.2m on 10-16-2007 with model fit. $T_c = 2454390.73863 \pm 0.00031$.

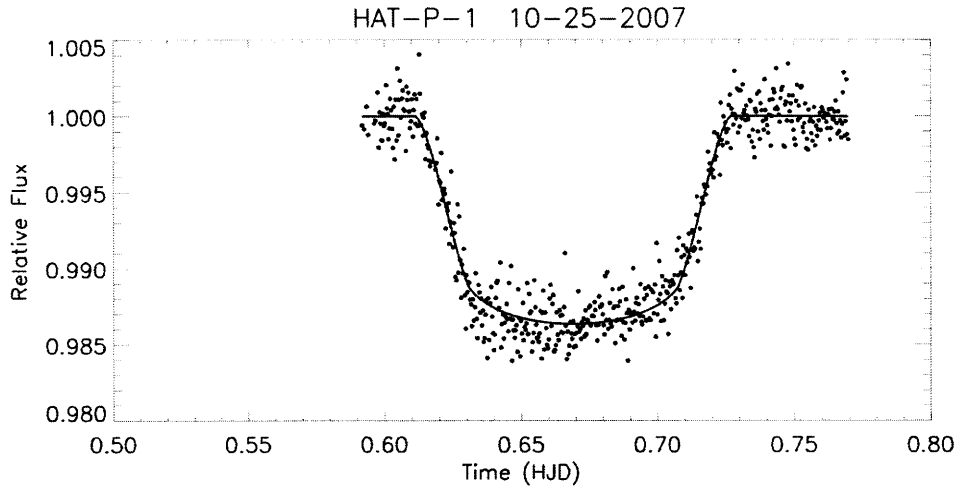

Figure B-26: HAT-P-1 observation (epoch 2) on FLWO 1.2m on 10-25-2007 with model fit. $T_c = 2454399.66916 \pm 0.00022$.

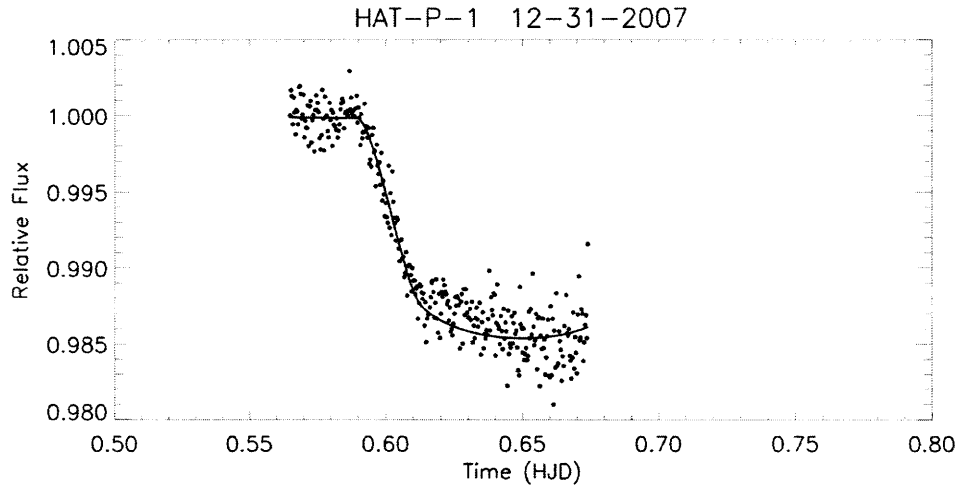

Figure B-27: HAT-P-1 observation (epoch 17) on FLWO 1.2m on 12-31-2007 with model fit. $T_c = 2454466.64817 \pm 0.00040$. Model is not a good for for the data, and data was not used in fitting for the ephemeris.

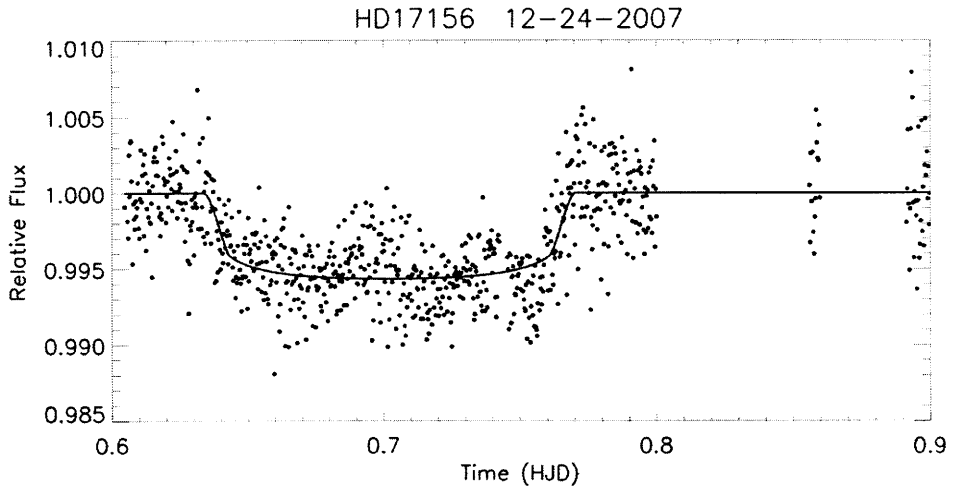

Figure B-28: HD17156 observation (epoch 0) on FLWO 1.2m on 12-24-2007 with model fit. $T_c = 2454459.70211 \pm 0.00045$. Noise appears very correlated.

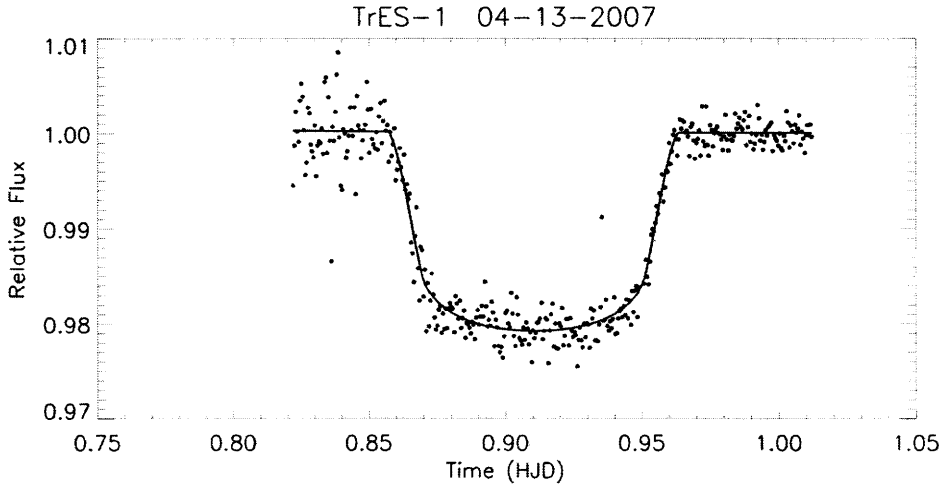

Figure B-29: TrES-1 observation (epoch 0) on FLWO 1.2m on 04-13-2007 with model fit. $T_c = 2454204.91034 \pm 0.00036$.

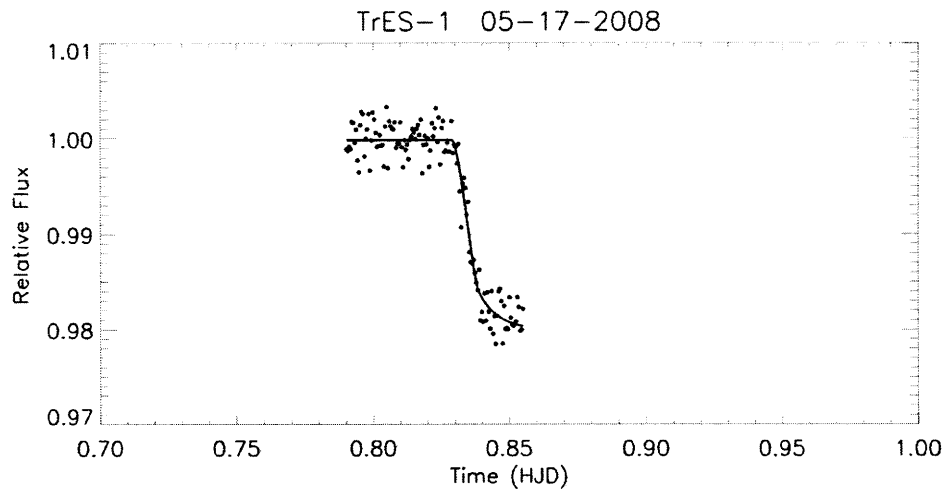

Figure B-30: TrES-1 observation (epoch 132) on FLWO 1.2m on 05-17-2008 with model fit. $T_c = 2454604.8811 \pm 0.00032$. Because such a small transit segment was observed, this data was not used in fitting for the ephemeris.

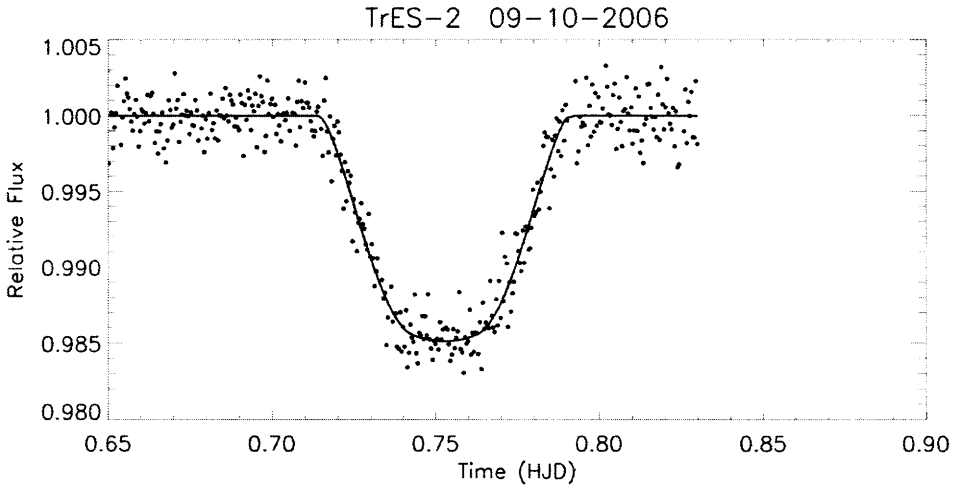

Figure B-31: TrES-2 observation (epoch -131) on FLWO 1.2m on 09-10-2006 with model fit. $T_c = 2453989.7526 \pm 0.00024$.

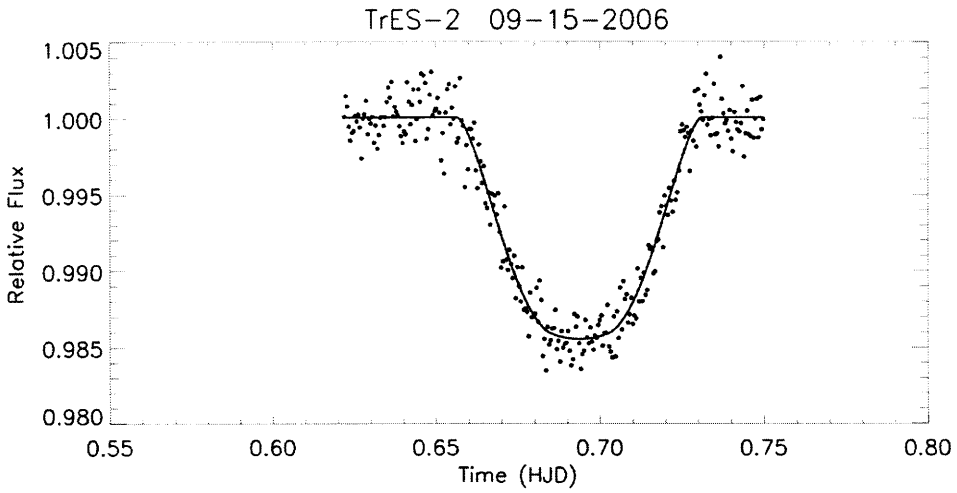

Figure B-32: TrES-2 observation (epoch -129) on FLWO 1.2m on 09-15-2006 with model fit. $T_c = 2453994.6938 \pm 0.00023$.

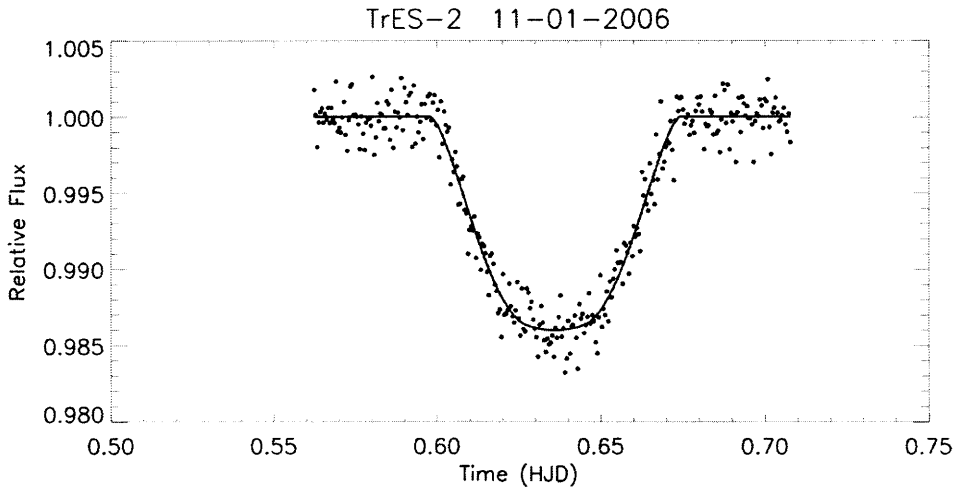

Figure B-33: TrES-2 observation (epoch -110) on FLWO 1.2m on 11-01-2006 with model fit. $T_c = 2454041.6360 \pm 0.00024$.

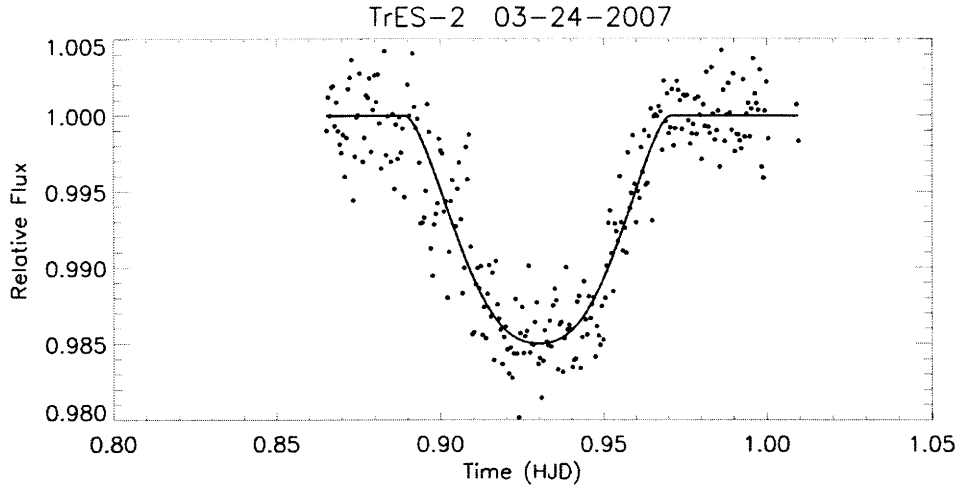

Figure B-34: TrES-2 observation (epoch -52) on FLWO 1.2m on 03-24-2007 with model fit. $T_c = 2454184.9299 \pm 0.00027$. Light curve is noisy in an asymmetric way, and was thus was not used in fitting for the ephemeris.

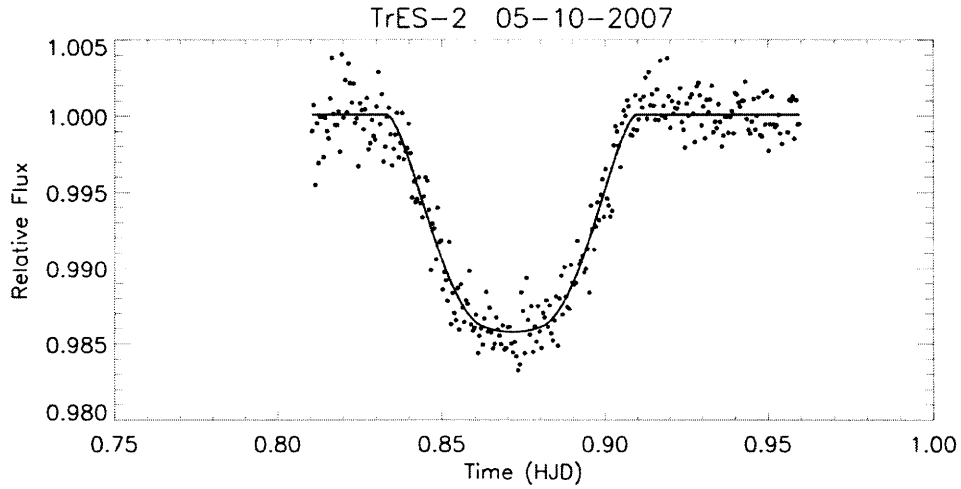

Figure B-35: TrES-2 observation (epoch -33) on FLWO 1.2m on 05-10-2007 with model fit. $T_c = 2454231.8714 \pm 0.00024$.

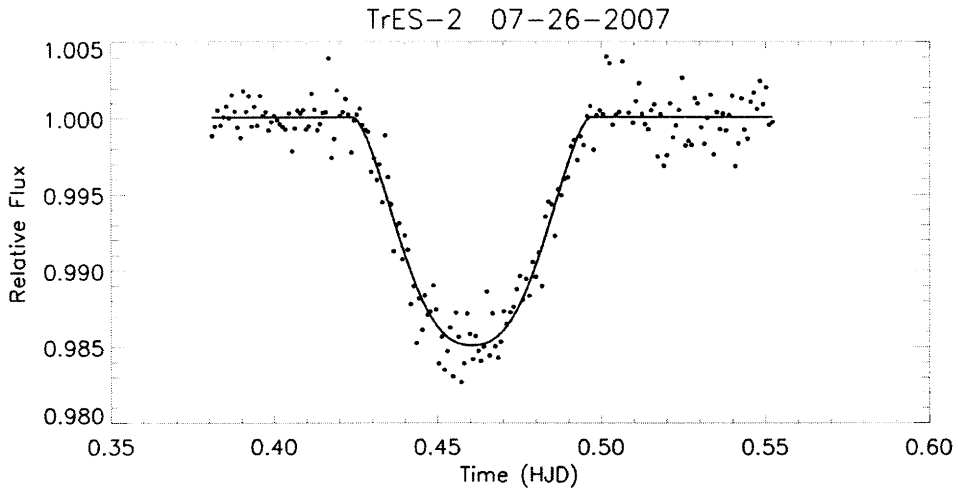

Figure B-36: TrES-2 observation (epoch -2) on Wise 1m on 07-26-2007 with model fit. $T_c = 2454308.4604 \pm 0.00025$.

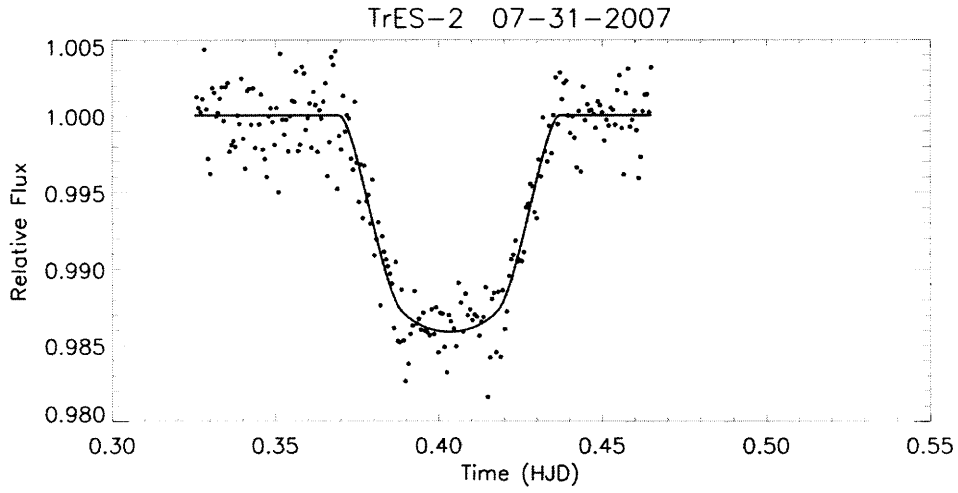

Figure B-37: TrES-2 observation (epoch 0) on Wise 1m on 07-31-2007 with model fit. $T_c = 2454313.4032 \pm 0.00027$.

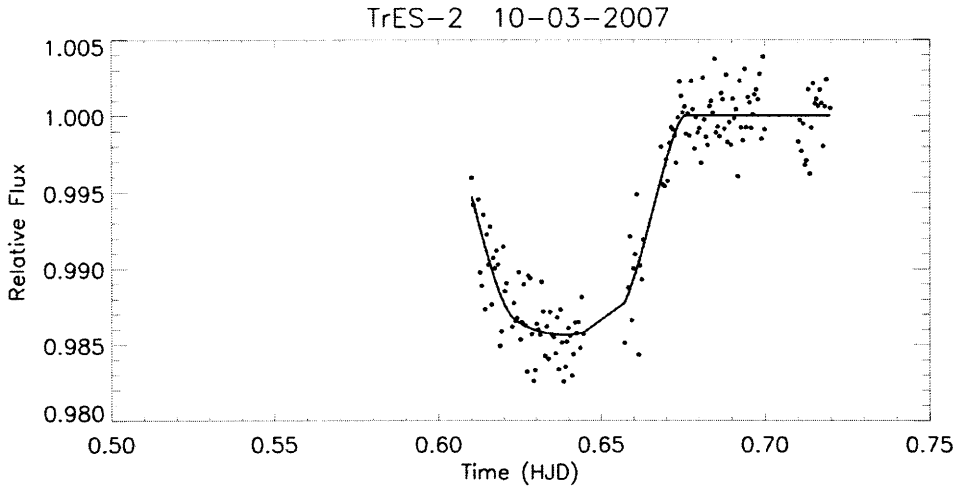

Figure B-38: TrES-2 observation (epoch 26) on FLWO 1.2m on 10-03-2007 with model fit. $T_c = 2454377.6386 \pm 0.00027$. Only a partial transit was observed, and thus the data was not used in fitting for the ephemeris.

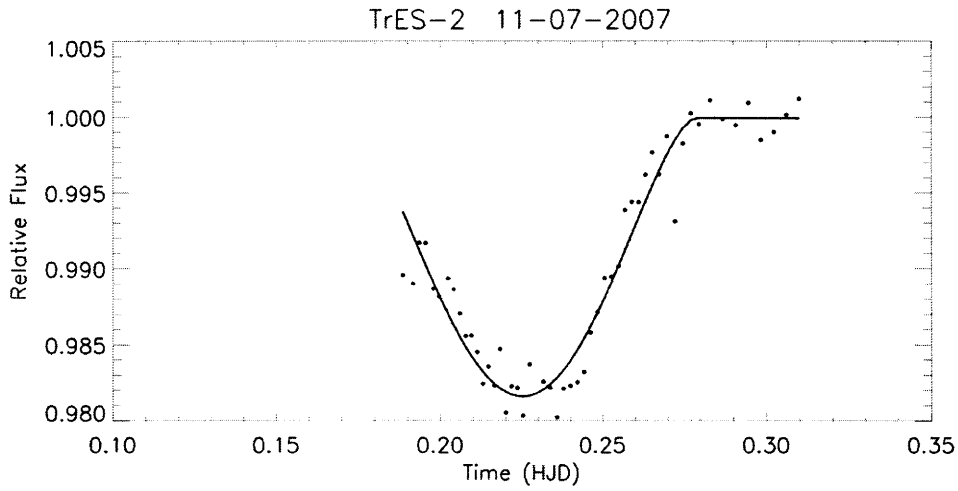

Figure B-39: TrES-2 observation (epoch 40) on Wise 1m on 11-07-2007 with model fit. $T_c = 2454412.2252 \pm 0.00029$. Time sampling is poor and model does not appear a good fit to the data. This observation was thus not used in fitting for the ephemeris.

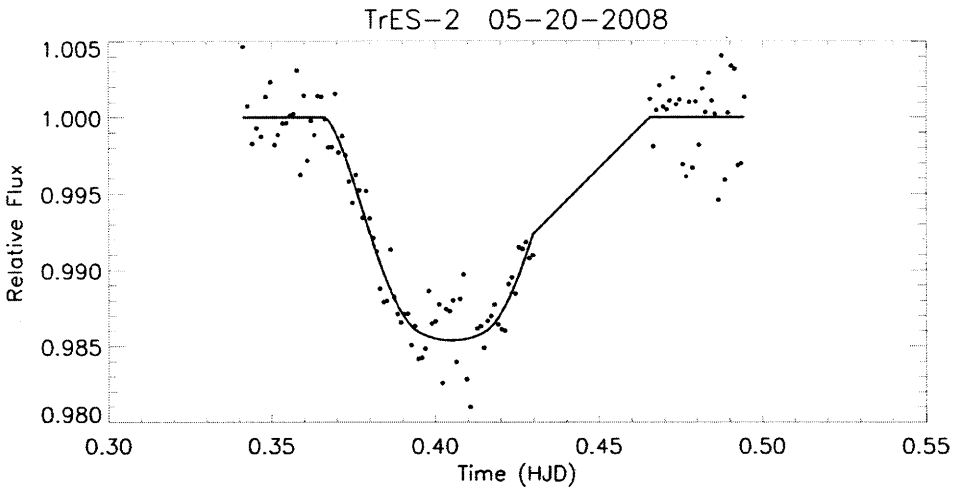

Figure B-40: TrES-2 observation (epoch 119) on Wise 1m on 05-20-2008 with model fit. $T_c = 2454607.4049 \pm 0.00037$. Data is noisy and missing a segment; this observation was not used in fitting for the ephemeris.

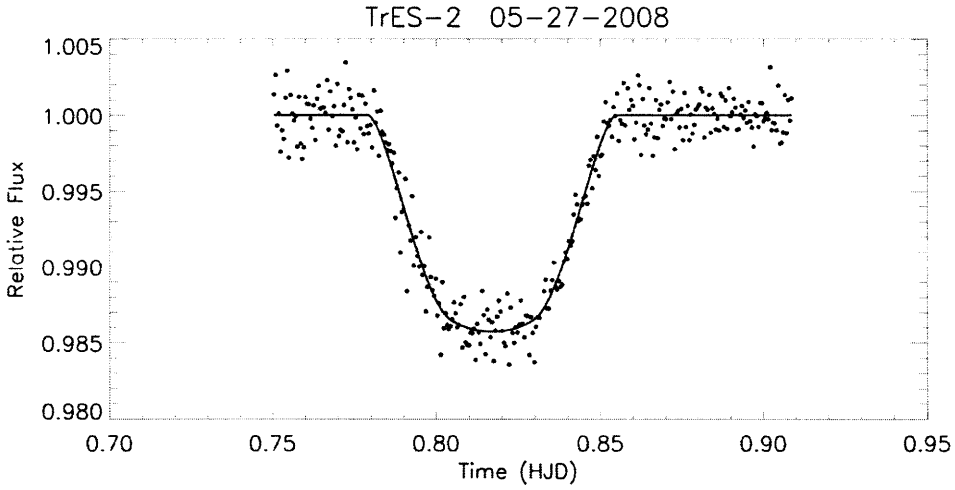

Figure B-41: TrES-2 observation (epoch 122) on FLWO 1.2m on 05-27-2008 with model fit. $T_c = 2454614.8170 \pm 0.00024$.

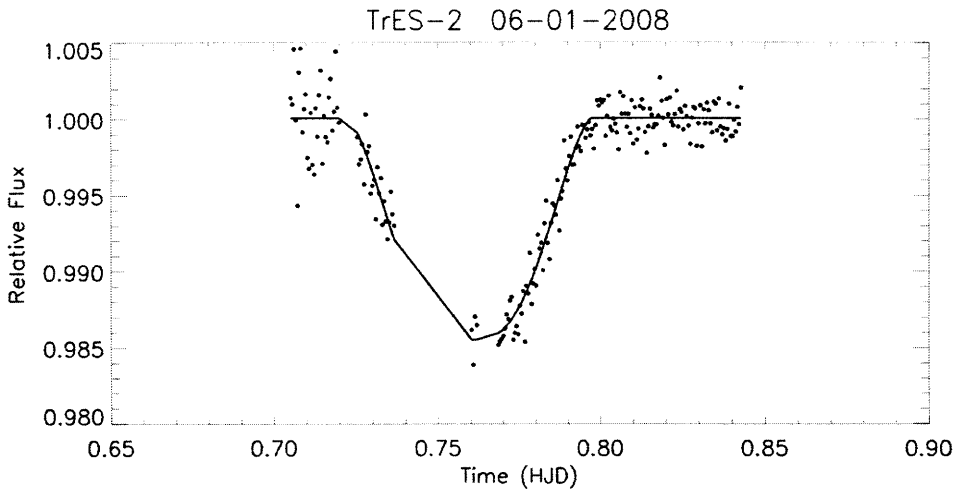

Figure B-42: TrES-2 observation (epoch 124) on FLWO 1.2m on 06-01-2008 with model fit. $T_c = 2454619.7600 \pm 0.00028$.

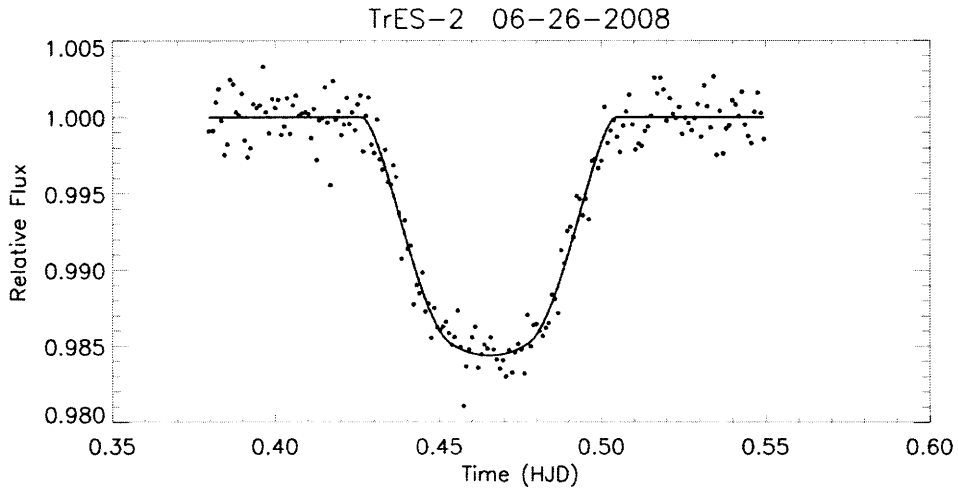

Figure B-43: TrES-2 observation (epoch 134) on Wise 1m on 06-26-2008 with model fit. $T_c = 2454644.4654 \pm 0.00026$.

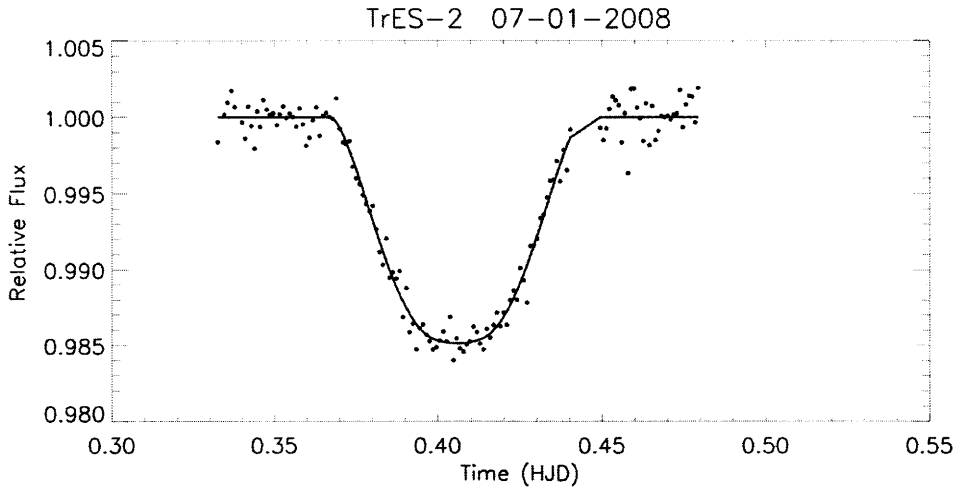

Figure B-44: TrES-2 observation (epoch 136) on Wise 1m on 07-01-2008 with model fit. $T_c = 2454649.4059 \pm 0.00024$.

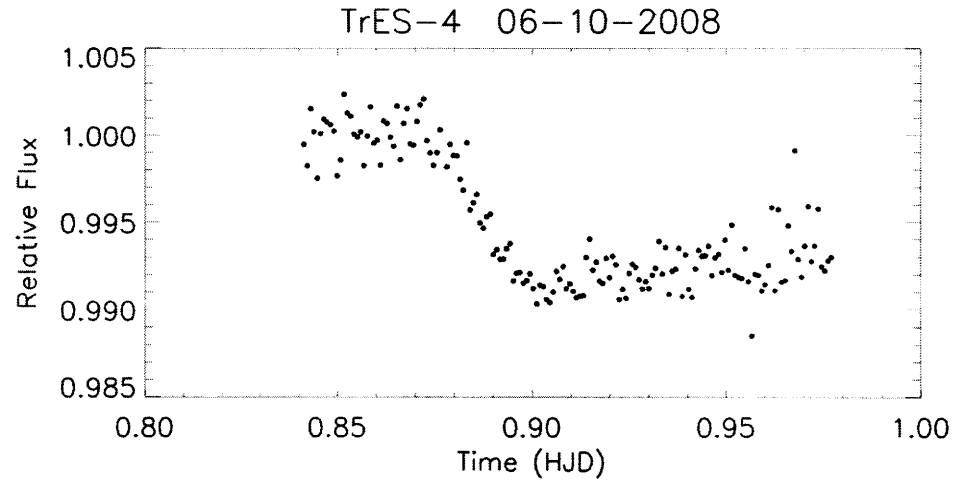

Figure B-45: TrES-4 observation on FLWO 1.2m on 06-10-2008. Data did not span enough of the transit and had too much correlated noise to give a good model-fitting and was thus not used.

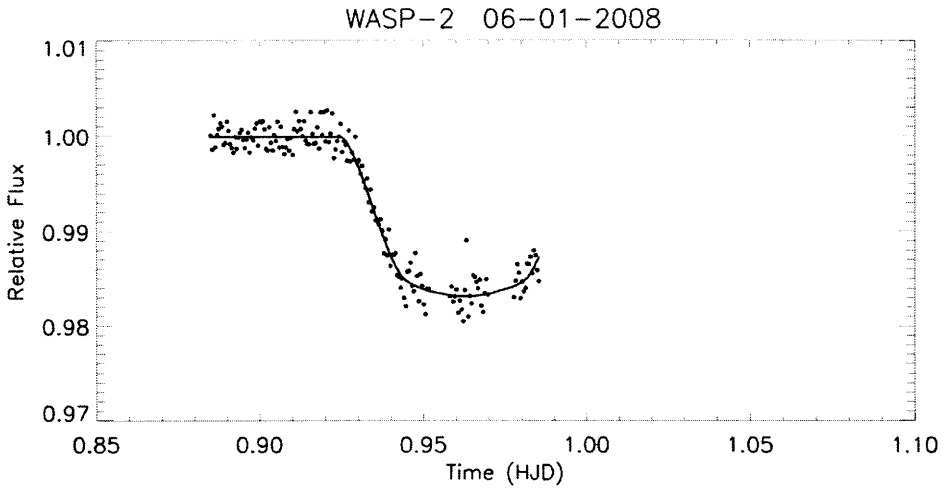

Figure B-46: WASP-2 observation (epoch 0) on FLWO 1.2m on 06-01-2008 with model fit. $T_c = 2454619.96275 \pm 0.00038$.

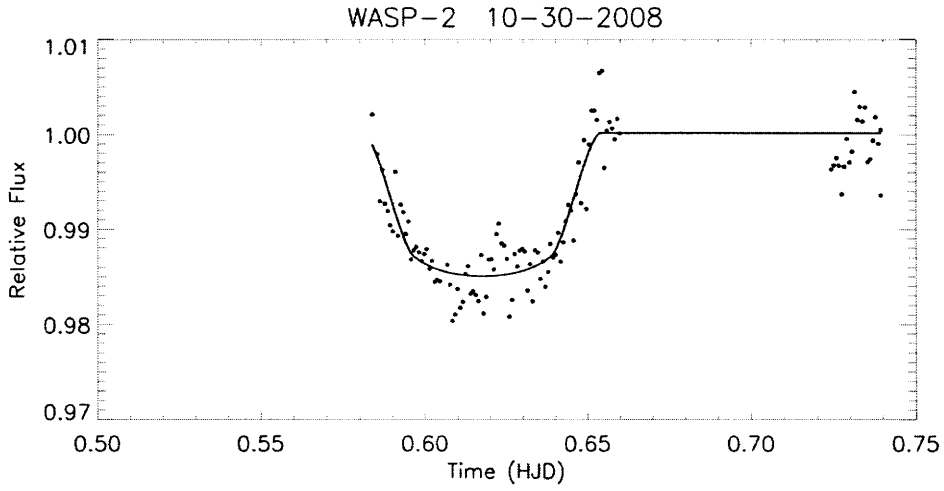

Figure B-47: WASP-2 observation (epoch 70) on FLWO 1.2m on 10-30-2008 with model fit. $T_c = 2454770.61757 \pm 0.00033$.

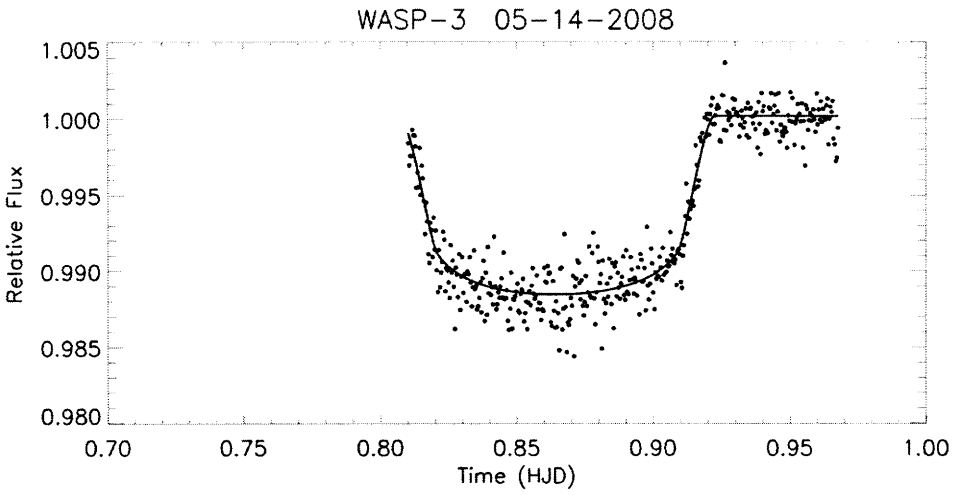

Figure B-48: WASP-3 observation (epoch -14) on FLWO 1.2m on 05-14-2008 with model fit. $T_c = 2454601.8649 \pm 0.00029$.

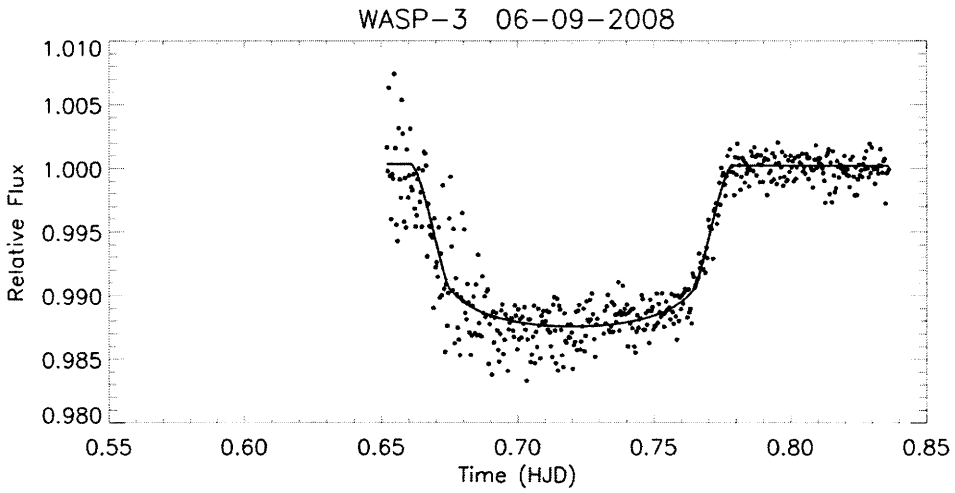

Figure B-49: WASP-3 observation (epoch 0) on FLWO 1.2m on 06-09-2008 with model fit. $T_c = 2454627.7198 \pm 0.00034$.

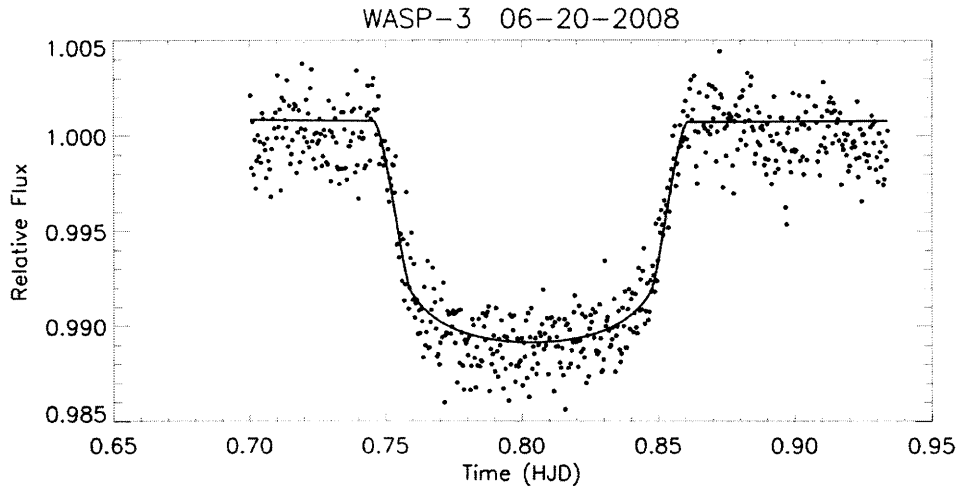

Figure B-50: WASP-3 observation (epoch 6) on FLWO 1.2m on 06-20-2008 with model fit. $T_c = 2454638.8028 \pm 0.00022$.

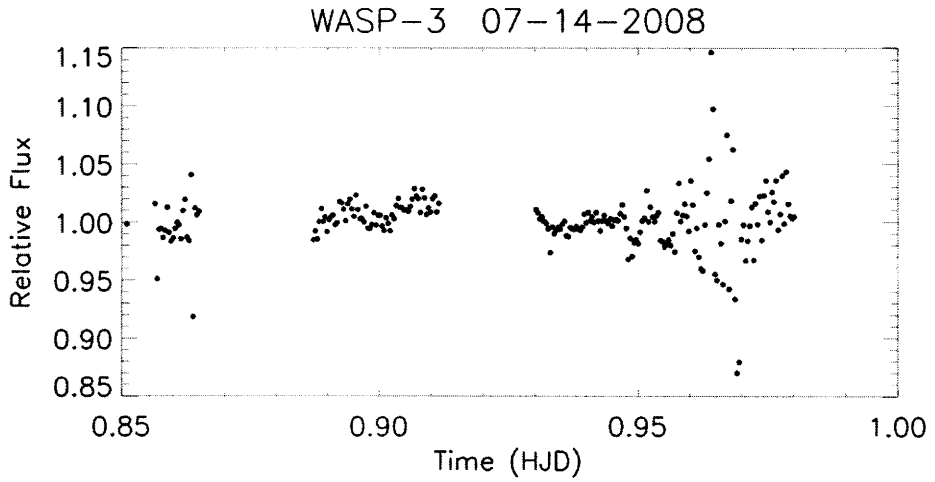

Figure B-51: WASP-3 observation on FLWO 1.2m on 07-14-2008. Data is terrible due to poor weather on the night of observation, and was not used in this thesis.

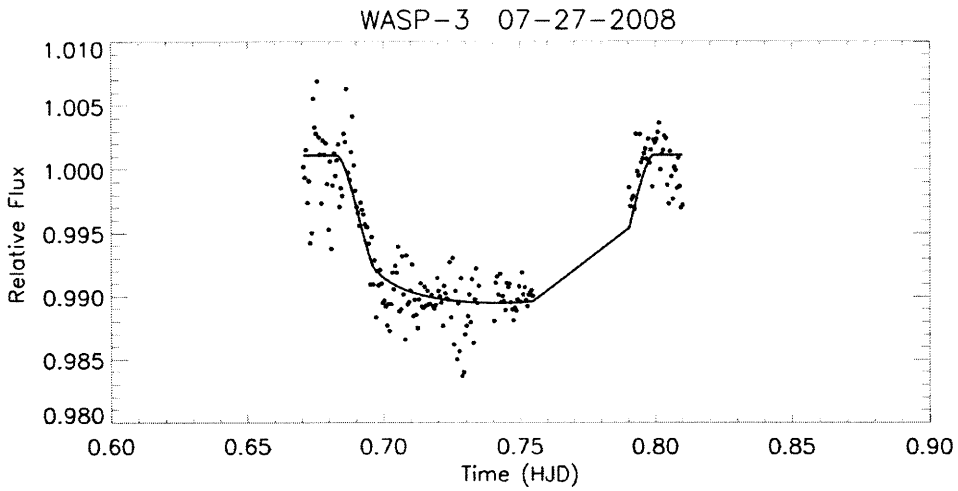

Figure B-52: WASP-3 observation (epoch 26) on FLWO 1.2m on 07-27-2008 with model fit. $T_c = 2454675.7413 \pm 0.00031$. This observation was not used in fitting for the ephemeris.

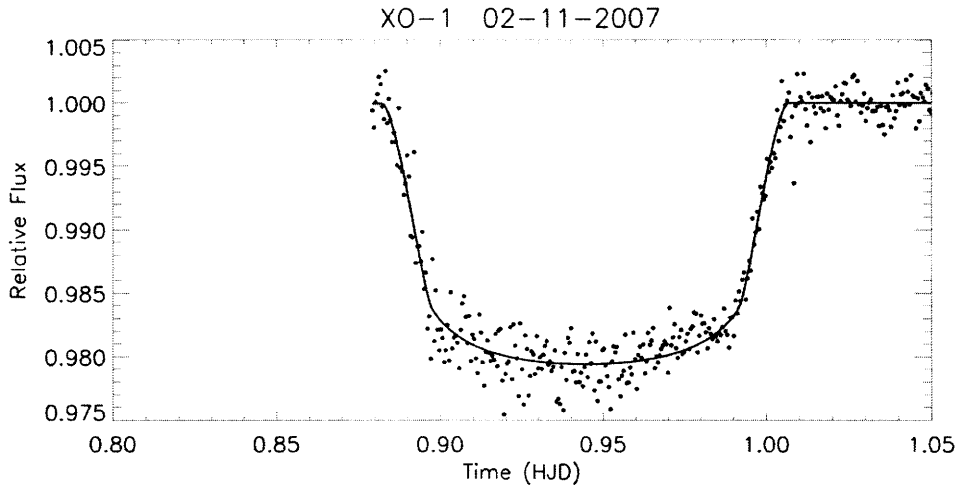

Figure B-53: XO-1 observation (epoch 0) on FLWO 1.2m on 02-11-2007 with model fit. $T_c = 2454143.94454 \pm 0.00020$.

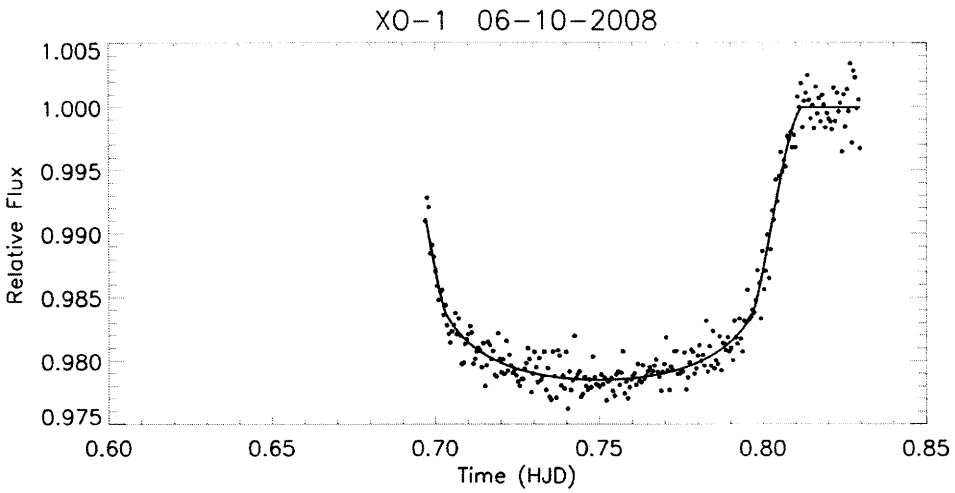

Figure B-54: XO-1 observation (epoch 123) on FLWO 1.2m on 06-10-2008 with model fit. $T_c = 2454628.74996 \pm 0.00020$.

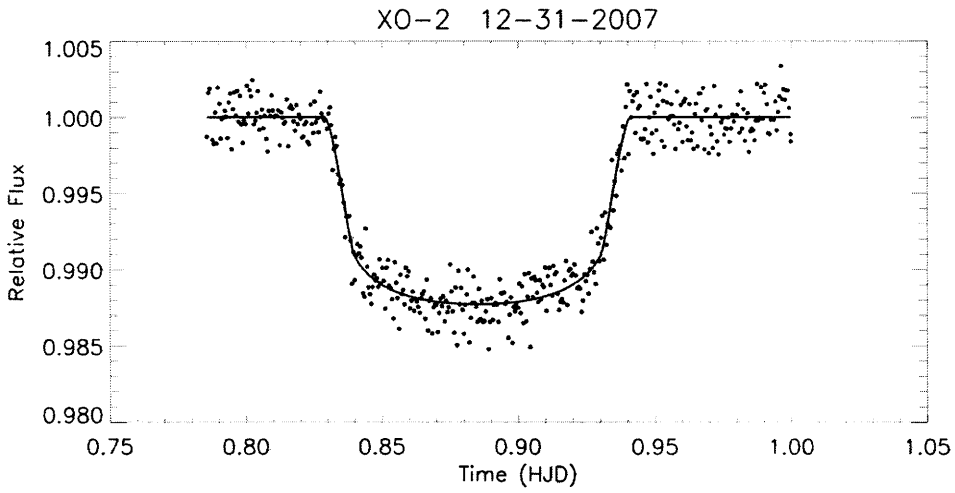

Figure B-55: XO-2 observation (epoch -5) on FLWO 1.2m on 12-31-2007 with model fit. $T_c = 2454466.88488 \pm 0.00023$.

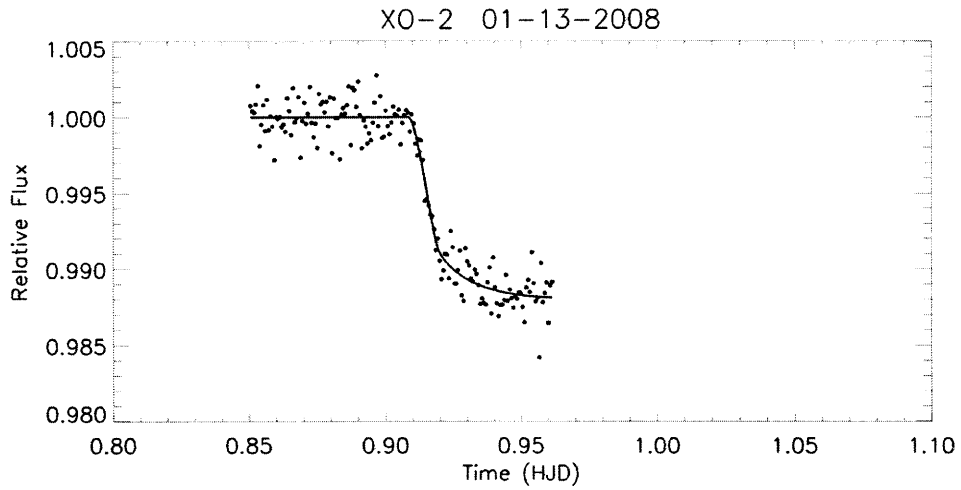

Figure B-56: XO-2 observation (epoch 0) on FLWO 1.2m on 01-13-2008 with model fit. $T_c = 2454479.96485 \pm 0.00033$.

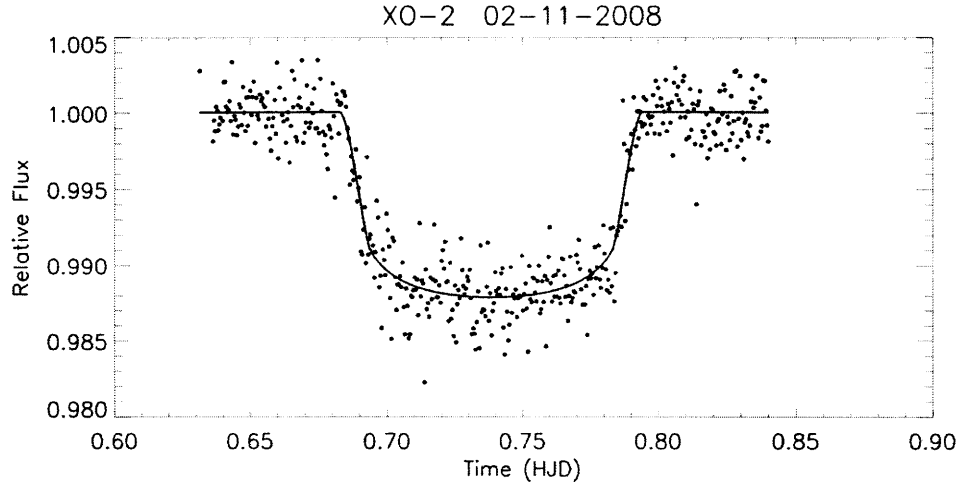

Figure B-57: XO-2 observation (epoch 11) on FLWO 1.2m on 02-11-2008 with model fit. $T_c = 2454508.73847 \pm 0.00023$.

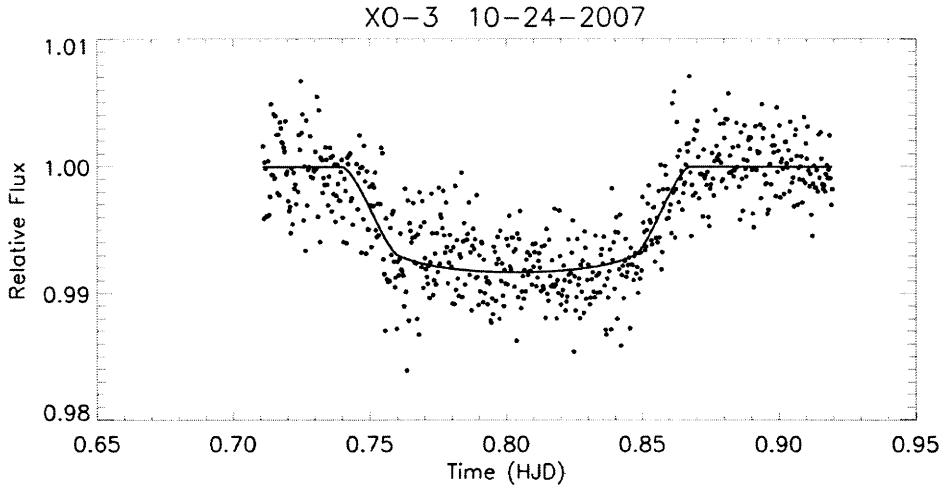

Figure B-58: XO-3 observation (epoch -16) on FLWO 1.2m on 10-24-2007 with model fit. $T_c = 2454398.80370 \pm 0.00032$.

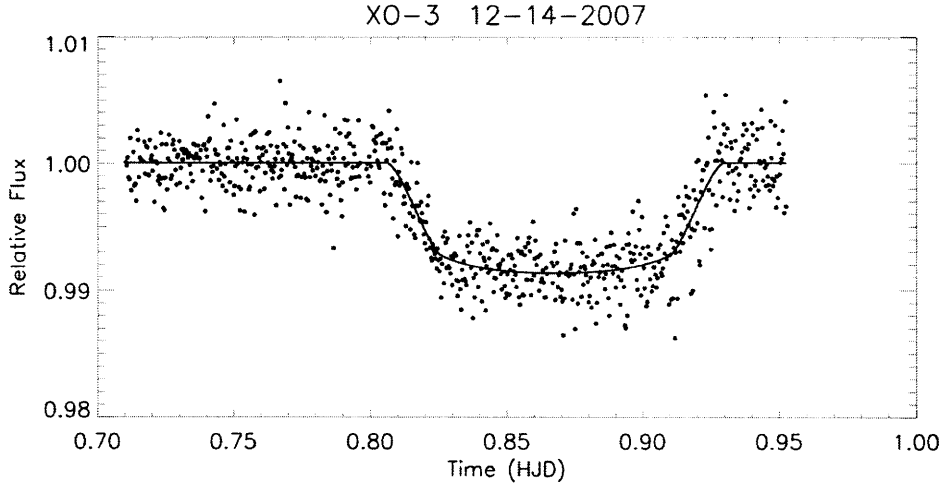

Figure B-59: XO-3 observation (epoch 0) on FLWO 1.2m on 12-14-2007 with model fit. $T_c = 2454449.86779 \pm 0.00028$.

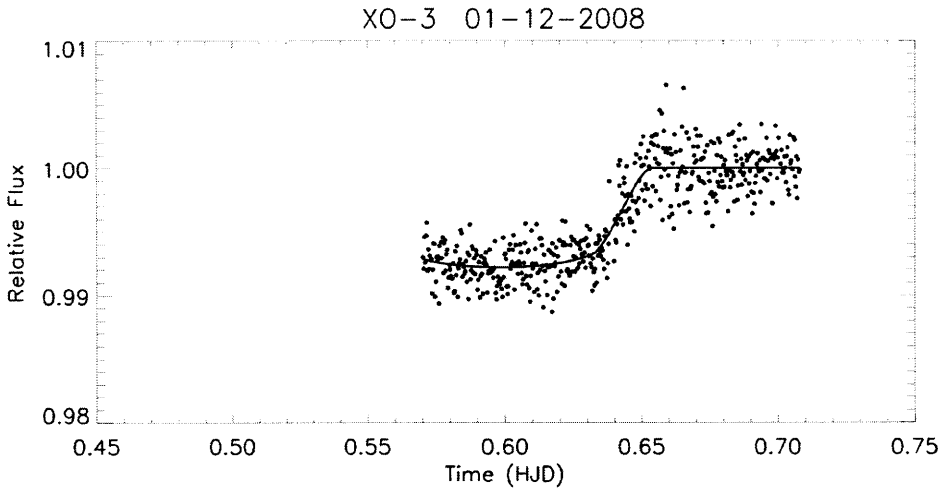

Figure B-60: XO-3 observation (epoch 9) on FLWO 1.2m on 01-12-2008 with model fit. $T_c = 2454478.59831 \pm 0.00041$.

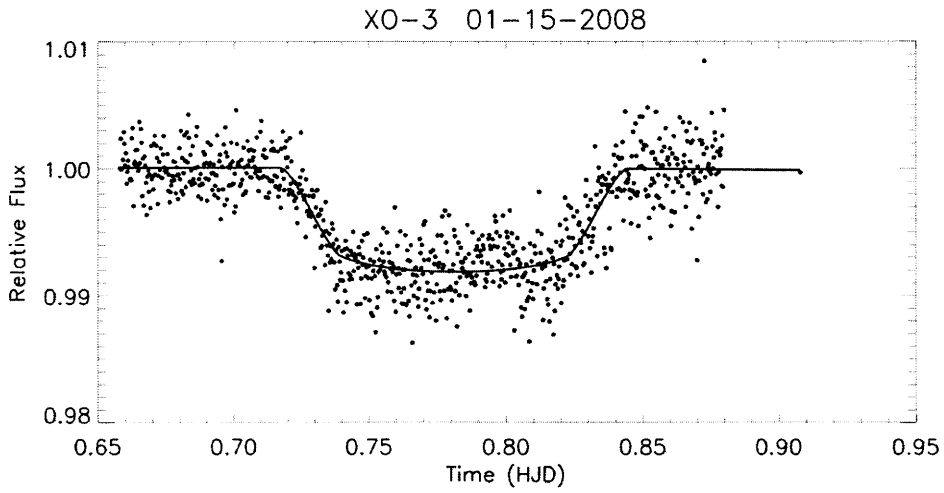

Figure B-61: XO-3 observation (epoch 10) on FLWO 1.2m on 01-15-2008 with model fit. $T_c = 2454481.78076 \pm 0.00031$.

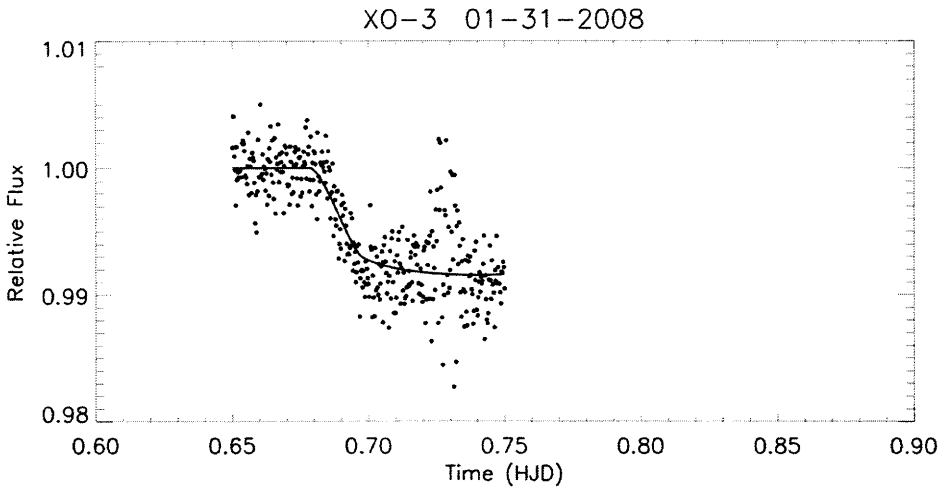

Figure B-62: XO-3 observation (epoch 15) on FLWO 1.2m on 01-31-2008 with model fit. $T_c = 2454497.73964 \pm 0.00037$. Only a partial transit was observed, and there seems to be some correlated noise. This observation was not used in fitting for the ephemeris fitting.

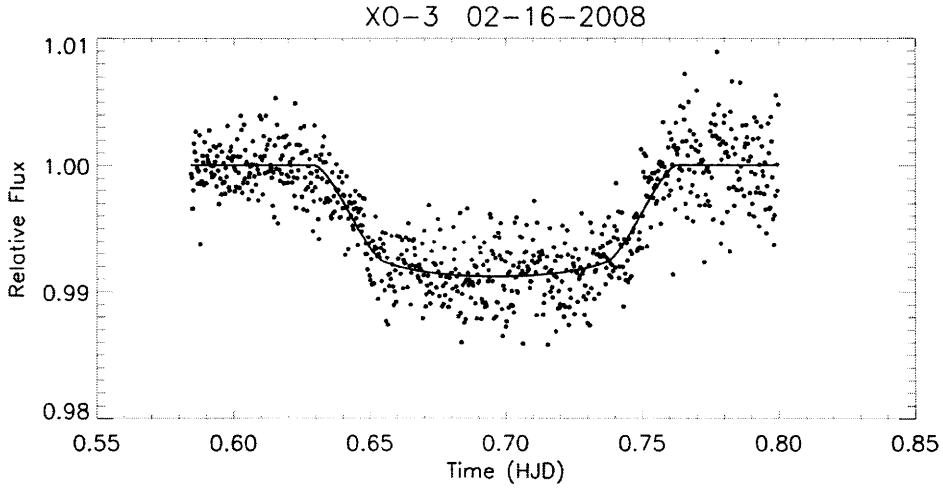

Figure B-63: XO-3 observation (epoch 20) on FLWO 1.2m on 02-16-2008 with model fit. $T_c = 2454513.69605 \pm 0.00032$.

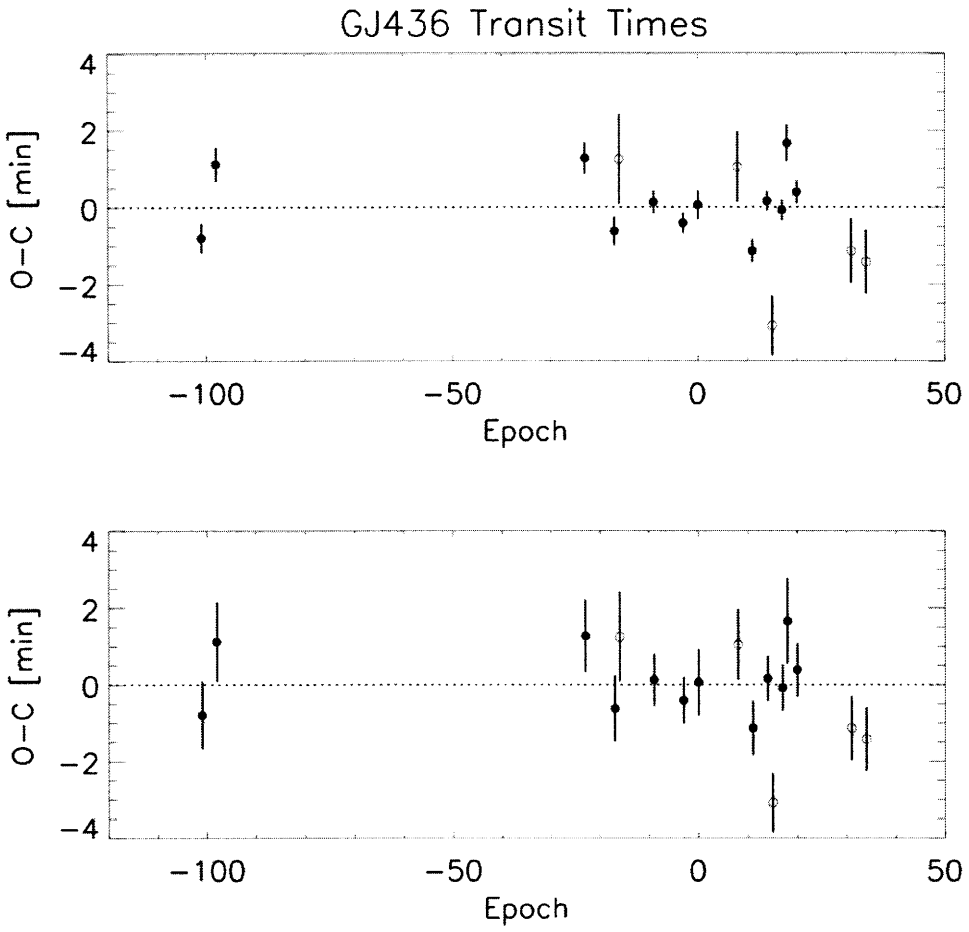

Figure B-64: Deviations (Observed-Calculated) of GJ436 transit times from ephemeris: $HJD_0 = 2454510.80069 \pm 0.00015$ and $P = 2.643896 \pm 0.000004$. Upper plot shows error bars exactly as given from Markov Chain. Lower plot shows error bars scaled such that χ^2 per degree of freedom is one, and the resultant fit. All data points are from this thesis, but only filled-in points were used in the fit.

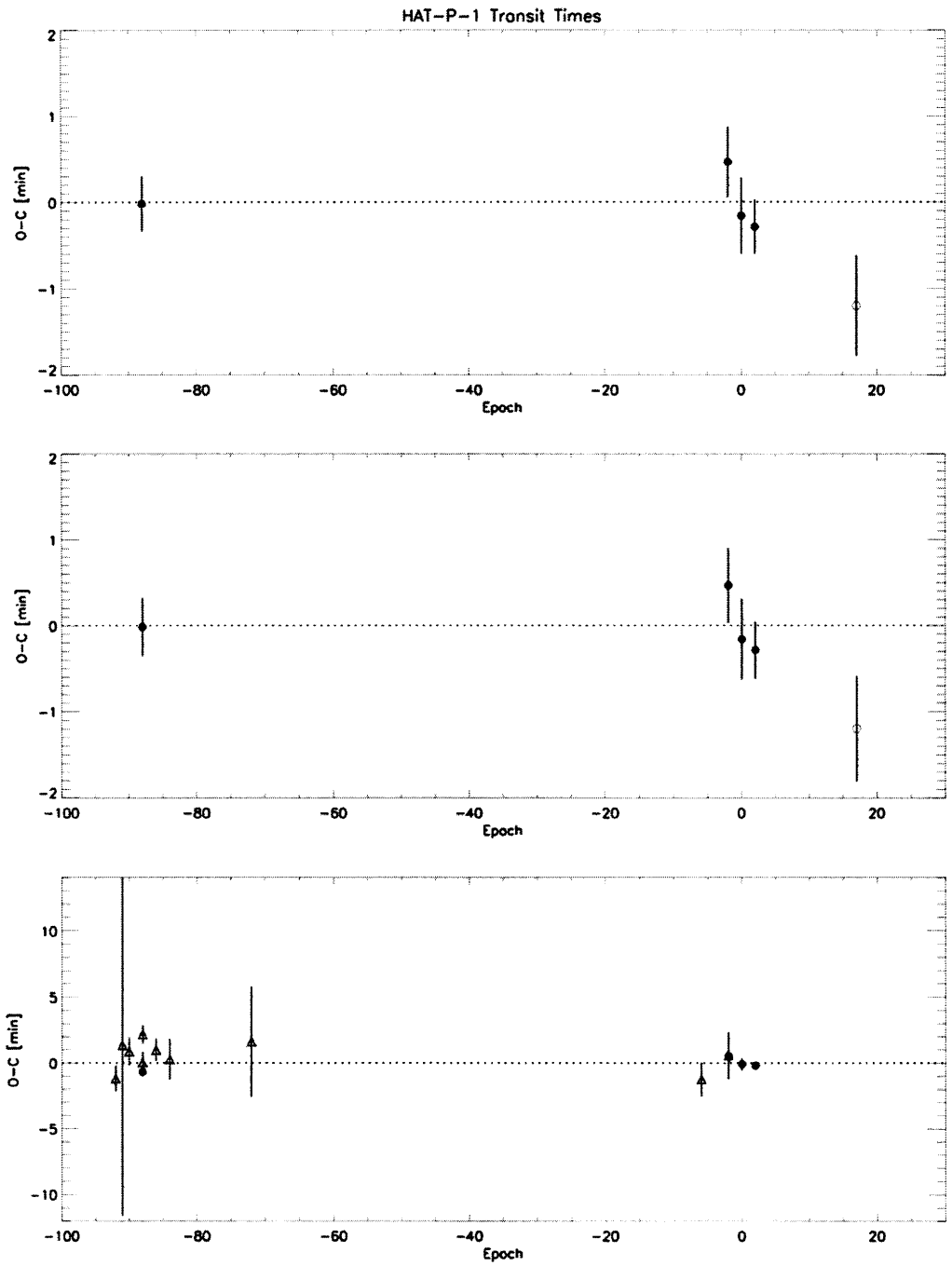

Figure B-65: Deviations (Observed-Calculated) of HAT-1 transit times from ephemerides: $HJD_0 = 2454390.73871 \pm 0.00016$ and $P = 4.4653094 \pm 0.0000037$ for upper two plots and $HJD_0 = 2454390.73870 \pm 0.00016$ and $P = 4.4653036 \pm 0.0000026$ for lower plot. Upper plot shows error bars exactly as given from Markov Chain. Middle plot shows error bars scaled such that χ^2 per degree of freedom is one, and the resultant fit. Lower plot shows data from this thesis combined with published transit times (see Table A.5. Circles indicate data from this thesis that was not used in the fit, filled-in circles indicate data from this thesis used in the fit, and triangles indicate published data that was also used in the fit.

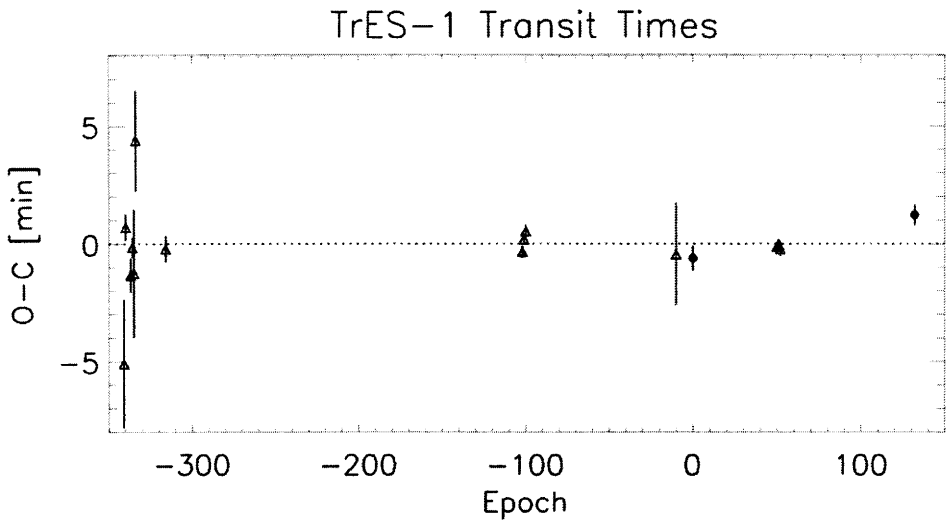

Figure B-66: Deviations (Observed-Calculated) of TrES-1 transit times from ephemeris: $HJD_0 = 2454204.910619 \pm 0.000058$ and $P = 3.0300727 \pm 0.0000005$. Circles indicate data from this thesis that was not used in the fit, filled-in circles indicate data from this thesis used in the fit, and triangles indicate published data that was also used in the fit.

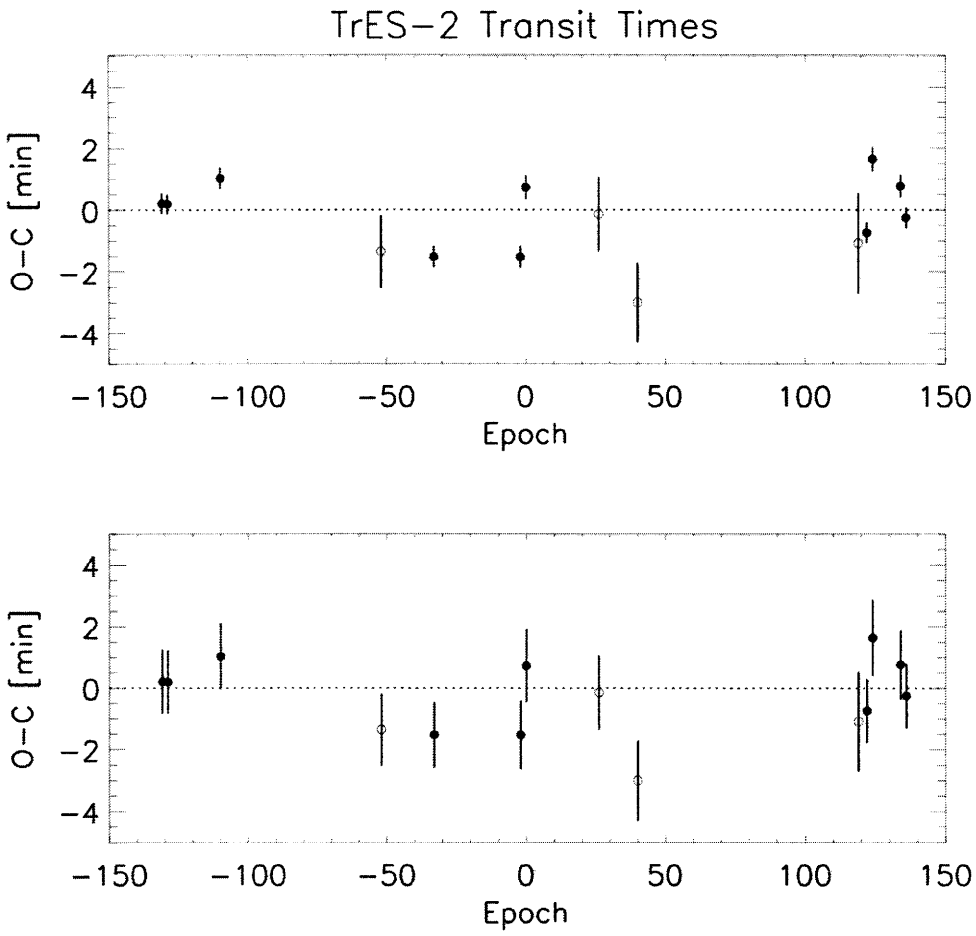

Figure B-67: Deviations (Observed-Calculated) of TrES-2 transit times from ephemeris: $HJD_0 = 2454313.402728 \pm 0.00024$ and $P = 2.470613 \pm 0.0000022$. Upper plot shows error bars exactly as given from Markov Chain. Lower plot shows error bars scaled such that χ^2 per degree of freedom is one, and the resultant fit. All data points are from this thesis, but only filled-in points were used in the fit.

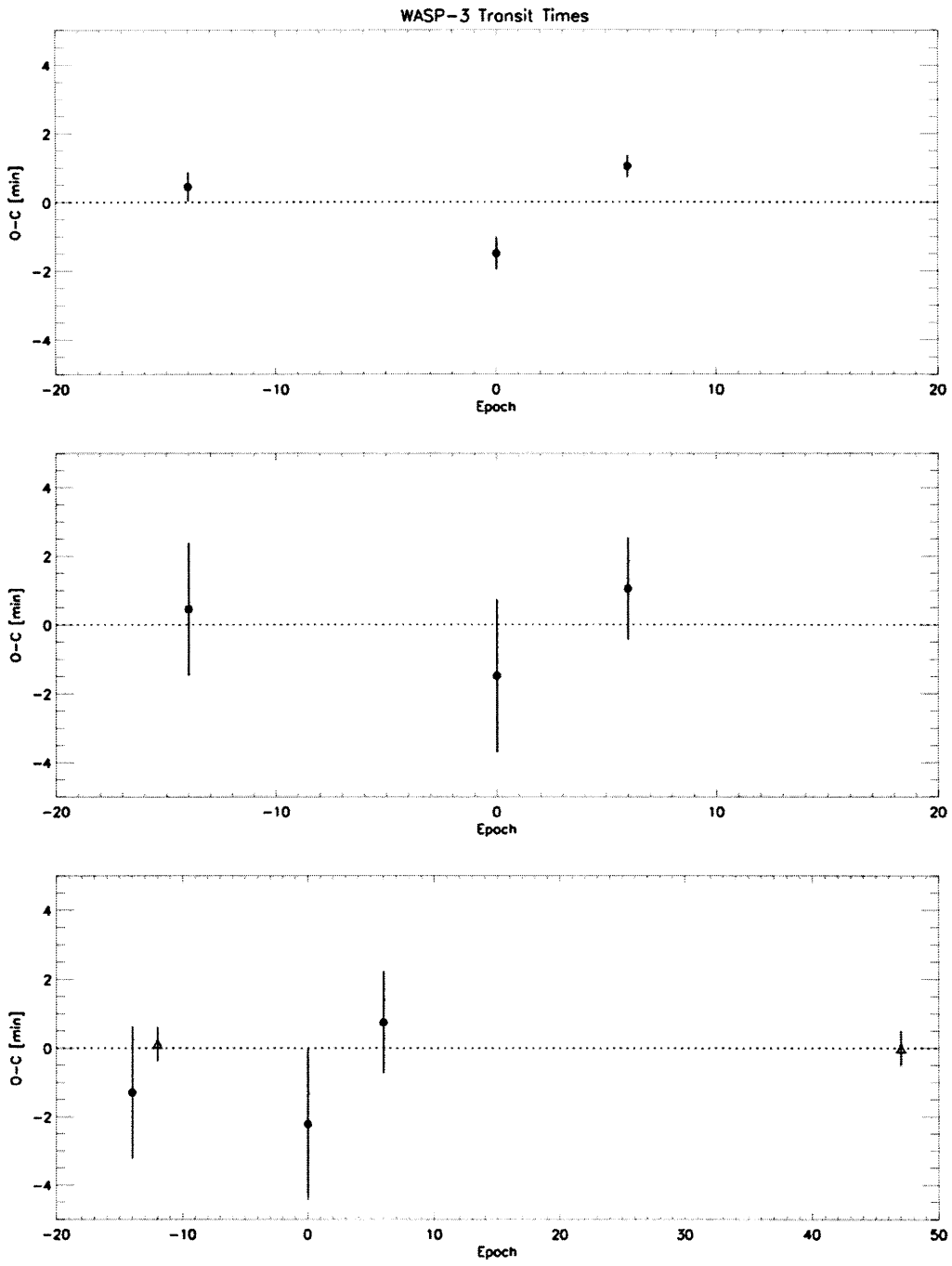

Figure B-68: Deviations (Observed-Calculated) of WASP-3 transit times from ephemerides: $HJD_0 = 2454619.96275 \pm 0.00038$ and $P = 2.1522117 \pm 0.0000072$ for upper two plots and $HJD_0 = 2454627.72137 \pm 0.00027$ and $P = 1.8468242 \pm 0.0000083$ for lower plot. Upper plot shows error bars exactly as given from Markov Chain. Middle plot shows error bars scaled such that χ^2 per degree of freedom is one, and the resultant fit. Lower plot shows data from this thesis combined with published transit times (see Table A.5. Circles indicate data from this thesis that was not used in the fit, filled-in circles indicate data from this thesis used in the fit, and triangles indicate published data that was also used in the fit.

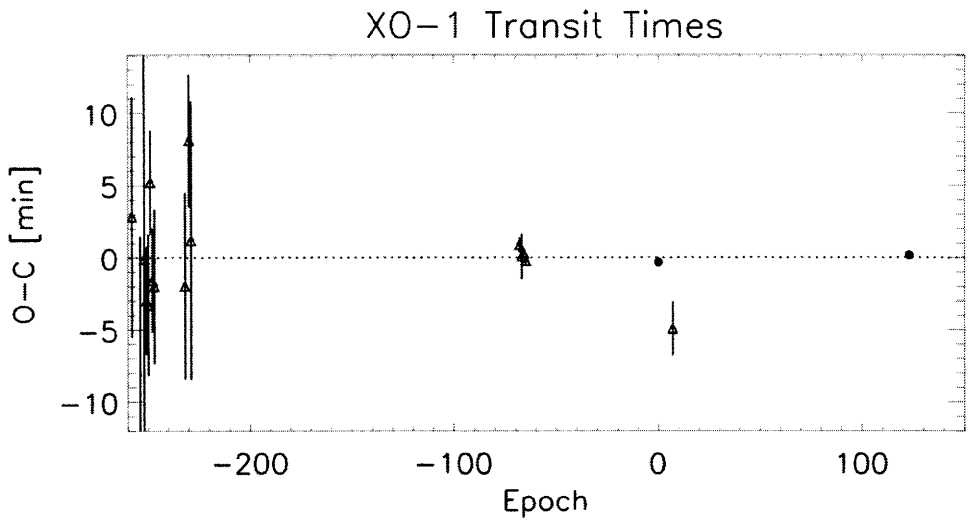

Figure B-69: Deviations (Observed-Calculated) of XO-1 transit times from ephemeris: $HJD_0 = 2454143.94476 \pm 0.000091$ and $P = 3.9415047 \pm 0.0000012$. Circles indicate data from this thesis that was not used in the fit, filled-in circles indicate data from this thesis used in the fit, and triangles indicate published data that was also used in the fit.

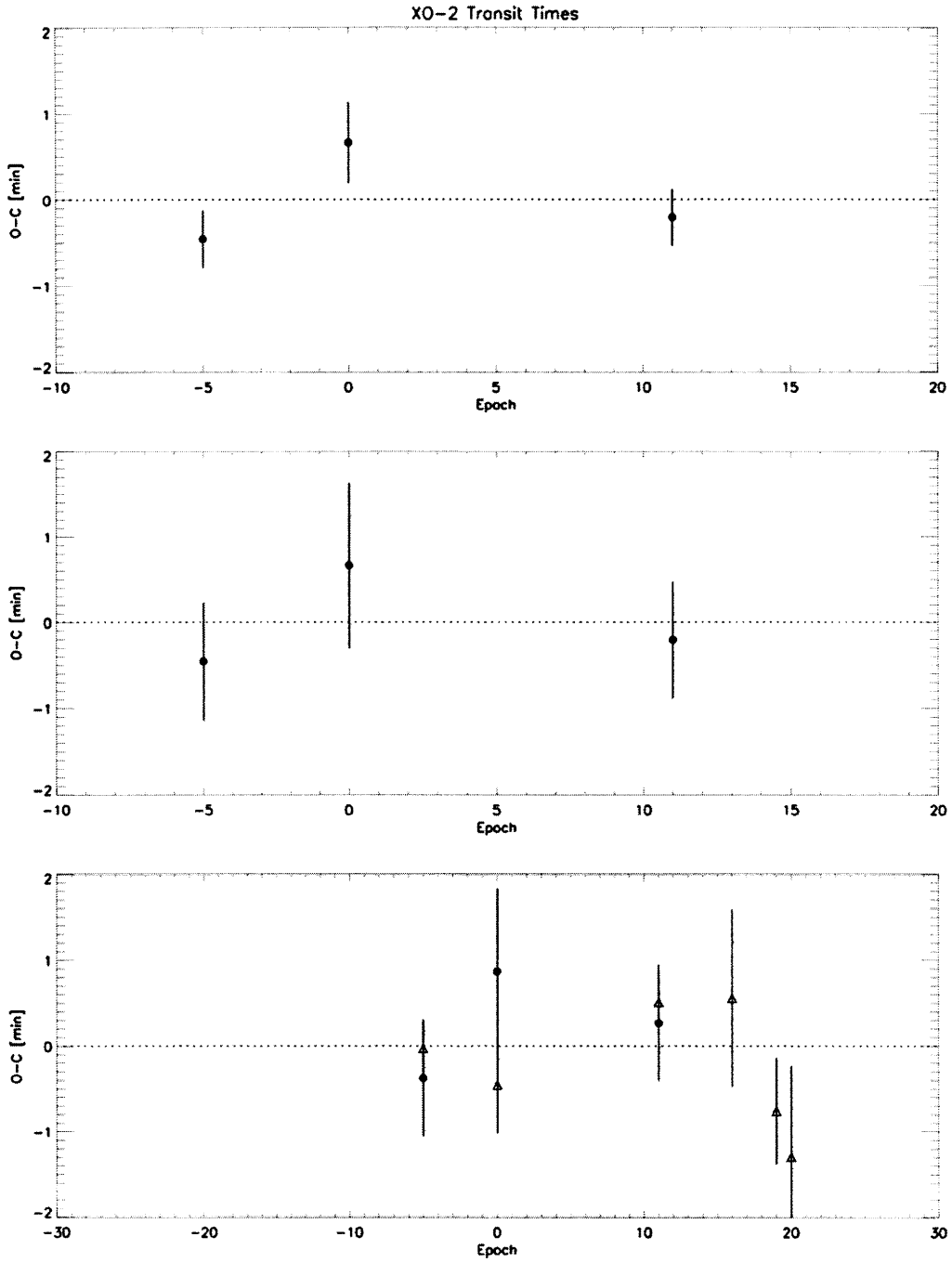

Figure B-70: Deviations (Observed-Calculated) of XO-2 transit times from ephemeris: $HJD_0 = 2454479.96429 \pm 0.00032$ and $P = 2.615843 \pm 0.000041$ for upper two plots and $HJD_0 = 2454479.96425 \pm 0.00014$ and $P = 2.615822 \pm 0.000014$ for lower plot. Upper plot shows error bars exactly as given from Markov Chain. Middle plot shows error bars scaled such that χ^2 per degree of freedom is one, and the resultant fit. Lower plot shows data from this thesis combined with published transit times (see Table A.5. Circles indicate data from this thesis that was not used in the fit, filled-in circles indicate data from this thesis used in the fit, and triangles indicate published data that was also used in the fit.

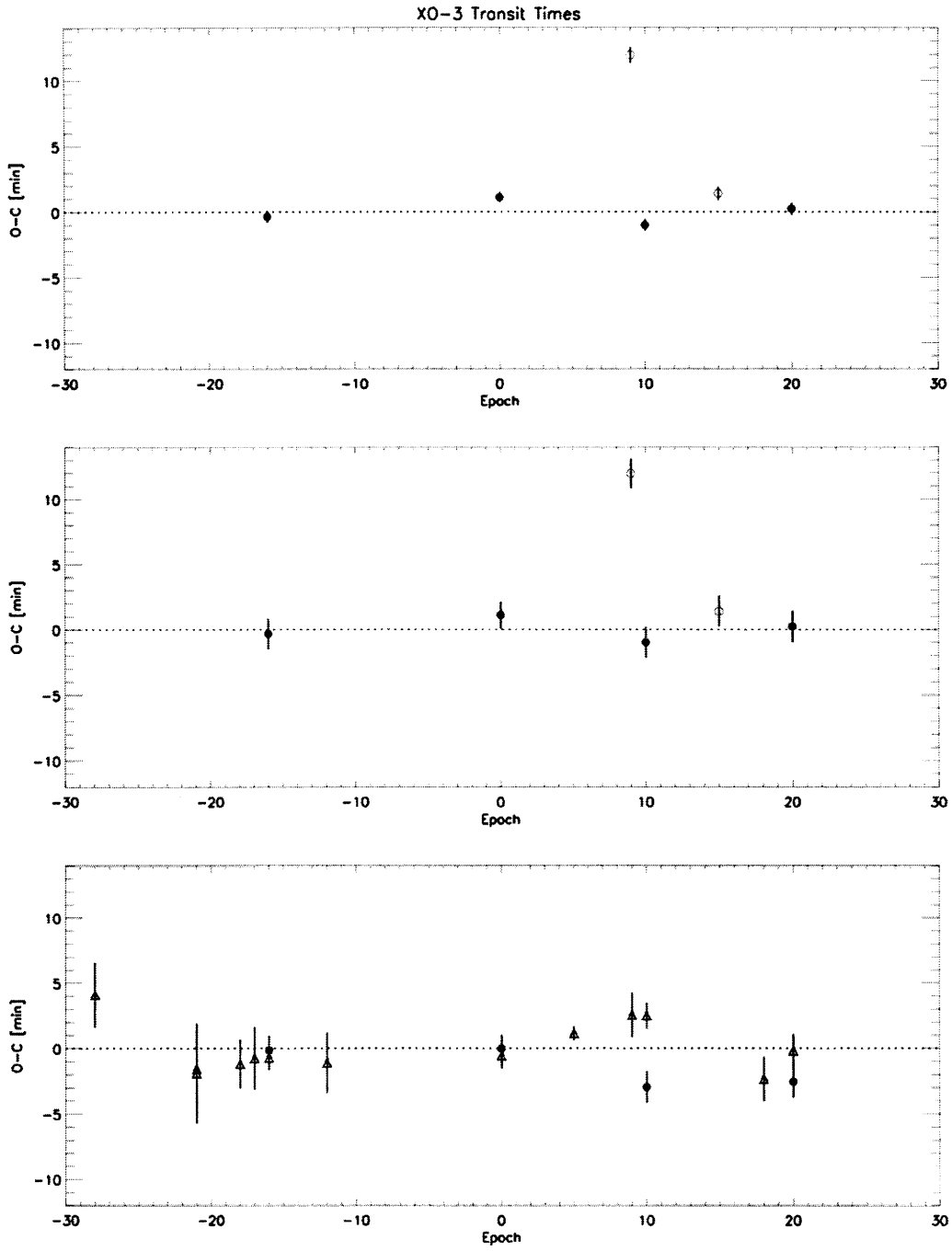

Figure B-71: Deviations (Observed-Calculated) of XO-3 transit times from ephemeris: $HJD_0 = 2454449.86703 \pm 0.00041$ and $P = 3.1914418 \pm 0.000031$ for upper two plots and $HJD_0 = 2454449.86782 \pm 0.00020$ and $P = 3.191500 \pm 0.000016$ for lower plot. Upper plot shows error bars exactly as given from Markov Chain. Middle plot shows error bars scaled such that χ^2 per degree of freedom is one, and the resultant fit. Lower plot shows data from this thesis combined with published transit times (see Table A.5. Circles indicate data from this thesis that was not used in the fit, filled-in circles indicate data from this thesis used in the fit, and triangles indicate published data that was also used in the fit.

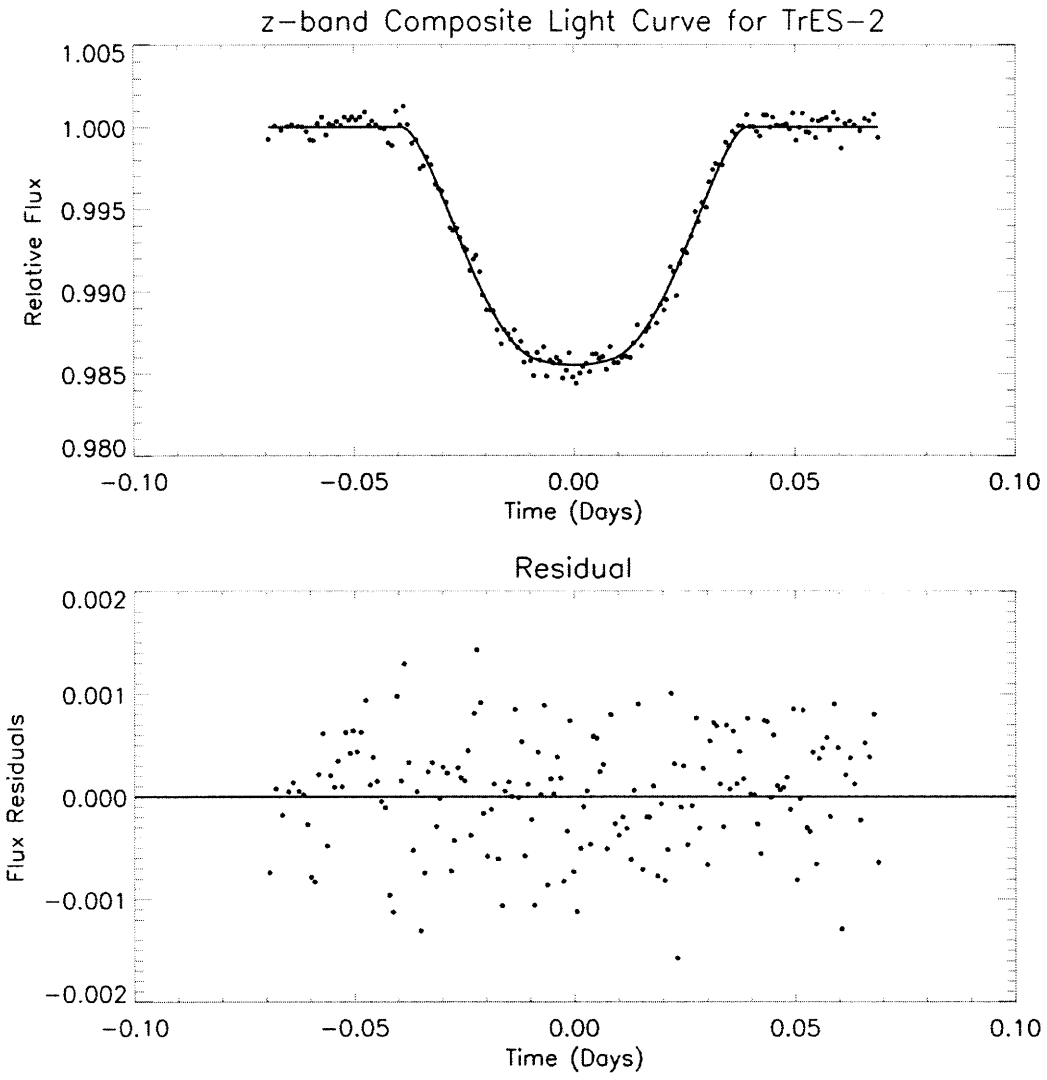

Figure B-72: TrES-2 Fitted Composite Light Curve (z-band)

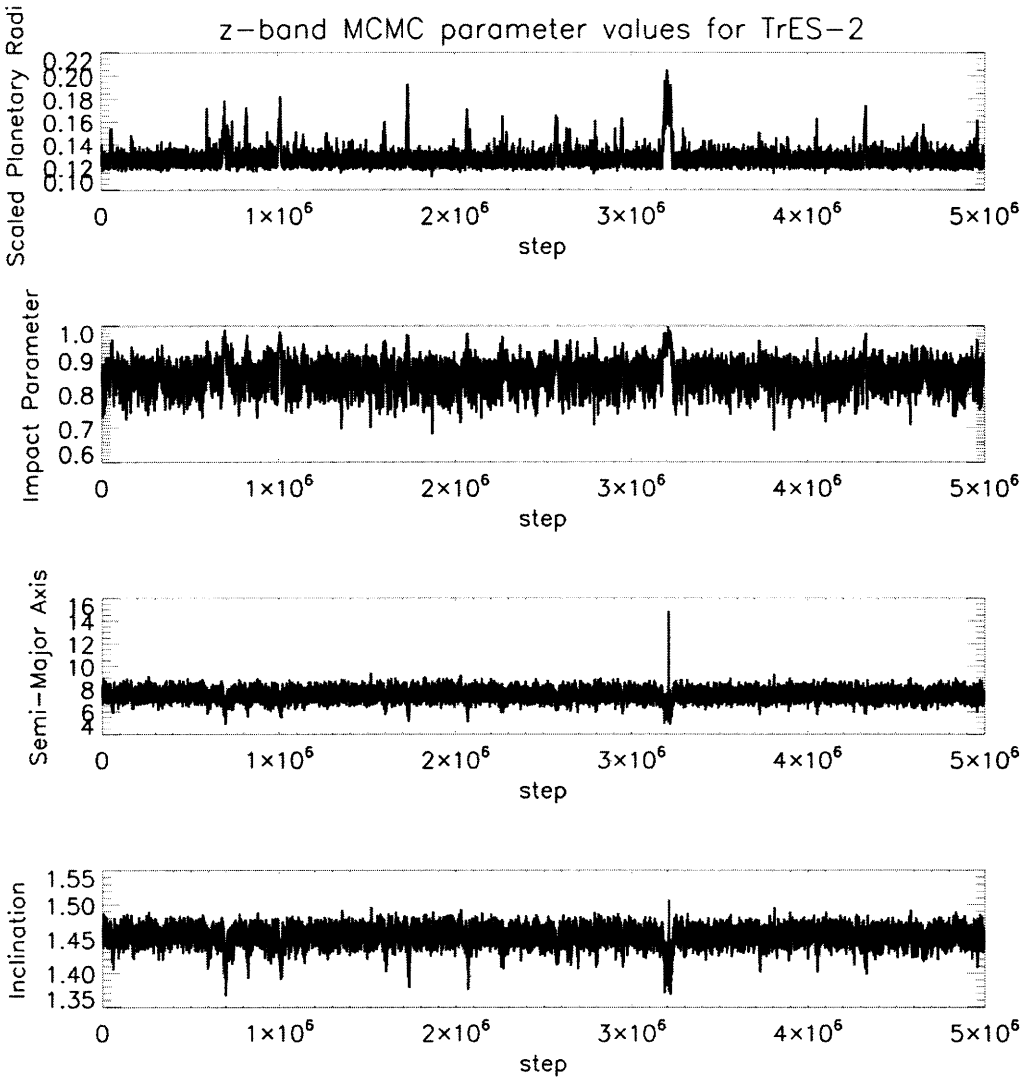

Figure B-73: TrES-2 MCMC Parameter Values (z-band)

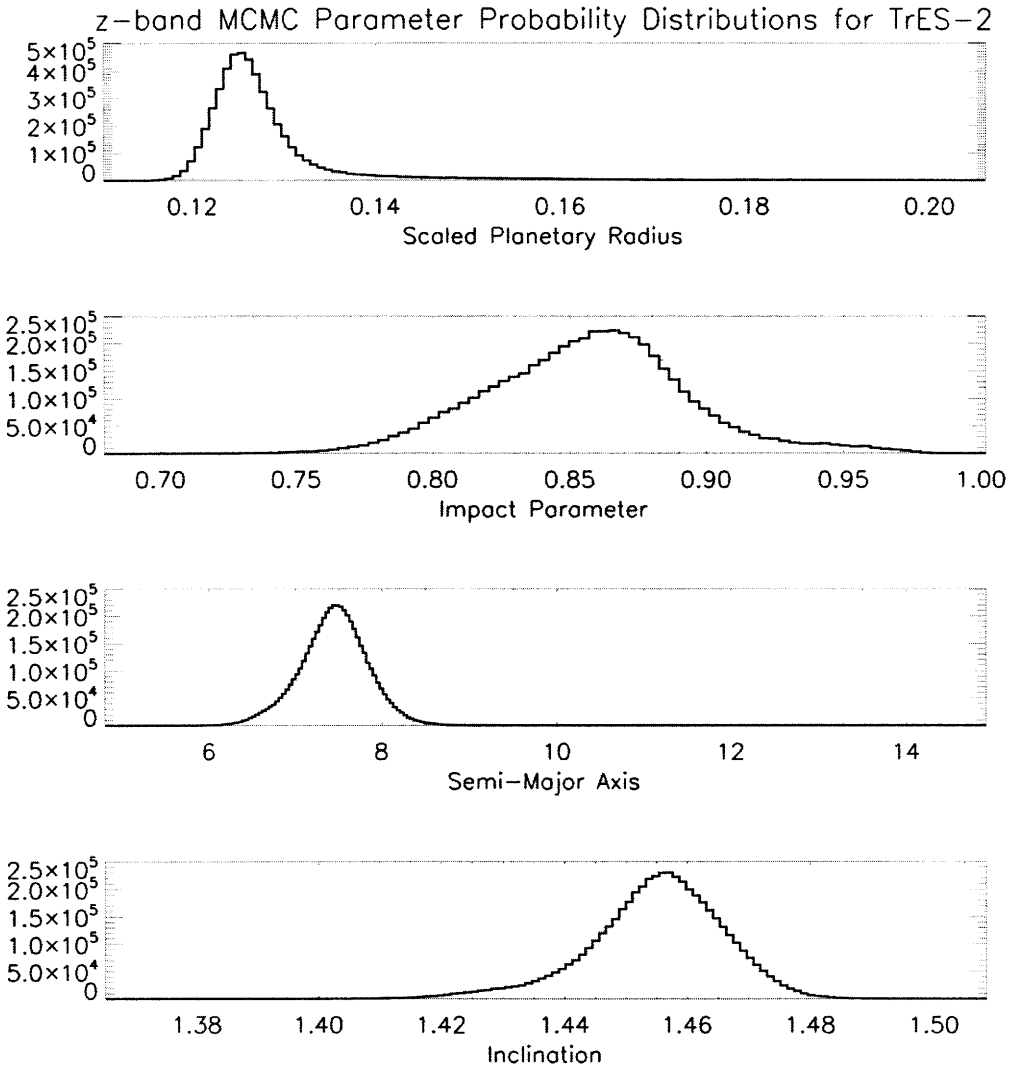

Figure B-74: TrES-2 Parameter Probability Distribution (z-band)

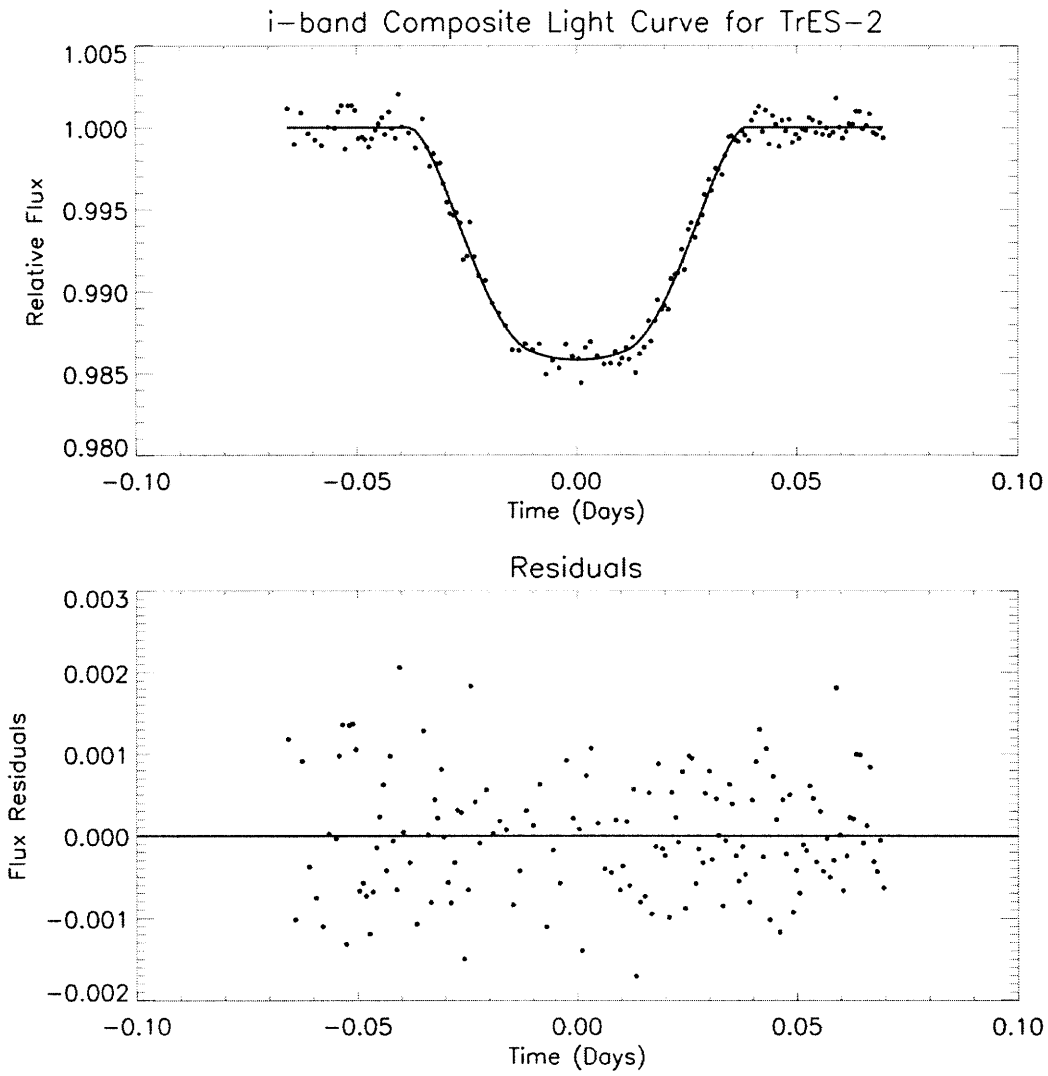

Figure B-75: TrES-2 Fitted Composite Light Curve (i-band)

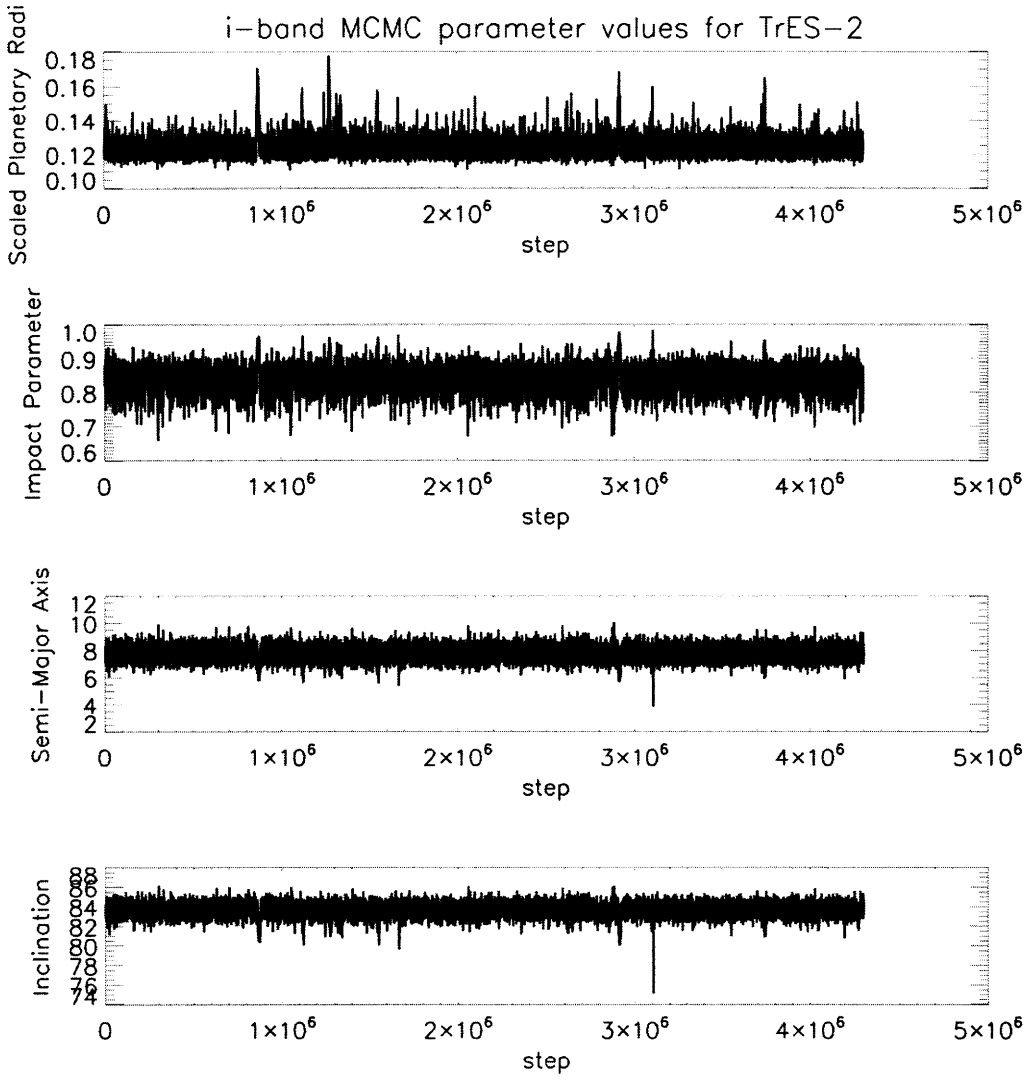

Figure B-76: TrES-2 MCMC Parameter Values (i-band)

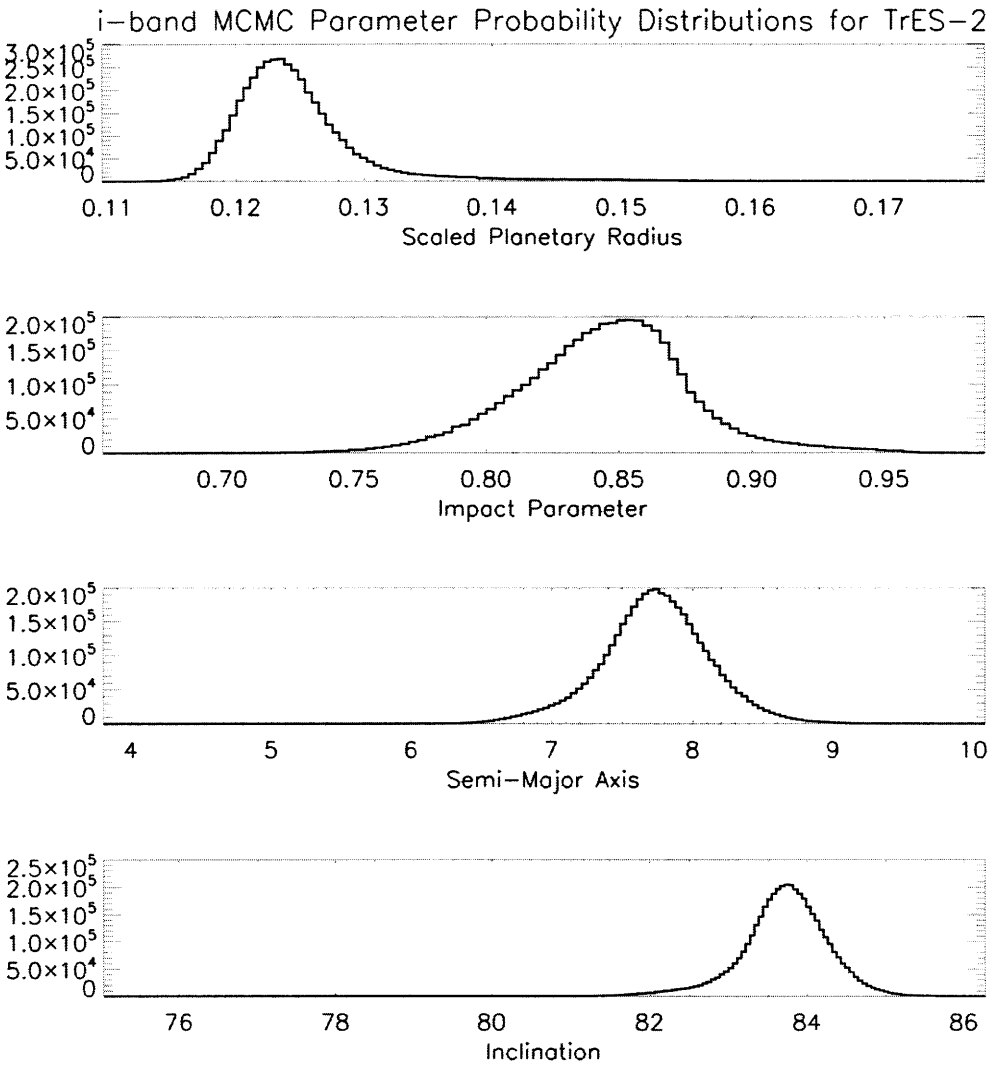

Figure B-77: TrES-2 Parameter Probability Distribution (i-band)

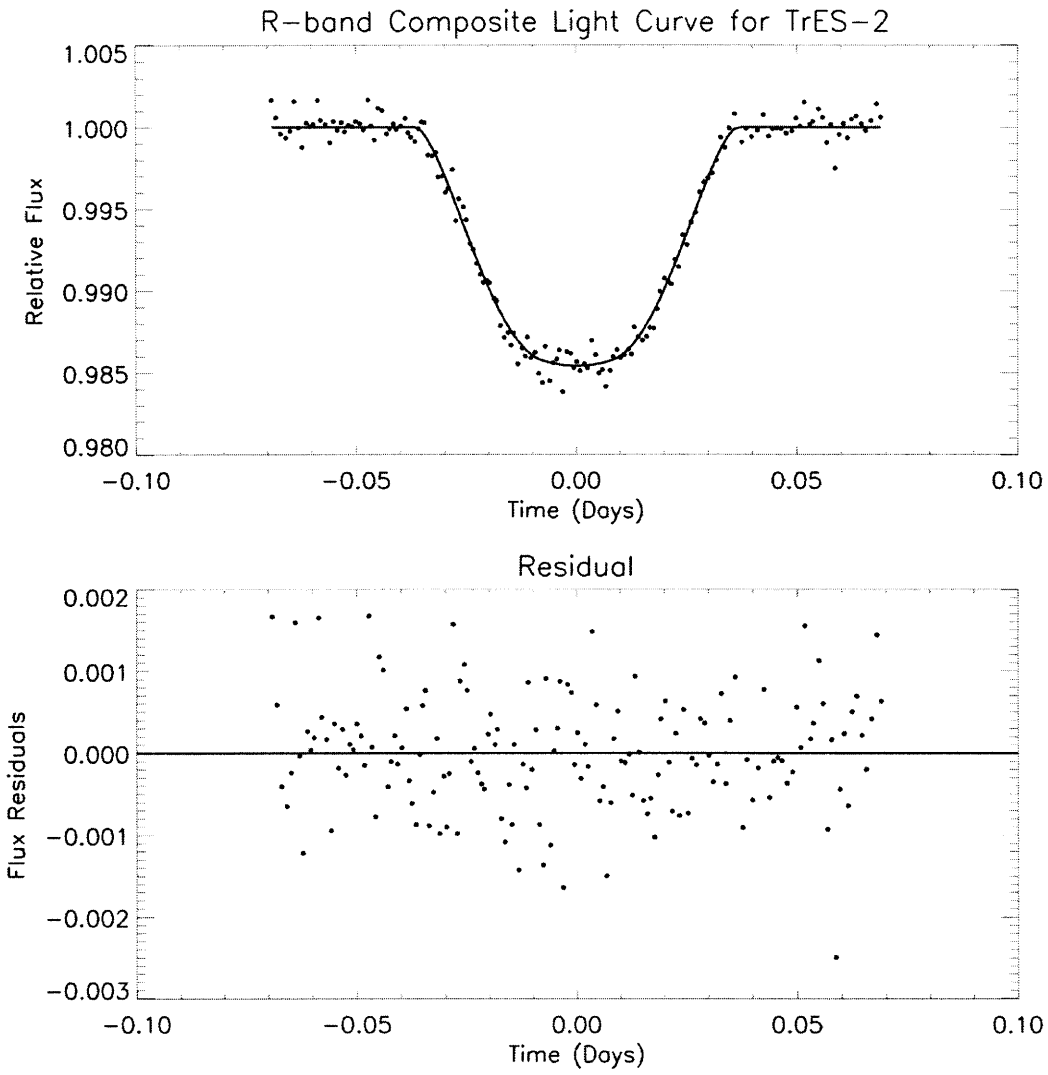

Figure B-78: TrES-2 Fitted Composite Light Curve (R-band)

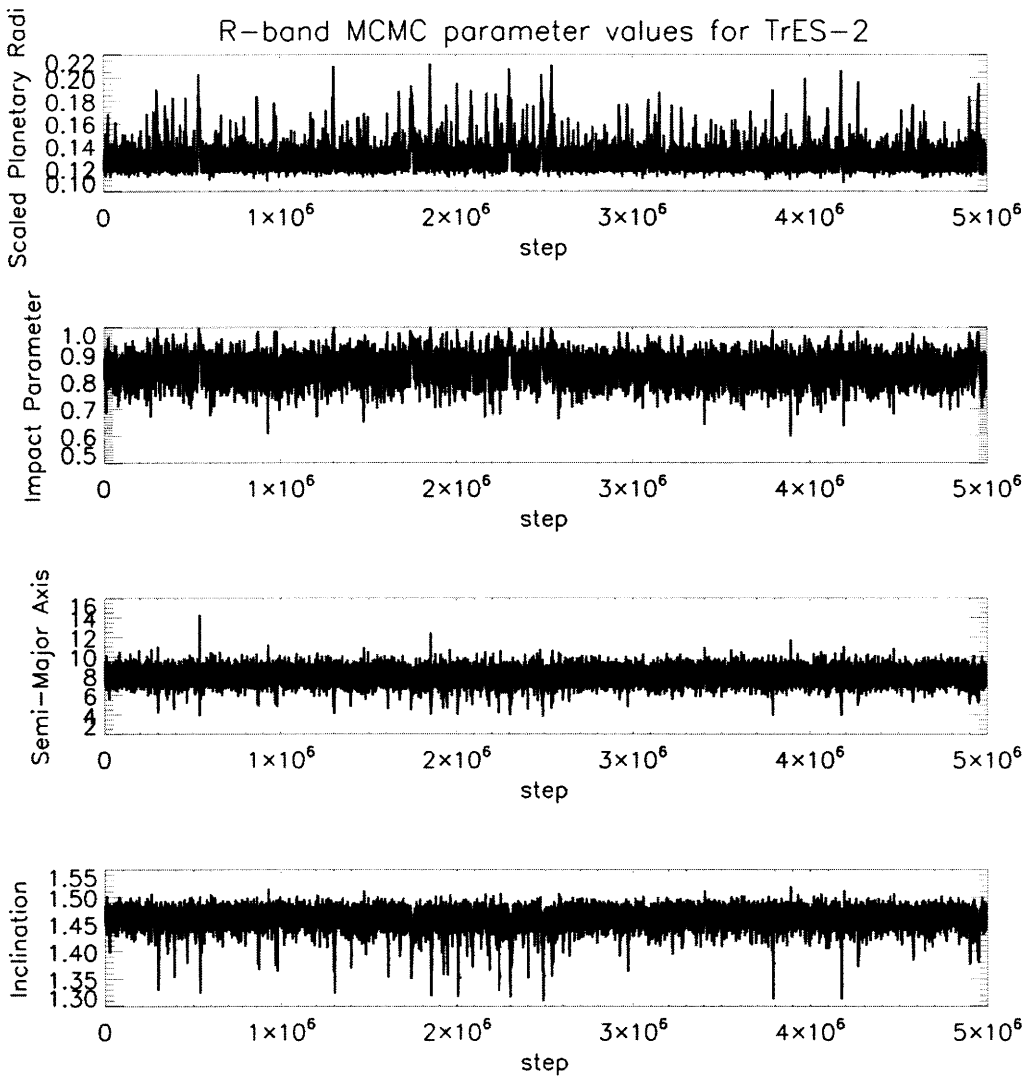

Figure B-79: TrES-2 MCMC Parameter Values (R-band)

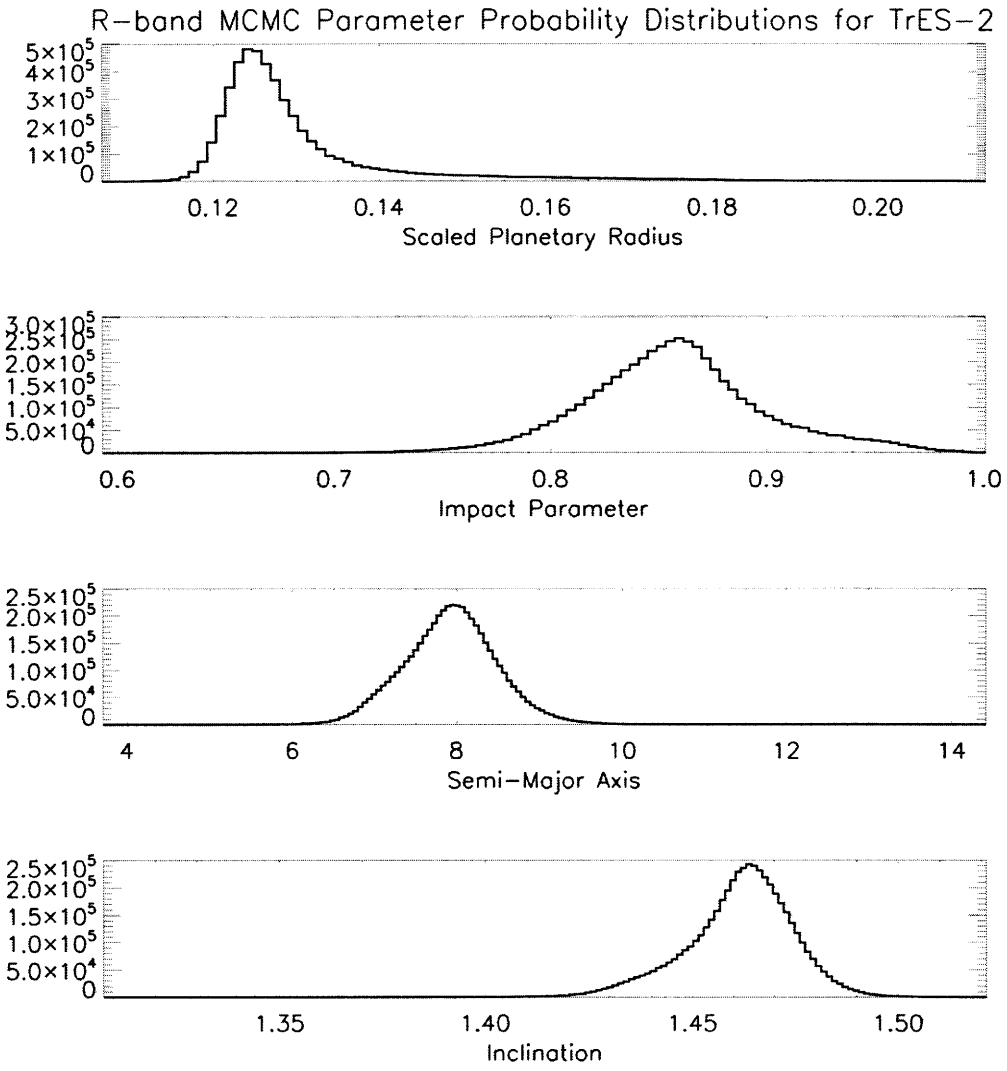

Figure B-80: TrES-2 Parameter Probability Distribution (R-band)

Bibliography

R. Alonso et al., *A&A* **482**,21 (2008).

G.A.Bakos et al., *ApJ* **670**,826 (2007).

M. Barbieri et al., *A&A* **476L**,13B (2007).

F. Bouchy et al., *A&A* (2008).

D. Charbonneau et al., *ApJ* **626**,523C (2005).

A. Claret et al., *A&A* **363**,1081 (2000).

A. Collier Cameron et al., *MNRAS* **375**,951 (2007).

J. Fernandez et al., *arXiv e-prints* 0903.2687F (2009).

E.B.Ford, *AJ* **129**,1706 (2005).

N.P. Gibson et al., *A&A* **492**,603 (2008).

M. Gillon et al., *A&A* **472**,13G (2007).

Holman & Murray, *Science* **307**,1288 (2005).

M. Holman et al., *ApJ* **652**,1715 (2006).

M. Holman et al., *ApJ* **664**,1185 (2007).

Hrudkova et al., *IAUS* **253** (2008).

J.A.Johnson et al., *ApJ* **686**,649J (2008).

Mandel & Agol, *ApJ* **580**,L171 (2002).

G. Mandushev et al., *ApJ* **667**,195 (2007).

N. Narita et al., *PASJ* **60L**,1N (2008).

A. Shporer et al., *ApJ* **694**,1559 (2009).

A. Simon et al., *A&A* **470**,727S (2007).

Steffen & Agol, *MNRAS* **364L**,96S (2005).

Tegmark et al., *Phys Rev D* **69**,103501 (2004).

G. Torres et al., *ApJ* **677**,1324 (2008).

M. Vanko et al., *arXiv e-print* 0901.0625V (2009).

P. Veres et al., *CoSka* **39**,34V (2009).

D.M. Wilson et al., *PASP* **118**,1245 (2006).

J. Winn et al., *AJ* **134**,1707 (2007).

J. Winn et al., *ApJ* **657**,1098 (2007b).

J. Winn et al., *ApJ* **682**,1283 (2008).

J. Winn et al., *ApJ* **683**,1076 (2008).

J. Winn et al., *ApJ* **693**,794 (2009).